SIMPLIFIED DESCRIPTION OF TRANSPORT IN TWO-PHASE ENVIRONMENTS

Ekkehard Holzbecher[a]*

Keywords: Two-phase; biogeochemistry; retardation; porous media; sediment chemistry.

The concept of retardation is usually applied successfully for the description of transport in two-phase systems of different kind with one moving and one stagnant phase. It simplifies understanding the multitude of processes in the two phases. Retardation factors can be derived from measurements and also mathematically from basic transport equations in the single phases, and thus form a link between practice and theory. The author recently presented a generalization of the theoretical derivations for systems with two moving and/or diffusive phases, in which so called *R*-factors were introduced. Like retardation factors, *R*-factors reduce the complexity of the description of a two-phase system. Here conditions are examined in detail under which the generalized *R*-factor approach is applicable. A demonstration example shows steady states depending on phase dependent reaction rates. A final example application demonstrates how the approach works interpreting real world data.

* Corresponding Authors
Fax: +968 2206 1000
E-Mail: ekkehard.holzbecher@gutech.edu.om
[a] German University of Technology in Oman (GUtech),
PO Box 1816, 130 Muscat, Oman

Introduction

There are very different real world situations, in which transport in 2-phase environments is of relevance. Usually one may think of two liquid phases, like water and oil, or one gaseous and one liquid phase, like oil and gas. However, there are much more other examples. A porous medium is by definition a 2-phase system, which consists of a solid and a fluid part. In most applications the fluid is moving, and thus subject to the processes of advection and diffusion or dispersion. In contrast the solid part can often be conceived as fixed, but there are also important instances, in which the solid phase is also moving or subject to alterations that can be described as diffusion. Sediments are a prominent example of such an environment, which is outlined in more detail below. Here a 2-phase system is understood in the outlined general sense, and a mathematical analytical framework is developed.

Mass transport in 2-phase systems can be generally described by two differential equations, each one including storage, diffusion, advection, reaction and phase exchange for a single phase, where subscripts denote phases 1 and 2. φ_1 and φ_2 represent volumetric shares of the phases, D_1 and D_2 are the diffusivities, V_1 and V_2 the velocity vectors and λ_1 and λ_2 the linear production or consumption terms of the phases. For positive λ_1 or λ_2 there is production, for negative values there are losses. The inter-phase exchange terms are denoted by q_{12} and q_{21}. The equations describe the mass balance for each phase.

$$\frac{\partial}{\partial t}\varphi_1 c_1 = \nabla \times (\varphi_1 D_1 \nabla c_1) - \nabla \times (\varphi_1 V_1 c_1) + \\ + \varphi_1 \lambda_1 c_1 - q_{12} \qquad (1)$$

$$\frac{\partial}{\partial t}\varphi_2 c_{12} = \nabla \times (\varphi_2 D_2 \nabla c_2) - \nabla \times (\varphi_2 V_2 c_2) + \\ + \varphi_2 \lambda_2 c_2 - q_{21} \qquad (2)$$

In the sequel we discuss conditions to be fulfilled that the system can be described by only one equation (eqn. 3) with additional factors, denoted here by R, R_{diff}, $\mathbf{R}_{\text{adv}}$ and R_{reac} in the following called *R*-factors. The term *R*-factor was first introduced by Holzbecher[1] in a study on the transient change of equilibria in a chain of radionuclides. Holzbecher[2] generalized the approach for multi-process 2-phase systems. Explicit formulae for the *R*-factors are derived below. As it was derived by adding the concentrations in both phases, equation (3) is the conservation equation for the total amount of the concerned chemical species in the system.

$$\varphi_1 R \frac{\partial}{\partial t} c_1 = \varphi_1 D_1 \nabla \times (R_{\text{diff}} \nabla c_1) - \\ \varphi_1 V_1 \times (\mathbf{R}_{\text{adv}} \nabla c_1) + \varphi_1 R_{\text{reac}} \lambda_1 c_1 \qquad (3)$$

The advantage of eqn. (3) is that it is much easier to understand than eqns. (1) and (2). The number of parameters is reduced, the exchange parameter cancelled out. Moreover for the single processes the coefficients can be combined to effective parameters. For example, by comparing eqn. (3) with the common transport equation, $\varphi_1 D_1 R_{\text{diff}}$ can be understood as an effective diffusivity. Parameter discussions and evaluations become easier that way.

Eqn. (3) as a single equation simplifies the original system consisting of two equations. Thus the wide variety of approaches and solutions for the single transport equation can be utilized. There is a multiplicity of numerical tools. Application example 2 demonstrates the use of a numerical tool. Concerning analytical solutions Ogata and Banks[3] provided a formula for the unsteady 1D advection-diffusion case. Van Genuchten and Alves[4] list much more solutions valid for different boundary conditions, and including reactions. Wexler[5] additionally presents solutions for transport in 2D and 3D.

A plethora of solutions of all kind can be found in the book of Bruggeman.[6] New numerical techniques can be employed easily, such as presented by Wang et al.[7] for high Péclet- and Courant numbers.

Here conditions are discussed in detail, which have to be fulfilled to make the transition from description (1) and (2) to eqn. (3). At first, the underlying idea is illustrated best by re-calling the concept of retardation factors. Further, the final part shows the applicability of the *R*-factor approach for a real world situation.

Retardation factors

To illustrate the idea of the simplified description the concept of retardation is briefly re-called here. This concept can be derived rigorously for a 2-phase system, if there is one immobile (static) and one mobile (dynamic) phase. The immobile phase is fixed in the chosen coordinate system. The mobile phase is subject to dispersion and advection. Moreover it is assumed that the inter-phase exchange is governed by equilibrium sorption. In analogy to eqns. (1) and (2) for both phases, separate mass balances can be set up as follows, where c = concentrations, φ = volumetric share of the mobile phase, $\mathbf{D}$ = dispersion tensor, V = velocity, and q_{mi} = inter-phase exchange term. The subscripts are: *m* for the mobile phase, *i* for the immobile phase. φ, $\mathbf{D}$ and V in equation (4) may vary in space. The term q_{mi} denotes the net flux from the mobile to the immobile phase.

$$\varphi \frac{\partial}{\partial t} c_m = \nabla \times (\varphi \mathbf{D} \nabla c_{\mathrm{m}}) - \nabla \times (\varphi V c_{\mathrm{m}}) - q_{\mathrm{mi}}$$

$$(1-\varphi) \frac{\partial}{\partial t} c_1 = q_{\mathrm{mi}} \qquad (4)$$

As q_{mi} can hardly be quantified in practice, especially if sorption processes are fast, it is convenient to proceed with a formulation in which the exchange term disappears. This is achieved by adding both equations of system (4).

$$\varphi \frac{\partial}{\partial t} c_m + (1-\varphi) \frac{\partial}{\partial t} c_1 = \nabla \times (\varphi \mathbf{D} \nabla c_{\mathrm{m}}) - \nabla \times (\varphi V c_{\mathrm{m}}) \qquad (5)$$

On the right side of the equation, the concentration of the mobile phase c_{m} remains as the only unknown. The same can be achieved on the left side, if the sorption equilibrium can be described by an isotherm $c_{\mathrm{i}}(c_{\mathrm{m}})$. Then the differential equation (5) can be rewritten as eqn. (6).

$$\left(\varphi \frac{\partial}{\partial t} c_{\mathrm{m}} + (1-\varphi) \frac{\partial}{\partial t} c_{\mathrm{i}} \right) = \nabla \cdot (\varphi \mathbf{D} \nabla c_{\mathrm{m}}) - \nabla \cdot (\varphi \mathbf{v} c_{\mathrm{m}}) \qquad (6)$$

The chain rule is applied for the function $c_{\mathrm{i}}(c_{\mathrm{m}}(t))$. In comparison with the transport equation for a tracer component only the term in the brackets on the left side makes a difference.

$$R = 1 + \frac{1-\varphi}{\varphi} \frac{\partial c_{\mathrm{i}}}{\partial c_{\mathrm{m}}} \qquad (7)$$

Thus we may interpret R as parameter that describes the change in the time scale. In case of time independent R one can formally express this by re-writing $R\partial/\partial t = \partial/\partial(t/R)$. Because R obviously is greater than 1, there is always a prolongation of the time scale. Thus R is called the retardation factor. Retardation is not a physical process itself, but is a combined result from single phases processes, coupled by phase interaction.

In case of linear isotherms formula (7) can be modified. In porous media studies, it is common to measure fluid phase concentrations c_{f} ($=c_{\mathrm{m}}$) in relation to fluid volume, and solid phase concentrations c_{s} in relation to the rock mass ($c_{\mathrm{i}}=\rho_{\mathrm{s}} c_{\mathrm{s}}$ with solid phase density ρ_{s}). Using bulk density $\rho_{\mathrm{b}}=(1-\varphi)\rho_{\mathrm{s}}$ the linear isotherm $c_{\mathrm{s}}=K_{\mathrm{d}} c_{\mathrm{f}}$ leads to the well-established formula (for example Roberts *et al*.,[8] Fitts[9]):

$$R = 1 + \frac{\rho_{\mathrm{b}}}{\varphi} K_{\mathrm{d}} \qquad (8)$$

The given derivation follows basic texts on transport in groundwater, for example Kinzelbach[10] or Goode and Konikow.[11] Bouwer[12] gives a derivation of the retardation factor without using the chain rule.

The concept of retardation has turned out to be useful in many porous media and groundwater applications. Extensions of the presented basic approach have been derived with respect to upscaling,[13,14] time-dependence,[15] heterogeneity[16] or colloid transport.[17,18] For the noted cases these extensions can be performed on top of the generalized approach suggested here, eventually considering some further conditions.

R – factors for two mobile phases

R-factors can be introduced for two phase systems with two mobile phases in the same way as presented above for *R* in the mobile-immobile system. Before we come to the general description in this section, it should be noted that additional processes like diffusion and reaction are not taken into account, in order to keep focused on the conditions. Examples are environmental systems with two fluids, like a gas and a liquid, or with two liquids, with advection as dominating intra-phase process. Sediments can be considered as systems with two mobile phases, if sedimentation is taken into account as due to sedimentation, the solid phase has to be described by an advective term, in the Lagrange coordinate system.[19] The considered processes are storage, advection and inter-phase exchange. The basic expression of the 2-phase system reads as system (9), where subscripts denote phases 1 and 2, φ_1 and φ_2 represent volumetric shares of the phases, and V_1 and V_2 are velocities of the phases. The inter-phase exchange terms are denoted by q_{12} and q_{21}.

$$\frac{\partial}{\partial t}(\varphi_1 c_1) = -\nabla \times (\varphi_1 V_1 c_1) - q_{12} \qquad (9)$$

$$\frac{\partial}{\partial t}(\varphi_2 c_2) = -\nabla \times (\varphi_2 V_2 c_2) - q_{21} \qquad (10)$$

Condition 1:
Chemical equilibrium, mathematically expressed as: $q_{21} = -q_{12}$

Summing up eqns. (9) and (10) leads to a single differential equation. The exchange terms disappear from the formulation

$$\frac{\partial}{\partial t}(\varphi_1 c_1) + \frac{\partial}{\partial t}(\varphi_2 c_2) = -\nabla \times (\varphi_1 V_1 c_1) - \nabla \times (\varphi_2 V_2 c_2) \quad (11)$$

Condition 2:
No temporal changes of volumetric shares (i.e. porosity)

The volumetric shares can be taken out of the time derivative on the left hand side.

$$\varphi_1 \frac{\partial}{\partial t} c_1 + \varphi_2 \frac{\partial}{\partial t} c_2 = -\nabla \times (\varphi_1 V_1 c_1) - \nabla \times (\varphi_2 V_2 c_2) \quad (12)$$

Condition 3: Existence of an isotherm

Under the assumption that an isotherm $c_2(c_1)$ exists eqns. (9) and (10) can be reformulated as eqn. (13).

$$\varphi_1 \left(1 + \frac{\varphi_2}{\varphi_1}\frac{\partial c_2}{\partial c_1}\right)\frac{\partial}{\partial t} c_1 = -\varphi_1 \mathbf{v}_1 \times \nabla c_1 - \varphi_2 \mathbf{v}_2 \times \nabla c_2 - [\nabla \cdot (\varphi_1 \mathbf{v}_1)] c_1 - [\nabla \cdot (\varphi_2 \mathbf{v}_2)] \quad (13)$$

The term in the brackets on the left side of the equation is equivalent to the well-known retardation factor R, corresponding to the definition in equation (7). The right hand side has been changed using the product rule in order to prepare the next step.

Condition 4: Steady state flow

Mathematically it can be stated as $\nabla \times (\varphi_1 V_1)$ and $\nabla \times (\varphi_2 V_2)$ and finally the equation simplifies to the formulation (14), with matrix $\mathbf{R}_{adv}$, containing advection R-factors. In 2D, using velocity components v_{1x} and v_{1y} of V_1 and v_{2x} and v_{2y} of V_2, the detailed formulation is given by formulation (15).

$$\varphi_1 R \frac{\partial}{\partial t} c_1 = \varphi_1 V_1 \times (\mathbf{R}_{\mathrm{adv}} \nabla c_1) \quad (14)$$

$$\mathbf{R}_{\mathrm{adv}} = \begin{pmatrix} R_{\mathrm{advx}} & 0 \\ 0 & R_{\mathrm{advy}} \end{pmatrix}$$

with

$$R_{\mathrm{advx}} = 1 + \frac{\varphi_2}{\varphi_2}\frac{v_{2x}}{v_{1x}}\frac{\partial c_2}{\partial c_1}$$

and

$$R_{\mathrm{advy}} = 1 + \frac{\varphi_2}{\varphi_2}\frac{v_{2y}}{v_{1y}}\frac{\partial c_2}{\partial c_1} \quad (15)$$

The new factors R_{advx}, R_{advy} (and R_{advz} in 3D) are diagonal components of the $\mathbf{R}_{adv}$ matrix appearing in the advection term. The factors are bigger or equal than 1. $\mathbf{R}_{adv}$ reduces to the unity matrix in case of $V_2 = 0$, i.e. if the second phase is immobile. The ratio R/R_{advx} can be interpreted as the factor changing the time scale of the advection process in x-direction. R_{advx} depends on the ratio between velocities in x-direction of the two phases.

In porous media problems the velocities in the phases are often determined by the hydraulic gradient, but with different hydraulic conductivities. Under this condition the ratios v_{2x}/v_{1x} and v_{2y}/v_{1y} are identical and one ends up with only one advection R-factor, denoted by R_{adv}:

$$\varphi_1 R \frac{\partial}{\partial t} c_1 = -\varphi_1 R_{\mathrm{adv}} V_1 \times \nabla c_1 \quad (16)$$

For linear exchange, characterized by the constant $K=c_2/c_1$, follows: $R=1+K\varphi_1/\varphi_2$ and and $R_{adv}=1+K_2\varphi_2/V_1\varphi_1$. With the usual definition of K_d (see above) in the fluid-solid system one obtains: $R_{adv}=1+K_d\rho_b V_s/V_f\varphi$. If both phases move with the same velocity, holds: $R_{adv}=R$.

Formulation of the general case

A general situation is considered in which both phases may involve the storage, diffusion, advection, reaction and interphase exchange. The basic mathematical description of this situation is given by eqns. (1) and (2). Concerning reactions we consider linear production or consumption of the species.

In the case of a chemical equilibrium (condition 1) one can reduce the system of eqns. (1) and (2), to a single differential equation. On adding both the equations, the exchange terms vanish, resulting in eqn. (17).

$$\frac{\partial}{\partial t}(\varphi_1 c_1) + \frac{\partial}{\partial t}(\varphi_2 c_2) = \nabla \times (\varphi_1 D_1 \nabla c_1) + \nabla \times (\varphi_2 D_2 \nabla c_2) - \nabla \times (\varphi_1 V_1 c_1) - \nabla \times (\varphi_2 V_2 c_2) + \varphi_1 \lambda_1 c_1 + \varphi_2 \lambda_2 c_2 \quad (17)$$

If the phase space does not change temporarily (condition 2), one obtains eqn. (18).

$$\varphi_1 \frac{\partial}{\partial t} c_1 + \varphi_2 \frac{\partial}{\partial t} c_2 = \nabla \times (\varphi_1 D_1 \nabla c_1) + \nabla \times (\varphi_2 D_2 \nabla c_2) - \nabla \times (\varphi_1 V_1 c_1) - \nabla \times (\varphi_2 V_2 c_2) + \varphi_1 \lambda_1 c_1 + \varphi_2 \lambda_2 c_2 \quad (18)$$

If an isotherm exists (condition 3), one can write

$$\varphi_1 R \frac{\partial}{\partial t} c_1 = \nabla \times (\varphi_1 D_1 \nabla c_1) + \nabla \times (\varphi_2 D_2 \nabla c_2) - \nabla \times (\varphi_1 V_1 c_1) - \nabla \times (\varphi_2 V_2 c_2) + \varphi_1 \lambda_1 c_1 + \varphi_2 \lambda_2 c_2 \quad (19)$$

or

$$\varphi_1 R\frac{\partial}{\partial t}c_1 = \nabla c_1 \times \nabla(\varphi_1 D_1) + \varphi_1 D_1 \nabla^2 c_1 + \\ +\nabla c_2 \times \nabla(\varphi_2 D_2) + \varphi_2 D_2 \nabla^2 c_2 - \\ -c_1 \nabla \times (\varphi_1 V_1) - \varphi_1 V_1 \times \nabla c_1 - \\ -c_2 \nabla \times (\varphi_2 V_2) - \varphi_2 V_2 \times \nabla c_2 + \\ +\varphi_1 \lambda_1 c_1 + \varphi_2 \lambda_2 c_2 \quad (20)$$

If $\nabla \times (\varphi_1 D_1), \nabla \times (\varphi_2 D_2), \nabla \times (\varphi_1 V_1)$, and $\nabla \times (\varphi_2 V_2)$ are negligible (condition 4) then

$$\varphi_1 R\frac{\partial}{\partial t}c_1 = \varphi_1 D_1 \nabla^2 c_1 + \varphi_2 D_2 \nabla^2 c_2 - \varphi_1 V_1 \times \nabla c_1 - \\ -\varphi_2 V_2 \times \nabla c_2 + \varphi_1 \lambda_1 c_1 + \varphi_2 \lambda_2 c_2 \quad (21)$$

which can be re-written as eqn. (22), in line with eqn. (3), using the additional *R*-factors

$$R_{diff} = 1 + \frac{\varphi_2}{\varphi_1}\frac{D_2}{D_1}\frac{\partial c_2}{\partial c_1}$$

and (22)

$$R_{\mathrm{reac}} = 1 + \frac{\varphi_2}{\varphi_1}\frac{\lambda_2}{\lambda_1}\frac{c_2}{c_1}$$

For the linear isotherm in the fluid-solid system with the diffusivity D_s in the solid phase and D_f in the fluid phase the diffusion *R*-factor can be written as $R_{diff}=1+K_d\rho_b D_s/D_f\varphi$. When both diffusivities are in the same range, one obtains R_{diff} in the same range as the retardation factor *R*. In case of strong sorption the factor may be several orders of magnitude greater than 1. If velocity ratios in the coordinate directions are the same ($v_{2x}/v_{1x}=v_{2y}/v_{1y}=v_{2x}/v_{1x}=v_{2z}/v_{1z}$) one can re-write eqn. (22) as eqn. (23).

$$\varphi_1 R\frac{\partial}{\partial t}c_1 = \varphi_1 D_1 \nabla \times (R_{\mathrm{diff}} \nabla c_1) - \\ \varphi_1 R_{\mathrm{adv}} V_1 \times \nabla c_1 + \varphi_1 R_{\mathrm{reac}} \lambda_1 c_1 \quad (23)$$

Equation (23) provides the clues how the relevance of a process changes in relation to a single-phase system. There are three process-dependent time scaling factors namely R/R_{diff} for diffusion, R/R_{adv} for advection, and R/R_{reac} for linear reactions. If there is no diffusion in the second phase, R_{diff} is equal to 1 and retardation by factor *R* is valid for diffusion. When there is no advection in the second phase, R_{adv} is equal to 1 and the retardation by *R* is valid for advection. When there is no production or degradation in the second phase, R_{reac} is equal to 1 and the retardation factor *R* is valid concerning reactions. The concept of genuine retardation, as described, is valid only if all factors are equal to unity i.e., $R_{diff} = R_{adv} = R_{reac} = 1$. The derived single differential equation delivers a tool to understand the relevance of the involved processes for the transport dynamics.

Examples of Application

Steady-state phase dependent reactions

Here we give an example for the 1D steady state, if all coefficients are constants. The general solution can be obtained easily with the following ansatz.

$$c(x) = C_1 \exp(\delta x) + \overline{C_1}\exp(\bar{\delta} x) \quad (24)$$

Putting this in the differential eqn. (3) one obtains

$$\delta, \bar{\delta} = \frac{1}{2R_{\mathrm{diff}}D}\left(R_{\mathrm{adv}}v \pm \sqrt{R_{\mathrm{adv}}^2 V^2 + 4R_{\mathrm{reac}}R_{\mathrm{diff}}\lambda D}\right) \quad (25)$$

The solution (24) and (25) can also be expressed in terms of the non-dimensional Péclet and Damköhler numbers. In the presented approach both non-dimensional numbers depend on *R*-factors:

$$P_e = \frac{R_{adv} V L}{R_{diff} D}$$

and (26)

$$D_a = \frac{R_{decay}\lambda L^2}{R_{diff} D}$$

The solution is then given by eqn. (27).[20]

$$c(x) = c\exp(\delta \bar{x}) + \bar{c_1}\exp\left(\bar{\delta}\bar{x}\right) \\ \delta, \bar{\delta} = \left(\frac{P_e}{2} \pm \sqrt{D_a + \frac{P_e^2}{4}}\right) \quad (27)$$

where $\bar{x} = x / L$ denotes the non-dimensional space variable. The Péclet and Damköhler numbers determine the steady state solutions, as illustrated for example by Holzbecher.[21]

The integration constants c_1 and $\bar{c}_1$ have to be determined by boundary conditions. If there is Dirichlet boundary condition $c(0) = 1$ at $x = 0$ and the Neumann condition $\partial c / \partial x = 0$ at $x = L$, then

$$\frac{c(\bar{c})}{c_0} = \frac{\bar{\delta}\exp\left(\bar{\delta}\right)\exp(-\delta\overline{x}) - \delta\exp(-\delta)\exp(\bar{\delta}\overline{x})}{\bar{\delta}\exp\left(\bar{\delta}\right) - \delta\exp(\delta)} \quad (28)$$

As an example a detailed look is presented into an environment, in which one of the phases is subject to degradation and inter-phase exchange only. A typical example for such a system is a porous medium with a fluid and a solid phase, the latter fixed in space. We denote the fluid as phase 1 and the solid as phase 2. As there is no advection and no diffusion in the solid phase, R_{adv}=1, and R_{diff}=1 (according to eqns. (15) and (20)). Hence eqn. (3) reduces to eqn. (29) with *R* and R_{reac}:

$$R\frac{\partial}{\partial t}\varphi_1 c_1 = \varphi_1 D_1 \nabla^2 c_1 - \varphi_1 V_1 \times \nabla c_1 - R_{\text{reac}}\varphi_1 \lambda_1 c_1 \quad (29)$$

$$R = 1 + \frac{\varphi_2}{\varphi_1}\frac{\partial c_2}{\partial c_1}$$

and (30)

$$R_{reac} = 1 + \frac{\varphi_2}{\varphi_1}\frac{\lambda_2}{\lambda_1}\frac{c_2}{c_1}$$

The degradation rate in the mobile phase is $\lambda_1 > 0$ and in the immobile phase it is $\lambda_2 > 0$. It is usual that the degradation characteristic is different, i.e., phase dependent. In case of radio-nuclides the degradation rates, i.e., rates for radioactive decay are identical, which is a special case of phase independent reaction. Altogether we can distinguish 5 different cases.

1. No reaction in immobile phase, $\lambda_2 = 0$, $R_{\text{reac}}=1$, $Da = \lambda_1 L^2/D$.

2. $0<\lambda_2<\lambda_1$, $1<R_{\text{reac}}<R$, example: $R = 2$, $\lambda_2 = \lambda_1/2$, $Da = R_{\text{reac}}\lambda_1 L^2/D = 1.5\lambda_1 L^2/D$.

3. Reaction in both the phases is identical, $\lambda_1=\lambda_2$, $R_{\text{reac}}= R =2$, $Da = 2\lambda_1 L^2/D$.

4. $\lambda_2>\lambda_1$, $R_{\text{reac}}>R$, $R = 2$, $\lambda_2 = 2\lambda_1$, $Da = R_{\text{reac}}\lambda_1 L^2/D = 3\lambda_1 L^2/D$.

5. No reaction in mobile phase, $\lambda_1=0$; the last term in (29) is $\varphi_2\lambda_2 C_1(C_1)$, $Da = \lambda_2 K L^2/D$.

Results for several combinations of *Pe* and *Da* are depicted in Figure 1. If $\lambda_1 L^2/D = 1$, in case of no reaction in the immobile phase the relevant Damköhler number is also equal to unity and the corresponding steady state profiles are given by the uppermost graphs in all sub-figures, depending on the Péclet number.

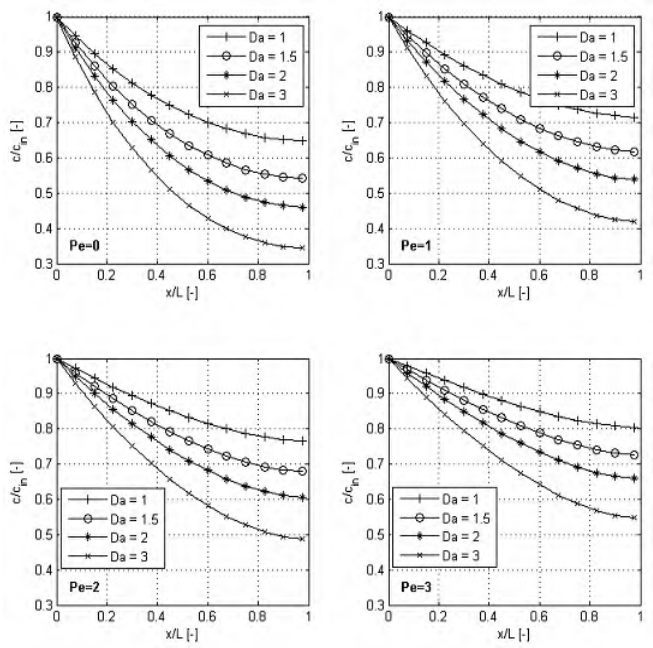

Figure 1. Steady state profiles in dependence of *Pe* and *Da*; *Pe* = 0 (top left), *Pe* = 1 (top right), *Pe* = 2 (bottom left), *Pe*= 3 (bottom right); profiles decrease stronger for higher *Da*-numbers.

In the example in case 2 with $0<\lambda_2<\lambda_1$ holds $Da = 1.5$ with second from top profiles shown in the sub-figures. In the special case of phase independent decay rates *Da* becomes equal to 2 (cf. the corresponding curves in Figure 1).

In the example case 4 with $\lambda_2>\lambda_1$ holds $Da = 3$. The graphs for the latter cases for four different Péclet numbers are the ones with lowest concentrations in the sub-figures. A comparison with case 5 in this series is not possible without further parameter specifications.

The illustrations in each sub-plot of Figure 1 demonstrate the decrease of the concentrations with increasing decay constant, provided all other parameters remain at a constant value. The Damköhler-number is different in the cases defined above, and the change in it is due to the different R_{reac} factor, on which it depends.

Transient phase-dependent diffusion

As was mentioned above aquatic sediments constitute a physical system in which diffusive and advective processes are relevant in both the fluid and the solid phase. Diffusion is not only caused by processes on molecular scale but also on a larger scale due to the activity of biological species, such as worms, which is referred to as bio-turbation.[22,23] Worm activity results in re-arrangements in the sediment structure and it is assumed that this can be described as a diffusion process.

Work et al.[24] documented laboratory experiments with aquatic sediments. The experiments were performed in a box with a sediment layer of 23 cm thickness, consisting of medium sand, kaolinite, and topsoil. The overlying free water column was 15 cm deep. The experimental test box was initially filled by a 1 ppt NaCl tracer solution, and then circulated by tracer-free water. Experiments were first done with pure sediments, then worms of type *Lumbriculus variegatus* were introduced as bio-turbators. Several of such experiment series were performed with different flow speed in the free water column and with different bed materials.

Salinity was measured at several locations of a sampling grid in several depths between 2.5 and 21 cm below the sediment-water interface. Sampling times were selected differently, but typically included 1, 3, 6, 12, and 24 h. Evaluating the different profiles from both situations, without and with worms, the effect of bio-turbation could be studied. For two experiments (B9 without worms and B10 with worms, using the notation of Work et al.[24]) the measured profiles for NaCl in the sediments after 24 h are depicted by markers in Figure 2. Moreover Work et al.[24] compared the observed concentration profiles with analytical solutions for situations in which only diffusion is a driving process. Reducing the RMS error between measurements and the analytical solution they were able to obtain best-fit values for diffusivities. Their results are listed in Table 1. D_e denotes the effective diffusivity in case without bio-turbation, D_b the effective diffusivity in case of bio-turbation. In all cases the effective diffusivity is increased after the introduction of the worms.

Table 1. Changes of effective diffusivities due to bio-turbation in the experiments of Work et al.[24]

Experiment	D_e [cm²/s]	D_b [cm²/s]	R_{diff}
B1, B2	5.4×10^{-5}	3.4×10^{-4}	6.3
B3, B4	3.2×10^{-5}	4.2×10^{-5}	1.31
B5, B6	6.7×10^{-5}	2.1×10^{-4}	3.13
B7, B8	4.7×10^{-5}	1.0×10^{-4}	2.13
B9, B10	1.9×10^{-4}	3.5×10^{-4}	1.84
B11, B12	3.4×10^{-5}	5.5×10^{-5}	1.62

The Péclet number, as given in eqn. (26), is a measure for the relative importance of advective in comparison to diffusive processes. If there is diffusion in the solid phase we have to consider a factor R_{diff} in the denominator of equation (26). The ratio between the Péclet number without bio-turbation, P_e, and with bio-turbation, P_{eb}, is given by eqn. (31).

$$P_e \big/ P_{eb} = \frac{R_{adv} v L}{D_e} : \frac{R_{adv} v L}{R_{diff} D_e} = \frac{D_b}{D_e} = R_{diff} \qquad (32)$$

Table 1 shows the resulting values for R_{diff} for the different experiments. In correspondence with the derivations here the values are all above 1, ranging between a minimum value of 1.31 and a maximum of 6.3. The experimental results confirm the validity of the theoretical approach.

Based on the mathematical analytical approach given above a 1D numerical model was set up to simulate the concentration distribution in the sediment columns. The initial condition is given by $c = 1$, representing high salinity in non-dimensional units. At $t = 0$, we assume a fast fresh water inflow in the surface water and thus set the boundary condition $c = 0$ at the upper boundary, the sediment-water interface. At the lower boundary a no-flow condition for mass transport is required. The numerical model was set-up using the finite element code COMSOL Multiphysics.[25]

The model was first run at constant diffusivity for the entire column. For a second run the model region was divided into two parts. The upper sediments are assumed to be affected by worm activity, in our approach implicating an increased diffusivity. The thickness of the upper layer is 6 cm, following Work et al.[24] The value stems from the usual length of the worms, which ranges between 2-5 cm. The value of diffusivity is 10^{-4} cm^2 s^{-1} without bio-turbation and is 4×10^{-4} cm^2 s^{-1} with bio-turbation, corresponding to a value of 4 for R_{diff} (eqn. 31). In this way two related experiments were modelled, one without and one with diffusion in the solid phase, i.e., without and with bio-turbation.

Figure 2 depicts the results of the numerical modelling for experiments B9 (without bio-turbation) and B10 with bio-turbation. The comparison with the measurements shows a rough agreement. For the B9 experiment the uppermost observation is highly overestimated, while others are underestimated. Thus the slope within the profile is not matched, while the mean square error is minimal. Probably one reason for the underestimation is that the $c = 0$ boundary condition is not matched in reality as it neglects the time to wash out high salinity at the bottom of the surface water.

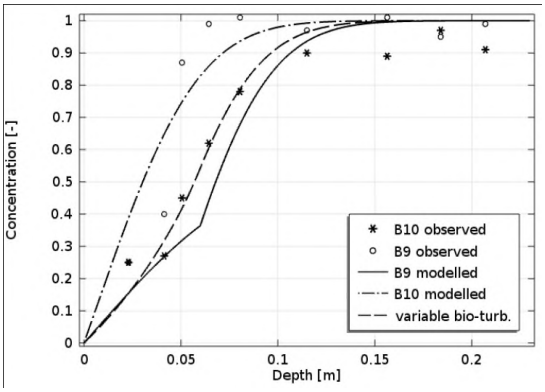

Figure 2. Concentration profiles of NaCl in aquatic sediments with and without worm activity; normalized concentration is plotted versus depth; markers indicate measured values and curves visualize numerical solutions.

The B10 experiment with bio-turbation seems to match better. Concentrations in the uppermost layer are underestimated, while there is an overestimation by the numerical model in the lower part. The latter may not be taken as serious, because the initialisation of the physical model with equally high NaCl concentrations may not have fully completed, as mentioned by the experimenters,[24] and as seen in the fluctuations of the measured values. Thus it seems to be more probable that the slope of the concentration profile is shifted to lower concentration values by the numerical model.

In order to obtain a better fit in the mentioned sense, a third model run was performed in which the bio-turbation model was varied from a high value at the top to a low background value at the bottom. This takes into account that the worms are of different size and they may not drill vertically to reach deeper levels. The re-arrangements in the sediment structure can thus be expected to be highest near to the sediment-water interface and decrease gradually with distance from it. Thus the diffusivity is assumed to vary linearly from a high value at the upper boundary to the bottom of the upper sediment layer. Correspondingly R_{diff} changes from a value of 4 at the sediment-water interface to 1 to the interior sediment interface.

Figure 2 also depicts the simulation results of the third model run. Obviously these match better than the former results in the sense noted above. The deviations between measurements and model at the end of the column can be attributed to difficulties of the experimental set-up. However the slope of the concentration profile is predicted exactly by the model.

Conclusion

The presented approach reduces the complexity of transport processes in general two-phase multi-process environments. Assuming the validity of chemical equilibrium the description can be reduced to a single differential equation, in which coefficients are modified by *R*-factors. For the involved processes *R*-factors were introduced in analogy to the derivation of the well-known retardation factor for the storage process.

The reduction to a single equation allows the utilization of classical approaches and results concerning the advection-diffusion-reaction equation. As example we present analytical solutions for the 1D steady state. In contrast to the retardation factor the *R*-factors have an effect not only on the transient development but also on the steady state. The effect can easiest be evaluated by the use of extended definition of Péclet - and Damköhler numbers.

In an application concerning aquatic sediments the theoretical results are contrasted with the outcome from laboratory experiments. The comparison shows that the theory gives a correct explanation for the behaviour observed in the sediments. It also shows how a quantification of the effect of bio-turbation is given by the R_{diff} factor. The utilization of the *R*-factor approach in a numerical model with spatially varying bio-turbation delivered a better match with measurements.

References

[1]Holzbecher, E., *J. Environ. Hydrol.*, **1997**, 5.

[2]Holzbecher, E., *Toxicol. Environ. Chem.*, **2017**, *9*(*7-8*), 1096-1116. doi.org/10.1080/02772248.2016.1241881

[3]Ogata, A., Banks, R. B., *A solution of the differential equation of longitudinal dispersion in porous media*, *U.S. Geol. Survey*, **1961**, Professional Paper No. 411-A.

[4]van Genuchten, M. Th., Alves, W. J., *Analytical solutions of the one-dimensional convective-dispersive solute transport equation*, Technical Bulletin No. 1661 (U.S. Dep. of Agriculture)**1982**

[5]Wexler, E. J., *Techniques of Water-Resources Investigations of the United States Geological Survey*, Book 3, **1992,** Chapter B7.

[6]Bruggeman, G. A., *Analytical Solutions of Geohydrological Problems*, Elsevier, Amsterdam, **1999**.

[7]Wang, W., Dai, Z., Li, J., Zhou, L., *Comput. Geosci*., **2012**, *12*, 182-189. doi.org/10.1016/j.cageo.2012.05.020

[8]Roberts, P. V., Reinhard, M., Valocchi, *J. AWWA*, **1982**,*74* (*8*), 408-413.

[9]Fitts, C., *Groundwater Science*, Academic Press, London, **2002**.

[10]Kinzelbach, W., *Numerische Methoden zur Modellierung des Transports von Schadstoffenim Grundwasser*, *Oldenbourg*, München, **1987**.

[11]Goode, D. J., Konikow, L. F., *Modification of a method-of-characteristics solute-transport model to incorporate decay and equilibrium-controlled sorption or ion exchange*, Water-Resources Investigations Report 89-4030 (U.S. Geological Survey), **1989**.

[12]Bouwer, H., *Groundwater*, **1991**, *29* (*1*), 41-46.

[13]Deng, H., Dai, Z., Wolfsberg, A. V., Ye, M., Stauffer, P. H., Lu, Z., Kwicklis, E., *Chemosphere*, **2013**, *91*, 248-257. doi.org/10.1016/j.chemosphere.2012.10.105

[14]Soltanian, M. R., Ritzi, R., Huang, C., Dai, Z., Deng, H., (2015) *Transport Porous Med*., **2015**, *108*, 355-366. doi: 10.1007/s11242-015-0480-2

[15]Soltanian, M. R., Ritzi, R., Huang, C., Dai, Z., *Water Res. Res*., **2015**, 51, 1586-1600. doi: 10.1002/2014WR016353

[16]Dentz, M., Castro, A., *Geophys. Res. Lett.*, **2009**, *36*, L03403. doi:10.1029/2008GL036846

[17]Holzbecher, E., Dizer, H., *Colloids Surf. A*, **2006**, 278, 204-211.

[18]Kim, M., Kim, S.-B., , *Hydrogeol. J.*, **2007**, *15* (*7*), 1433–1437.

[19]Holzbecher, E., *Hydrol. Sci. J.***,** ,**2002**, *47* (*4*), 641-649.

[20]Holzbecher, E., Dizer, H., Lopez-Pila, J., Szewzyk, R., Nützmann, G., *Recharge systems for protecting and enhancing groundwater resources*, UNESCO IHP-VI Publ., UNESCO, Paris, **2006**, 377-383.

[21]Holzbecher, E., *Environmental Modeling – using MATLAB*, Springer, Berlin, **2012**.

[22]Schiffers, K., Teal, L.R., Travis, J. M. J., Solan, M., *PLoS ONE*, **2011**, *6* (*12*), e28028. doi.org/10.1371/journal.pone.0028028

[23]Kristensen, E., Penha-Lopes, G., Delefosse, M., Valdemarsen, T., Quintana, C.O., Banta, G. T., *Mar. Ecol. Prog. Ser*., **2012,** *446*, 285-302. doi.org/10.3354/meps09506

[24]Work, P. A., Moore, P. R., Reible, D. D., *Water Res. Res*., **2002**, *38* (*6*), 1088. doi: 10.1029/2001WR000302

[25]COMSOL Multiphysics, **2018**, www.comsol.com

Received: 24.06.218.
Accepted: 10.07.2018.

ISOLATION, CHEMICAL MODIFICATION AND CYTOTOXIC EVALUATION OF ATRANORIN, THE MAJOR METABOLITE OF THE FOLIOSE LICHEN *PARMOTREMA MELANOTHRIX*

Uppuluri Venkata Mallavadhani,[a,b]* Tiruveedhula Somasekhar,[a,b] Gudem Sagarika[c] and Sistla Ramakrishna[c]

Keywords: Lichen, Parmotrema melanothrix, atranorin, cytotoxicity, MTT assay.

The foliose lichen, *Parmotrema melanothrix* has been chemically screened for the first time and isolated the depside atranorin (**1**) in significant quantity (2 %) along with methyl 2,4-dihydroxy-3,6-dimethylbenzoate (**2**) and methyl 3-formyl-2,4-dihydroxy-6-methylbenzoate (**3**). In view of its abundance, interesting structural features and significant biological profile, atranorin was subjected to chemical modification and synthesised five diverse analogues in very good yields (70~93%). The synthesised analogues along with the three isolated compounds were evaluated for their cytotoxic potential against a panel of six human cancer cell lines using MTT assay. Among the tested compounds, **1a** showed enhanced activity than the parent compound (**1**) against almost all the tested cell lines. Significantly, **1a** showed highest activity (IC_{50} = 15.19 μM) against prostate cancer cell line (DU145). The results indicate that complete protection of the phenolic hydroxyls in atranorin as acetates enhances the cytotoxicity, especially against DU 145.

* Corresponding Author
E-Mail: uvmavadani@yahoo.com.
[a] Centre for Natural Products & Traditional Knowledge, CSIR-Indian Institute of Chemical Technology, Hyderabad-500007, India.
[b] Academic Council for Scientific and Industrial Research
[c] Applied Biology Department, CSIR-Indian Institute of Chemical Technology, Hyderabad-500007, India.

Introduction

Lichens are highly productive natural sources with a conglomerate of two organisms such as fungi and algae or cyanobacteria.[1] They can survive in a wide range of habitats and harsh environmental conditions such as low temperatures, prolonged darkness, drought and continuous light. These extreme conditions encourage the lichens to produce biologically active secondary metabolites such as depsides, depsidones, xanthones, dibenzofurans and chromones.[2] Most of these secondary metabolites are unique to lichens and are produced biosynthetically via the polyketide pathway.[3]

Lichen substances exhibit a wide range of biological activities such as antimicrobial, anti-inflammatory, HIV-1 integrase inhibitory, antioxidant, antipyretic and antiproliferative or cytotoxic.[4,5] The genus *Parmotrema*, belongs to the Parmeliaceae family, is the largest one in the lichen kingdom. The lichens of this family are characterized by the development of a foliose growth.[6]

The major secondary metabolites of *Parmotrema* genus are depsides, which possess two or more aromatic rings joined through ester linkages. Interestingly these metabolites are reported with several biological activities such as antimicrobial, antiviral, antiprotozoal, insecticidal, antitermite, cytotoxic, antioxidant, wound healing, antiherbivore, analgesic and anti-inflammatory.[7-9] Among the various *Parmotrema* lichens, *P. melanothrix* is unexplored both chemically and biologically. In a preliminary study different polar extracts *P. melanothrix* were tested and reported to exhibit antioxidant and antibacterial activity against *S. viridians*, *S. aureus* and Acinetobacter.[10] Virtually, no systematic chemical examination has been done on this species except the preliminary phytochemical screening of Spielmann and Marcelli who identified atranorin and protopraesorediosic acid by performing some spot tests.[11] As, there are no systematic chemical and biological studies were carried so far on *P.melanothrix*, we have now taken up its detailed chemical screening and chemical modification of atranorin, its major metabolite to identify potent cytotoxic leads.

Experimental

General experimental procedure

Silica gel 60 F254 TLC glass plates (Merck) were used to monitor purity of the isolated compounds and all the reactions. Column chromatography was carried out by using Acme grade silica gel (60-120 mesh). Melting points were determined on Buchi melting point apparatus and are uncorrected. IR spectra were recorded on Nicollet 740 FTIR spectrophotometer using KBr pellets. ^{1}H and ^{13}C NMR spectra were recorded on Brucker 300 MHz or Varian 500 MHz in $CDCl_3$ with TMS as internal standard. Chemical shifts were expressed as Hertz (Hz). HRMS spectra were recorded on Agilent-ESI QTOF or JEOL mass spectrometers.

Lichen material

The lichen, *Parmotrema melanothrix* (250 g) was collected from rocks (saxicolous) in Tirumala Hills (13.67820N, 79.35220E), Tirupathi, Andhra Pradesh, India at an altitude of 976 meters (3,202 ft). The collected lichen material was identified according to their morphological characteristics.[12]

Extraction and isolation

The lichen material was washed under tap water to remove any foreign matter. It was shade dried and powdered in a pulveriser. The powdered lichen (250 g) was extracted with acetone (1 L) at room temperature overnight. Concentration of acetone solubles under vacuum to one quarter volume and keept at room temperature overnight followed by filtration yielded a brown coloured solid (5.5 g, 2.2 %) and an extract (5 g, 2 %). The brown colour solid on recrystallisation using hexane-ethanol solvent system, yielded pure compound **1** (5 g, 2 %). Repetitive Si gel column chromatographic separation of the acetone extract (5 g) afforded compounds **2** (1.0 g, 0.4 %) and **3** (0.5 g, 0.2 %).

3-Hydroxy-4-(methoxycarbonyl)-2,5-dimethylphenyl 3-formyl-2,4-dihydroxy-6-methylbenzoate (atranorin, 1)

Yield 2 %, m.p. 192-196 ^{0}C. IR (KBr): 3450, 1770, 1730, 1650, 1580,1260, 1145 cm$^{-1.1}$H NMR (300 MHz, $CDCl_3$) δ = 2.09 (s, 3H), 2.54 (3H, S), 2.69 (s, 3H), 3.98 (s, 3H), 6.40(1H,S) 6.51(s, 1H), 10.36 (1H,S),11.96 (1H,S), 12.51 (s, 1H), 12.56 (s, 1H); ^{13}C NMR (125 MHz, $CDCl_3$) δ = 9.60, 24.24, 25.80, 52.56, 103.06, 108.78, 110.49, 113.07, 116.241, 117.01, 140.09, 152.21, 152.65, 163.09, 167.708, 169.30, 169.90, 172.41, 194.04. HRMS (ESI) *m/z* calcd. for $C_{19}H_{17}O_8$ $[M-H]^+$ 373.0923, found 373.0917.

Methyl 2,4-dihydroxy-3,6-dimethylbenzoate (2)

Yield 0.4 %, m.p 143-145 ^{0}C. IR (KBr): 3404, 3082, 2943, 1627, 1500, 1446, 1424, 1368 cm^{-1}. ^{1}H NMR (300 MHz, CDCl3) δ = 2.10 (s, 3H), 2.45 (s, 3H), 3.92 (s, 3H), 6.20 (s, 1H), 12.04 (s, 1H); ^{13}C NMR (125 MHz, CDCl3) δ = 7.37, 23.79, 51.53, 104.88, 108.29, 110.28, 139.85, 157.83, 162.82, 172.38. HRMS (ESI) *m/z* calcd. for $C_{10}H_{13}O_4$ $[M+H]^+$ 197.0814, found 197.0810.

Methyl 3-formyl-2,4-dihydroxy-6-methylbenzoate (3)

Yield 0.2 %, m.p 145-149 ^{0}C, ^{1}H NMR (300 MHz, $CDCl_3$) δ = 2.53 (s, 3H), 3.96 (s, 3H), 6.29 (s, 3H), 10.34 (s, 1H), 12.40 (s, 1H), 12.87 (s, 1H); ^{13}C NMR (125 MHz, $CDCl_3$) δ = 24.93, 52.03, 103.5, 108.1, 111.8, 152.0, 166.3, 168.0, 171.7, 193.6; HRMS (ESI): *m/z* calcd. for $C_8H_7O_3$ $[M-H]^+$ 151.0395, found 151.0394.

Preparation of 4-((3-acetoxy-4-(methoxycarbonyl)-2,5 dimethylphenoxy)carbonyl)-2-(diacetoxymethyl)-5-methyl-1,3-phenylene diacetate (1a).

A mixture of compound **1** (0.05 g, 0.13 mmol), acetic anhydride (5 mL) and pyridine (catalytic amount) was stirred at room temperature for 12 h. The reaction mixture was poured into 20 mL of ice water. The brown colored solid was collected by filtration and washed with ice water. The reaction mixture was diluted with water and extracted with ethyl acetate. The organic layer was dried over anhydrous sodium sulphate, concentrated under reduced pressure and chromatographed over silica gel column to afford compound **1a** as brown colored crystals (0.075 g, 93 %), m.p. 98-102 ^{0}C. IR (KBr): 2951 (C-H), 1776 ($OCOCH_3$), 1728 ($OCOCH_3$) cm$^{-1.}$ ^{1}H NMR (500 MHz, $CDCl_3$) δ = 2.01 (s, 3H, C8^1-CH_3), 2.06 (s, 3H, C9^1-CH_3), 2.30 (s, 3H, C9-CH_3), 2.301 (s, 3H, C4-$COCH_3$), 2.39 (s, 3H, C2-$COCH_3$), 2.57 (s, 3H, C3^1-$COCH_3$), 3.89 (s, 3H, C7^1-OCH_3), 6.94 (s, 3H, C5-H), 7.01(s, 1H, C6^1-H), 7.97 (s, 1H, HCOO); ^{13}C NMR (125 MHz, $CDCl_3$) δ = 10.01 (C3^1), 20.05 (C4-$COCH_3$), 20.37 (C2-$COCH_3$), 20.46 (C3^1-$COCH_3$), 20.67 (C8-$COCH_3$), 20.80 (C8-$COCH_3$), 21.80 (C8-$COCH_3$), 21.31 (C9^1-$COCH_3$), 52.17 (C7^1-OCH_3), 83.45 (C8), 119.61 (C4^1), 121.36 (C2^1), 123.71 (C6^1), 124.28 (C3), 124.48 (C5), 136.24 (C5^1), 141.88 (C6), 148.26 (C3^1) 148.9 (C2), 150.23 (C4), 150.99 (C1^1), 162.81(C8-C=O), 166.42 (C4-C=O), 168.27 (C2-C=O), 168.32 (C3^1-C=O), 168.66 (C7), 168.93 (C7^1). HRMS (ESI): *m/z* calcd. for $C_{29}H_{30}NaO_{14}$ $[M+Na]^+$, 625.1528, found 625.1549.

Preparation of 3-methoxy-4-(methoxycarbonyl)-2,5-dimethylphenyl 3-formyl-2, 4-dimethoxy-6-methylbenzoate (1b)

To atranorin **1** (0.1 g , 0.26 mmol) in dry acetone (5 mL), was added methyl iodide (0.049 ml, 0.80 mmol) and K_2CO_3 (0.1 g, 0.80 mmol) and stirred the reaction mixture for 12 h. In the process of purification, acetone was evaporated under vacuum conditions and the reaction mixture was diluted with water and extracted with ethyl acetate (3x10 mL). The combined organic layer was dried over anhydrous sodium sulphate followed by concentration under reduced pressure and chromatography over silica gel column afforded compound **1b** as colourless crystals (0.08g, 72 %), m.p. 109-112 ^{0}C. IR (KBr): 3421 (C-H), 2940 (C-H), 2864 (C-H), 1740 (C=O) cm$^{-1.}$ ^{1}H NMR, (300 MHz, $CDCl_3$) δ = 2.1(s, 3H, C8^1- CH_3), 2.3 (s, 3H, C9-CH_3), 2.5 (s, 3H, C9^1-CH_3), 3.8 (s, 3H, C4-OCH_3), 3.9 (s, 3H, C2-OCH_3), 3.9 (s, 3H, , C5^1-OCH_3), 6.6 (s, 1H, C5-H), 6.8 (s, 1H, C6^1-H), 10.4 (s, 1H, C8-CHO); ^{13}C NMR, (125 MHz, $CDCl_3$) δ = 9.58 (C8^1) , 19.13 (C9^1), 20.91 (C9), 52.20 (C7^1-OCH_3), 56.26 (C4-OCH_3), 61.51 (C2-OCH_3), 64.51 (C3^1-OCH3), 109.14 (C3), 116.35 (C1,), 119.10 (C5), 121.36 (C4^1), 122.12 (C6^1), 126.62 (C2^1), 134.62 (C5^1), 145.20 (C6), 150.61(C1^1), 156.70 (C3^1), 160.50 (C2), 163.31 (C4), 165.12 (C7), 168.24 (C7^1), 187.9 (C8). HRMS (ESI): *m/z* calcd. for $C_{22}H_{25}O_8$ $[M+H]^+$, 417.1544, found 417.1562.

Preparation of 3-methoxy-4-(methoxycarbonyl)-2,5-dimethylphenyl 3-(hydroxymethyl)-2,4-dimethoxy-6-methylbenzoate (1c)

Compound **1b** (0.05 g, 0.12 mmol) was reduced to its corresponding alcohol by using sodium borohydride (0.004 g, 0.12 mmol) in methanol at 0 ^{0}C, the reaction mixture was stirred for 1h. Methanol was removed under reduced pressure after the reaction is over. The reaction mixture was diluted with water and extracted with ethyl acetate (3x10 mL). The organic layer was dried over anhydrous sodium sulphate, concentrated under reduced pressure and chromatographed over silica gel column to afford compound **1c** as colorless crystals **(**0.042 g, 83 %), m.p: 104-107 ^{0}C. IR (KBr): 3422 (O-H), 2923 (C-H) cm^{-1}. ^{1}H NMR (500 MHz, $CDCl_3$) δ = 2.19 (s, 3H, C8^1-CH_3), 2.30 (s, 3H, C9-CH_3), 2.49 (s, 3H, C9^1-CH_3), 3.81 (s, 3H, C4-OCH_3), 3.91 (s, 3H, C2-OCH_3), 3.93 (s, 3H, C7^1- OCH_3), 3.94 (s, 3H, C3^1-OCH_3), 4.75 (s, 2H, C8- CH_2), 6.60 (s, 1H, C5-H), 6.81 (s,

3H, C6[1]-H); ^{13}C NMR (125 MHz, $CDCl_3$) δ = 9.34 (C8[1]), 18.92 (C9[1]), 20.16 (C9), 54.88 (C7[1]-OCH_3), 55.58 (C4-OCH_3), 61.74 (C2-OCH_3), 63.94 (C3[1]-OCH_3), 108.33 (C5), 118.97 (C6[1]), 120.03 (C4[1]), 121.89 (C2[1]), 126.22 (C1), 134.31 (C6), 138.18 (C5[1]), 150.55 (C1[1]), 156.45 (C3[1]), 157.14 (C4), 159.85 (C2), 165.66 (C7), 168.08 (C7[1]); HRMS (ESI): *m/z* calcd. for C22H26NaO8 $[M+Na]^+$, 441.152, found 441.1554.

Preparation of 3-(allyloxy)-4-(methoxycarbonyl)-2,5-dimethylphenyl 2,4-bis(allyloxy)-3-formyl-6-methylbenzoate (1d)

To atranorin **1** (0.05 g, 0.13 mmol) in analytical grade acetone solvent (5 mL), was added K_2CO_3 (0.05 g, 0.40 mmol) and allyl bromide (0.03 ml, 0.40 mmol) and stirred the reaction mixture at room temperature for 12h. After completion of the reaction as indicated by TLC, the reaction mixture was extracted with ethyl acetate (3x10 mL) and the combined organic layer was washed with water. The resultant organic layer was dried over anhydrous sodium sulphate. The dried organic layer was concentrated under reduced vapor pressure and chromatographed over silica gel column to afford compound **1d** as colorless crystals **(**0.055 g, 83 %), m.p. 82-86 ^{0}C; IR (KBr): 2923 (C-H), .2853 (C-H), 1646 (C=C), 1597 (C=C) cm^{-1}. ^{1}H NMR (500 MHz, $CDCl_3$) δ = 2.16 (s, 3H, , C8[1]), 2.29 (s, 3H, S,), 2.50 (s, 3H, C9[1]), 3.90 (s, 3H, C7[1]-OCH_3), 4.42(dt, 2H, J= 5.49, 1.39, C4-OCH_2), 4.59 (dt, 2H, J= 5.95, 1.2, C2-OCH_2), 4.69 (dt, 2H, J= 5.03,1.5, C3[1]-OCH_2), 5.24-5.28 (m, 2H, C4-allyl protons), 5.35-5.41 (m, 3H, C2- allyl protons), 5.47-5.52 (m, 1H, C4-allyl proton), 6.10-6.17 (m, 3H, C2- allyl protons); ^{13}C NMR, (125 MHz, $CDCl_3$) δ = 10.3 (C8[1]), 19.5 (C9[1]), 21.1 (C9), 70.0 (C4-O-C), 75.6 (C2-O-C), 78.3 (C3[1]-O-C), 110.5 (C4[1]), 117.7 (C2[1]), 118.7 (C4-allyl carbon), 119.0 (C2- allyl carbon), 119.6 (C3[1]- allyl carbon), 132.0 (C4- allyl carbon), 133.3 (C2- allyl carbon), 133.6 (C3[1]- allyl carbon), 134.8 (C5[1]), 145.0 (C6), 150.8 (C1[1]), 155.8 (C2), 159.1 (C4), 162.5 (C3[1]), 165.5 (C7), 168.5 (C7[1]), 188.2 (C8). HRMS (ESI): *m/z* calcd. for C28H30O8Na $[M+Na]^+$ 517.1838, found 517.1830.

Preparation of 3-hydroxy-4-(methoxycarbonyl)-2,5-dimethylphenyl 2,4-dihydroxy-6-methyl-3-((2-phenylhydrazono)methyl) benzoate (1e)

Phenyl hydrazine (0.014 g, 0.013 mmol) and sodium acetate (0.013 g, 0.16 mmol) were added slowly to atranorin (0.05g, 0.13mmol) in DCM (5 mL). The reaction mixture was diluted with water and extracted with dichloromethane (3x10 mL). The Organic layer was dried over anhydrous sodium sulphate and evaporated under reduced pressure. The resultant residue was purified over silica gel column to afford compound **1e** as colorless crystals (0.051 g, 82 %), m.p. 170-172 ^{0}C. IR (KBr): 3419 (C=N), 3338 (C-N), 2922 sodium sulphate and evaporated under reduced pressure. The resultant residue was purified over silica gel column to afford compound **1e** as colorless crystals (0.051 g, 82 %), m.p. 170-172 ^{0}C. IR (KBr): 3419 (C=N), 3338 (C-N), 2922 (C-H), 2854 (C-H), 1654 (C=C, aromatic), 1565 (C=C, aromatic), 1491 (C=C, aromatic) cm^{-1}. ^{1}H NMR (500 MHz, $CDCl_3$) δ = 2.10 (s, 3H, C2[1]) , 2.54 (s,3H, C6-CH_3), 2.66 (s, 3H, C5[1]-CH_3), 6.47 (s, 1H, C5-H), 6.52 (s, 1H, C6[1]-H), 6.91-6.96 (m, 3H, aromatic), 7.29-7.32 (m, 2H, aromatic), 8.37 (s, 1H, C8-H); ^{13}C NMR, (125 MHz, $CDCl_3$) δ = 9.34 (C8[1]), 24.0 (C9[1]), 102.78 (C1), 105.34 (C2[1]), 110.03 (C3), 112.53 (C5), 112.74 (NH-Ar), 116.21 (C6[1]), 116.88 (C4[1]), 120.84 (NH-Ar), 129.52 (NH-Ar), 136.84 (NH-Ar), 139.70 (NH-Ar), 143.38 (NH-Ar), 144.31 (C8), 152.32 (C1[1]),162.82(C2), 163.69 (C4), 170.16 (C7), 172.22 (C7[1]); HRMS (ESI): *m/z* calcd. for $C_{25}H_{25}N_2O_7$ $[M+H]^+$ 465.1662, found 465.1653.

Cytotoxicity Assay

The above isolated and synthesized compounds were screened for anticancer activity against five different cell lines including A549 (Lung Cancer), DU145 (Prostate Cancer), MCF-7(Breast Cancer), SiHa (Cervical Cancer), U87MG (Glioblastoma) cell lines. The cells were plated at a density of 5×10^3 cells per well in a 96 well plate supplemented with 10 % FBS and after 24 h of incubation at 37 ºC and 5 % CO_2, they were treated with respective concentration of the compounds dissolved in the culture media with vehicle controls and known standards for 48 h.

Cell viability was determined by adding 100 µL of 3-(4,5-dimethyl-2-thiazolyl)-2,5-diphenyl-2H-tetrazolium bromide, MTT reagent (0.5 mg mL^{-1}) dissolved in serum free media added to each well and incubated for 4 h. Then the media was aspirated and the formazan crystals were dissolved in 200 µL of DMSO and absorbance was taken at 570 nm in multimode plate reader (BioTek Instruments, Synergy 4, and Winooski, VT)). The percent cell inhibition in treated cells was calculated by normalizing the cells with 0 % inhibition with control group. Then the compounds which exhibited the percentage inhibition of more than 50 % at a concentration of 150 µM in the initial screening were further screened for dose response curve with series of 7 concentrations starting from initial 150 µM. MTT was performed as described previously and IC_{50} values were determined from DRC plot by linear regression method. Graph was plot between different concentration and percentage Inhibition. All the values were expressed as Mean ± SEM in three different experiments in which each treatment was performed in triplicates.

Results and discussion

Chemistry

P. melanothrix was collected from the lower temperate region of Tirumala Hills (13.65000 N 79.420 E) located in Andhra Pradesh, India. This region is having more saxicolous kind of *P. melanothrix*. Before carrying out extraction, it was washed with fresh water to remove foreign matter. The lichen material was shade dried, powdered in a pulveriser and extracted with acetone at room temperature overnight. The extract was concentrated to one quarter volume and left overnight at room temperature. Filtration of the extract yielded a brown coloured solid (2.2 %) and filtrate (2 %). The solid on recrystallisation from hexane-ethanol solvent system, yielded a single and pure compound **1** (Scheme 1). The residue obtained on evaporation of the filtrate, was subjected to silica gel flash column chromatography with n-hexane and ethyl acetate solvents as eluents to yield two pure compounds **2** and **3** (Scheme 1).

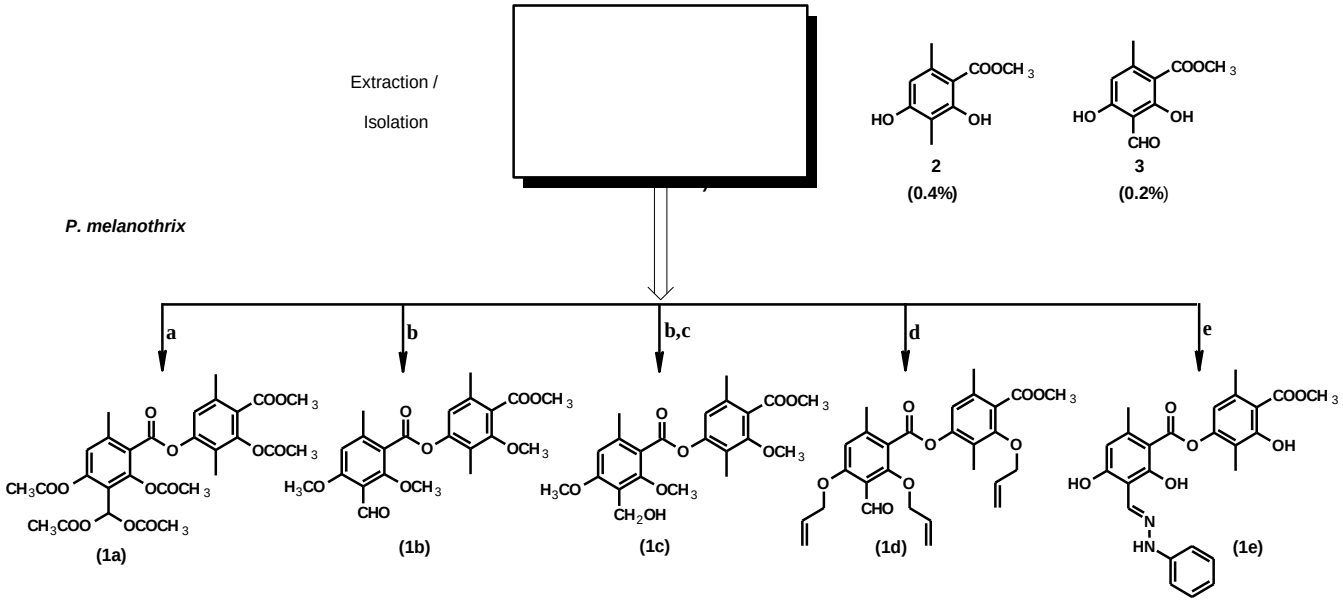

Scheme 1. Isolation of natural products from *P. melanothrix* and synthesized atranorin derivatives.

Table 1. Biological profile of atranorin derivatives over cancer cells.

S.No.	IC_{50} (µM)					
	A549	**DU145**	**HT-29**	**MCF-7**	**SiHa**	**U87MG**
1	96.70±0.92	52.03±5.72	45.16±4.66	71.9±4.66	86.41±3.48	>100
1a	29.25±4.40	15.19±2.90	19.16±0.72	30.35±1.54	22.07±2.55	16.96±1.83
1b	99.91±6.00	26.34±2.21	24.74±3.73	50.79±2.40	54.49±3.05	>100
1c	>100	42.7±2.42	63.04±5.97	67.09±2.06	>100	>100
1d	74.66±6.25	22.12±2.37	48.3±6.99	96.91±5.15	>100	>100
1e	58.96±1.70	27.52±5.36	>100	55.93±5.05	>100	>100
2	87.28±7.34	35.93±3.15	>100	84.53±4.91	83.93±6.18	80.44±6.88
3	>100	>100	>100	>100	>100	>100
Docetaxel	0.04	0.64	0.019	0.034	0.247	0.106

The structures of the isolated compounds were elucidated by their spectral data (^{1}H & ^{13}C NMR, IR and HRMS). Compound **1** was obtained as colourless crystals and its molecular formula was deduced as $C_{19}H_{18}O_8$ from its HRMS, which showed the molecular ion peak at m/z 373.0917 $[M-H]^+$.

The IR spectrum of the compound showed the absorption bands at 3450 and 1730 cm^{-1} corresponding to hydroxyl and ester functionalities respectively. ^{1}H and ^{13}C NMR spectra of the compound revealed its identity as atranorin. Its structure was further confirmed by comparing its physical and spectral data with reported values.[13] Atranorin was earlier isolated from few lichen species belonging to *Cladina*, *Evernia* and *Pseudoevernia* genera.[14-16] However, its present isolation assumes significance as it is now isolated in high yield (2 %). Compound **2** was obtained as colourless crystals (0.4 %). Its molecular formula was deduced as $C_{10}H_{12}O_4$ by ESI-HRMS, which showed the protonated molecular ion at m/z 197.0810 $[M+H]^+$. Its IR spectrum showed the absorption bands at 3404 and 1627 cm^{-1} corresponding to hydroxyl and ester functionalities respectively. Its ^{1}H and ^{13}C NMR spectra identifies its structure as methyl 2, 4-dihydroxy-3, 6-dimethylbenzoate. Its identity was further confirmed by comparing its spectral data with the reported values.[17] Compound **3** was obtained as colourless crystals (0.2 %) and its molecular formula was deduced as $C_{10}H_{10}O_5$ from ESI-HRMS, which showed the molecular ion peak at *m/z* 211.0608 $[M+H]^+$. Its IR spectrum showed absorption bands for hydroxyl (3404 cm^{-1}) and aldehydic carbonyl (1644 cm^{-1}) functionalities. Its ^{1}H and ^{13}C NMR spectra reveals its identity as methyl 3-formyl-2,4-dihydroxy-6-methylbenzoate.[18] Among the isolated metabolites, atranorin (**1**) was obtained in significant quantity (2%). It is to mention here that atranorin was reported to exhibit potent biological activities such as anticancer,[19] anti-inflammatory (Inhibition of LTB_4 biosynthesis).[20] Further atranorin was reported to be non toxic to normal cells and has an added advantage as a promising scaffold for making diverse analogues to identify potent bio-active lead molecules. Hence, compound **1** was fine tuned by chemical modification of its active functional groups (2 phenolic hydroxyls and 1 aldehydic group) and synthesised five diverse analogues as shown in scheme 1 (**1a**-**1e**). The structures of the synthesised analogues were confirmed by their spectral data (^{1}H and ^{13}C NMR, IR, HRMS). Treatment of **1** with acetic anhydride in presence of pyridine afforded compound **1a** in 93% yield. Its structure was confirmed by spectral data. The IR spectrum of compound **1a** showed sharp peaks at 1776 cm^{-1} and 1728

cm^{-1} corresponding to the carbonyl group in acetoxyl and ester functionalities. The ^1H NMR displayed peaks between δ 2.01 ~ 2.39, corresponding to the methyl protons of acetyl group. The ^{13}C NMR spectrum of compound **1a** showed peaks between δ 20.05-20.80 and δ 162.81- 168.66 corresponding to the methyl and carbonyl carbons of acetoxyl groups. The HRMS spectrum of compound **1a** showed the corresponding sodiated $[M+Na]^+$ molecular ion at *m/z* 625.1549 confirming its structure. Compound **1** when treated with alkyl halides (methyl iodide or allyl bromide) in presence of K_2CO_3 in acetone yielded the corresponding tri alkyl ethers (**1b** and **1d**) in good yield (72 & 83 %). The unsaturated ether (**1d**) showed the characteristic peaks in IR spectrum at 1597, 1458 and 1407 cm^{-1} confirming the presence of olefin groups. Its ^1H NMR spectrum showed the characteristic peaks between δ = 4.42-5.52 and δ = 6.10-6.17 corresponding to the methylene olefinic protons. The ^{13}C NMR spectrum while confirming these observations exhibited the carbon signal between δ 119.0-133.6. The HRMS spectrum of the compound confirmed its structure by exhibiting the sodiated molecular ion at *m/z* 517.1830 [M+Na]+ corresponding to $C_{28}H_{30}O_8Na$. Compound **1c** was obtained by the treatment of **1b** with $NaBH_4$ in presence of methanol in 83 % of yield. The IR spectrum of compound **1c** showed the characteristic absorption band at 3422 cm^{-1} corresponding hydroxyl group. The ^1H and ^{13}C NMR spectra of compound **1c** confirmed the absence of aldehydic group and presence of a hydroxy methylene group in the compound. The HRMS spectra of compound **1c** further confirmed its structure by exhibiting the sodiated molecular ion $[M+Na]^+$ at *m/z* 441.1554. The analogue **1e** was obtained, when compound **1** was treated with phenyl hydrazine in dichloromethane and sodium acetate to yield the product **1e** in 82 % yield. The structure of compound **1e** was identified by its spectral data, which exhibited absorption band at 1645 cm^{-1} corresponding to the imine functionality in IR spectrum and showed diagnostic signals at δ 8.37 and between δ = 7.29-7.32 in ^1H NMR spectrum corresponding to imine and aryl ring protons respectively. This further supported by the ^{13}C NMR spectrum, which showed characteristic signals δ = 143.38 corresponding to the imine carbons. The HRMS of compound **1e** showed $[M+H]^+$ molecular ion peak at *m/z* 465.1653 confirming its structure.

Cytotoxicity

The three isolated compounds (**1-3**) and five synthesized analogues **1a-1e** (Scheme-1), were screened for their cytotoxic potential against five human cancer cell lines such as A549 (lung cancer), DU145 (prostate cancer), MCF-7 (breast cancer), SiHa (cervical cancer), U87MG (glioblastoma) using docetaxel by employing MTT assay.[20] Analysis of data, presented in Table 1, revealed that the synthesised compounds showed enhanced activities than parent compound **1**. The cytotoxicity found to be increased when the three phenolic hydroxyls and aldehyde functionality were acylated as acetates (**1a**) against DU145 (IC_{50} = 15.19±2.90 μM), U87MG (IC_{50} = 16.96±1.83μM), HT-29 (IC_{50} = 19.16±0.72μM), SiHa (IC_{50} = 22.07±2.55 μM), A549 (IC_{50} = 29.25±4.40 μM) and MCF-7 (IC_{50} = 30.35±1.54 μM). When the methyl groups were introduced in compound **1** in the form of ethers (1b), cytotoxicity found enhanced against HT-29 (IC_{50} = 24.74±3.73μM) and DU145 ((IC_{50} = 26.34±2.21μM) cell lines. Interestingly, compound (**1d**) with allyl ether groups showed enhanced cytotoxic activity against the prostate cancer cell line DU145 ((IC_{50} = 27.52±5.36μM). Similarly, the phenyl hydrazone (**1e**) showed improved cytotoxicity against prostate cancer cell line DU145 ((IC_{50} = 22.12±2.37μM) than the parent compound **1**.

Conclusion

In conclusion, chemical screening of *P. melanothrix* resulted in the isolation three orcinol based metabolites (**1-3**) with the depside, atranorin (2 %) as the major metabolite. In view of its abundance and interesting skeletal features, compound (**1**) was subjected to chemical modification and synthesised five diverse analogues (**1a-1e**). Among the synthesised compounds, **1a** showed enhanced cytotoxicity against almost all the cancer cell lines screened with highest activity against the prostate cancer cell line with an IC_{50} of 15.19μM.

Acknowledgements

We are thankful to CSIR, New Delhi for the award of research fellowship to one of us (TSS). We are also thankful to Director, CSIR-IICT for keen interest and encouragement.

References

[1]Pierre, L. P., Anne-Cecile, L. L., Bandi S., Beatrice, L., Arnaud, B., Jerome, G., Denis, J., Isabelle, R., Solenn, F., Walter O, Suresh, B., Joel, B. , *J. Nat. Prod*., **2016**, *79*, 1005–1011.

[2]Imke, S., Thorsten, L, H., *Mol. Phylogenet. Evol*., **2004**, *33*, 43–55.

[3]Blanco, O., Crespol, A., Divakar, P, K., Elix, J, A., Lumbsch, H. T., *Mycologia*., **2005**, *97*, 150– 159.

[4] Neamati, N., Hong, H., Mazumder, A., Wang, S., Sunder, S., Nicklaus, M, C., Milne, G, W., Proksa, B., Pommier, Y., *J.Med.Chem*., **1997**, *40*, 942-951.

[5] Marion, M., Sophie, T., Elisabeth, S., Isabelle, R., Joel B., *J. Nat. Prod*., **2009,** *72*, 2177–2180.

[6] Buaruang, K., Mongkolsuk, P., Manoch, L., *J. Microsc. Soc. Thai.*, **2009**, *23*, 20-24.

[7]Bombuwala, K., Subramaniam, V., DeSilva, K, S., Karunaratne, V., Adikaram, N. K. B., Herat, H. M. T. B., *Cey. J. Sci. (Physical Sciences)*., **1999,** *6*, 8-12.

[8] Mitrovic, T., Stamenkovic, S., Cvetkovic, V., Nikolic, M., Tosic, S., Stojicic, D., *Biol. Nyssana*., **2011**, *2*, 1-6.

[9]Barreto, R. S. S., Junior, R. L. C. A., Filho, R.N.P., Quintans, J. S. S., Barreto, A, S., DeSantana, J. M., Filho, V. J. S., Santos, M. R. V., Bonjardim, L. R., Araujo A. A, S., Junior, L. J. Q., *Braz. J. Pharmacogn*., **2013,** *23*, 310-319.

[10]Prabhu, S, S., Sudha, S, S., *Int. J. Adv. Res. Biol.Sci*. **2015**, *2*, 177–181.

[11]Spielmann, A, A., Marcelli, M, P., *Hoehnea*. **2009**, *36*, 551–595.

[12]Awasthi, D. D., *A Compendium of the Macrolichens from India, Nepal and Sri Lanka*, Bishen Singh Mahendra Pal Singh, India, **2007**, p.344.

[13]Melo, M. G. D., Araújo, A. A. S., Rocha, C. P. L., Emyle, M. S. A., Almeida, R. D. S., Siqueira, B. L. R., Junior, L. J. Q., *Biol. Pharm. Bull.*, **2008**, *31*, 1977-1980 .

[14]Shukla, V., Joshi, G. P., Rawat, M. S. M., *Phytochem. Rev*., **2010**, 9, 303–314.

[15]Molina, M. D. C., Crespo, A., Blanco, O., Lumbsch, H. T., Hawksworth, D. L., *Lichenologist*, **2004**, *36*, 37–54.

[16]Kristmundsdottir, T., Jonsdottir, E., Ogmundsdottir, H. M., Ingolfsdottir, K., *Eur. J. Pharm. Sci.*, **2005**, *24*, 539–543.

[17] Elix, J. A., Norfolk, S., *Aust. J. Chem*., **1975**, *28*, 1113-24.

[18]Rojas, I. S., Hennsen, B. L., Mata, R., *J. Nat. Prod*., **2000**, *63*, 1396–1399.

[19]Zhou, R., Yang, Y., Park, S. Y., Nguyen, T. T., Seo, Y. W., Lee, K. H., Lee, J. H., Kim, K. K., Hur, J. S., Kim, H., *Sci. Rep*., **2017**, *7*, 8136.

[20]Sunil Kumar, K. C., Muller, K., *J. Nat. Prod*., **1999**, *62*, 817-820.

[21] Mosmann T., *J. Immunol. Methods*, **1983**, *65*, 55–63.

Received: 28.06.2018.
Accepted: 15.07.2018.

TOTAL PHENOLIC CONTENT, ANTIOXIDANT CAPACITY AND ANTIFUNGAL ACTIVITY OF EXTRACTS OF *CARTHAMUS TENUIS* AND *CEPHALARIA JOPPENSIS*

Abdullatif Azab[a,b]*

Keywords: *Carthamus tenuis*, *Cephalaria joppensis*, total phenolic content, antioxidant, antifungal, *Rhizopus stolonifer*.

Three different extracts (aqueous, ethanolic and ethyl acetate) of *Carthamus tenuis* and *Cephalaria jopprnsis* were prepared and tested for total phenolic content (TPC), antioxidant capacity and antifungal activity. Results for *C. tenuis* are meaningfully different of known findings. As for *C. joppensis*, the medicinal and biological properties of this plant were never published before. For each plant, TPC was highest in aqueous extracts and these had highest antioxidant capacity. Ethanolic extracts of both plants had strongest activity against *Rhizopus stolonifer* (black mold).

* Corresponding Authors
Fax: +972-(0)4-6356168, +972-(0)4-6205906
E-Mail: eastern.plants@gmail.com
[a] Triangle Research & Development Center, Box 2167, Kfar-Qari, Israel 30075
[b] Eastern Plants Company, Box 868, Arara, Israel 30026

Introduction

Plants and their products possess many health benefits and medicinal activities. One of the most important properties of plants in terms of healthy nutrition, is antioxidant capacity, where polyphenolic compounds are among the top of active antioxidants.[1] For this reason, many methods of determining antioxidant capacity were developed, and they are based on a wide variety of chemical reactions and analytical techniques.[2] Numerous studies have shown that there is a clear and strong correlation between total phenolic content of a plant and its antioxidant capacity.[3]

Plant extracts and essential oils are used for many other medicinal activities and medical treatments, which include anticancer, antidiabetic, antibacterial and antifungal. This last activity, antifungal, is drawing more and more research attention in the last few years due to it is immediate and practical applications for medical treatments and food storage and consumption, and its for this very reason, that many methods of testing antifungal activity were developed and published.[4] *Rhizopus stolonifer* (black mold), is one of the most common fungi and its dangers and damages can be found on almost all foods, especially bread and fruits.[5] Many studies were published with reports of new findings of possible treatments for *R. stolonifer*, and they include pure compounds from plant sources or origins (see reference 5, salicylic acid), synthetic compounds,[6] essential oils[7] and plants extracts.[8]

The genus *Carthamus* (Asteraceae) include around 47 species, where 15 of them can be found in the Middle East reagion and Western Asia.[9] Some of these species were studied for their medicinal properties, but strangely enough, *Carthamus tenuis* was very limitedly investigated, despite the fact that is very widespread in the western parts of the Middle East. Archeological studies of caves on Carmel mountain (Israel), indicate that humans used seeds of this plant, probably as food, around 48000-60000 years ago.[10] The same study found use of *Carthamus nitidus* in the Dead Sea area. In Lebanon, *C. tenuis* is used in traditional medicine to treat skin diseases (roots decoction) and hemorrhoids (roots extact).[11]

One of the earliest publications about medicinal activities of *C. tenuis* tested the TPC and antioxidant capacity of aqueous and methanolic extracts.[12] The same properties were reported in a later study, in addition to immunosuppresive activity of one of the compounds isolated from the plant.[13] All compounds that this group isolated were previously known. But the findings of these two studies are contradicting (see discussion). Methanolic extract of *C. tenuis* was also prepared by V. Kuete and his colleagues and tested for antibacterial (weak) and cytotoxic (inactive) activities.[14] They also indicate that the plant is traditionally used in Egypt to prevent abortion, to increase fertility and acts as aphrodisiac. A followup study that was conducted by authors of reference 13, showed that methnolic extract of *C. tenuis* and its fractions had immunosuppresive activity.[15] Ethanol/water (70%) extract was prepared and its TPC was found 41.8 mg g^{-1} dry extract (Folin-Ciocalteu reagent/ gallic acid method). The extract was *syriaca*),[21] and in Turkey to treat cancer (decoction of *C. specicosa*) and latex of *C. sparsipilosa* as antiseptic.[22]

Several studies were published so far and reported medicinal/biological activities of *Cephalaria* species, where some studies investigated some species collectively and some focused on a single species. Two novel triterpene-type glycosides were isolated and characterized from *C. scoparia* in a study that investigated four *Cephalaria* species.[23] These glycosides showed notable antioxidant capacity, as well as strong antibacterial activity. A year earlier, the same research group from Turkey reported another five novel triterpene-type glycosides, that have sufficient antimicrobial activity.[24] This group continued to isolate novel triterpene-type glycosides, and in 2012 they reported the isolation and characterization of two compounds from *C. gazipashensis*.[25] But the research of this group of the *Cephalaria* genus started more than two decades ago when they reported antimicrobial and antifungal activities of three new saponins

(triterpenic glycosides), that were isolated from the methanolic extract of *C. transsylvanica*.[26] From *C. paphlagonica* they succeeded in isolation of two novel saponis, and they reported their antioxidant and antimicrobial activities.[27] Strong antibacterial activity was reported by this group for another two novel saponins (hederagenin derivatives), that were isolated from *C. davisiana*.[28] The structures of these compounds are shown in Figure 1.

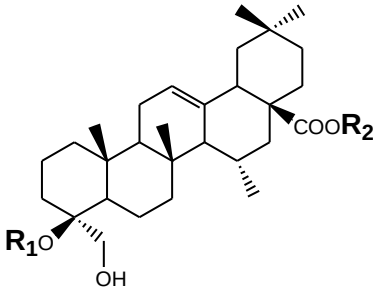

1 and 2 R_1 = Rha-β(1-4)Glc-β(1-3)Rha-β(1-2)Ara-(1-
1 R_2 = Glc-β(1-6)Glc-(1- **2 R_2 =** H

Figure 1. Saponins isolated from *C. davisiana*

When researchers of this group extracted *C. balansae* with n-butanol, they isolated and characterized four new saponins, that were tested and found active as immunomodulatory, hemolytic and cytotoxic.[29] The last publication of this group concerning saponins isolated from *Cephalaria*, reported the isolation of several compounds with branched saccharide side chains.[30] These compounds are reportedly having enhanced cytotoxic activity.

In addition to saponins, the fatty acids content of *Cephalaria* plants, was studied by several groups. Eight Turkish species were analyzed (n-hexane extract) by S. Kirmizigul and her colleages, that also tested the antioxidant activity of the extracts with several methods.[31] Long chain (>14 carbons) fatty acids are dominant in these oils. A follow up study was expanded by the same Turkish group, to investigate another ten species.[32] Method of extraction as well as antioxidant capacity and results in this study were very similar to those of previous cited (ref. 31), but the fatty acids composition of the *Cephalaria* species was clearly different having shorter carbon chains. Finally, in a comprehensive study, this group tested the acetone and ethanolic extracts of twenty one different species of *Cephalaria* against *Aedes aegypti*.[33] They found that ethanolic extract was more active, and they analyzed it by chromatographical methods, and found that eight compounds had measurable activity, where Luteolin-7-*O*-β-D-glycoside (Figure 2) was most active.

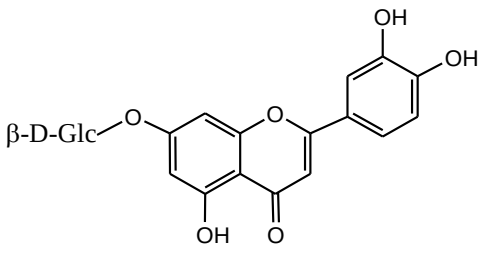

Figure 2. Structure of luteolin-7-*O*-β-D-glycoside

Essential oils of *Cephalaria* species were also studied. Ten of them were investigated by the group of S. Kirmizigul, where they analyzed the phytochemical composition of the oils.[34] They did not indicate any new compound. Recent study that extracted and analyzed the essential oil of *C. ambrosioides* also did not find new natural produtcs.[35] Another species that was extracted (90 % aqueous methanol) was *C. pastricensis*, afforded two known flavonoids, luteolin 7-*O*-glucoside and luteolin 7-*O*-arabino(1-6)glucoside, which had antioxidant activity.[36] Last study we cite here for biological activities, is comprehensive, despite the fact that it studied only *C. gigiantea* and did not report new compounds.[37]

Finally, despite being very widespread on the eastern parts of the Mediterranean basis, *Cephalaria jopponsis* was never studied before. Our wide search of published literature search could not find any study about the biological/medicinal activities of this species. The only publication we could find related to its nutrition benefits for lactating dairy cows.[38]

Experimental

Chemicals

All chemicals were purchased locally in at least analytical grade.

Plant Materials

Both studied plants (aerial parts) were harvested from the wild near our laboratory in Kfar-Qari (northern Israel). The green materials were washed with distilled water and air dried for 2 weeks. The dry matter of each plant was ground into a fine powder and stored at -12 °C in sealed containers.

Extraction

500 g of plant material were stirred in 1000 mL of solvent (water, ethanol, ethyl acetate) for 24 h at 50 °C. Suspensions were allowed to cool to room temperature and filtered (Munktell quant. Grade 393) to obtain clear solutions. These were evaporated to dryness with rotary evaporator: aqueous extracts at 60 °C, ethanol and ethyl acetate extracts at 50 °C. Extracts were stored at -12 °C.

Total Phenolic Content (TPC)

TPC was determined with the method described by Kumar and Jain (with no modifications).[39] The sample mixture that contains 3 mg of extract (or standard gallic acid solutions) dissolved in 1 mL of solvent, was obtained by dilution of 0.3 g of extract in 10 mL stock solution 10 folds. Then it was added to 10 mL volumetric flask containing 8 mL of dd H_2O. After that, 1mL of Folin-Ciocalteu's reagent was added to the mixture. After 3min, 1mL of 35% Na_2CO_3 solution was added with mixing to reach the reaction system to 10 mL. The reaction mixture was mixed thoroughly and allowed to stand for 90 min at 25 °C in the dark. Absorbance of all the sample solutions against a blank was measured at 725 nm.

Table 1. TPC and antioxidant capacity of *Carthamus tenuis* and *Cephalaria jopponsis* extracts.

Plant	Total phenolic content[a,b]			Antioxidant capacity[a,c]		
	Aqueous	Ethanolic	EtOAc[d]	Aqueous	Ethanolic	EtOAc
Carthamus tenuis	31.2	17.9	6.6	48.1	36.4	21.3
Cephalaria jopponsis	26.7	18.3	8.1	41.1	30.1	20.7

[a]Average values of three tests, [b]mg of gallic acid g^{-1} of dry extract, [c]mg of ascorbic acid g^{-1} of dry extract, [d]Ethyl acetate.

Table 2. Antifungal activity of *Carthamus tenuis* and *Cephalaria jopponsis* extracts against *Rhizopus stolonifer*.

Plant	Inhibition (%)[a]					
	Aqueous extract		Ethanolic extract		Ethyl acetate extract	
	10%	20%	10%	20%	10%	20%
Carthamus tenuis	28.4	36.5	38.2	42.9	25.1	30.0
Cephalaria jopponsis	31.5	33.2	41.4	51.6	30.9	33.3

[a]Extraction solvent in each experiment was used as control and resulted in 0 % inhibition.

Calibration curve was constructed with different concentrations of gallic acid (2–12 μg mL^{-1}) as the standard and dd H_2O was used as reagent blank. The results were expressed as mg gallic acid equivalents (GAE)/g dry extract.

Antioxidant capacity

Antioxidant capacity was determined by the phosphomolybdenum method described by Sharma and Singh (with slight modifications).[40] Tested aliquot of 0.1 mL (100 mg extract) was added to 1 mL of reagent solution (0.6 M sulfuric acid, 28 mM sodium phosphate, and 4 mM ammonium molybdate). The blank was 0.1 ml of ethanol. The tubes were capped and incubated in a boiling water bath at 95 °C for 90 min, then allowed to cool to room temperature. Absorbance of the aqueous solution of each was measured at 695 nm. The antioxidant capacity was expressed as an equivalent of ascorbic acid (mg of ascorbic acid g^{-1} of dried extract).

Antifungal activity

Agar plates were prepared according to Sanders, with slight modifications.[41] To prepare 20 petri agar plates, 400 mL of distilled water were heated to 60 °C and 9.2 g of potato agar was added to them. The suspention was stirred until clear solution was obtained, then it was poured into the plates and allowed to cool to room temperature. Agar plates were not stored but used immediately.

Antifungal assay was performed according to Salhi *et al*. with only changing the fungus and the plants.[42] *Rhizopus stolonifer* was grown on whole wheat bread and extracted with water. The center of each Petri dish was inoculated with 5 mm diameter disc of fungal mycelium, taken from pure culture (7 days old).Then, all inoculated dishes were incubated at 25 °C for 6 days and the radial mycelial growth was measured. The antifungal activity of each extract was calculated in terms of inhibition percentage of mycelia growth by using the following formula:

$$\% \text{ Inhibition} = [(dc - dt)/dc] \times 100$$

Where *dc* is the average increase in mycelia growth in control and *dt* is the average increase in mycelia growth in treated samples with extracts

In all experiments the control was the extraction solvent and we performed the antifungal tests using two concentrations for each extract: 10 % and 20 % (w/w).

Statistical analysis

All measurements were repeated three times and resutls introduced in the next section are average values.

Results and discussions

TPC (total phenolic content) and antioxidant capacity are shown in Table 1. Similarly, antifungal activity results are shown in Table 2.

Our TPC and antioxidant capacity tests of *C. tenuis* are notably different of previous studies. They are higher than the findings of Alali and his colleagues,[12] and with no agreement with the results of A. A. El-Hela and his colleages.[13] It is very important to notice that the reportings of these two groups are contradicting. While Alali *et al*. report that the aqueous extract has higher TPC than the methanolic (27.8 and 16.2 mg g^{-1} of dry extract, respectively), El-Hela *et al*. reported that methanolic extract had higher TPC than aqueous extract (65.8 and 18.2, respectively).

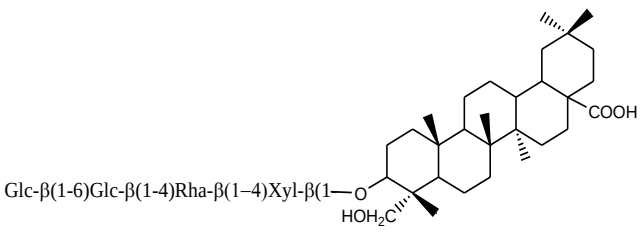

Figure 3. Structure of antifungal transsylvanoside A from *C. transsylvanica* (ref. 50).

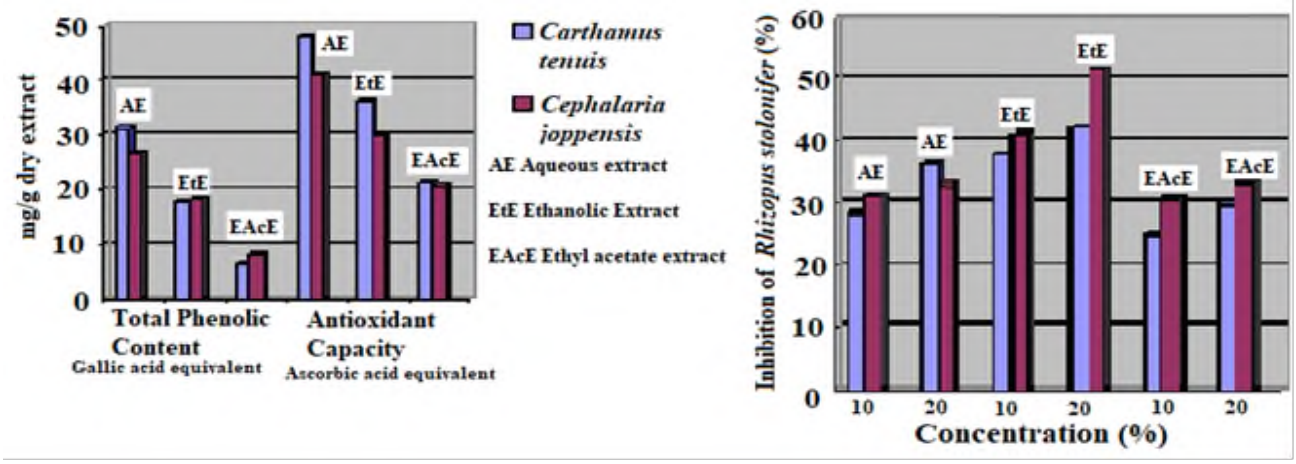

Figure 4. Total phenolic content, antioxidant capacity and inhibition of *Rhizopus stolonifer* of *Carthamus tenuis* and *Cephalaria joppensis*

Accordingly, their antioxidant tests resulted in contradicting findings, whereas Alali *et al*. measured 162.9 μmol g^{-1} of dry aqueous extract and 61.8 μmol g^{-1} for methanolic extract, El-Hela *et al*. reported 163.9 μmol g^{-1} for methanolic extract and 29.8 μmol g^{-1} for aqueous extract. The contradiction between these reports is even stranger based on the fact that both groups used exactly same methods to determine TPC (Folin-Ciocalteu reagent and gallic acid) and antioxidant capacity (ABTS and Trolox) of the extracts. Our findings are more consistent with those of Alali *et al*. in terms of that the aqueous extract had highest TPC and antioxidant capacity, even though we did not prepare methanolic extract but ethanolic.

The follow up study of the Egyptian research group (reference 13) that investigated the immunosuppressive activity of the matholic extract of *C. tenuis*,[15] discovered that this activity is due to the presence of choline in the extract. Despite the fact that this group did not isolate new natural products, and the immunosuppressive of plant derived choline is well known,[43] it is important to take this activity into account and possibly utilize it for future medicinal uses. Despite the fact that authors of reference 17 underestimated the global total number of *Carthamus* (25 instead of 37), and they concluded that this genus is not suitable as oil source, they actually contradict archeological evidences that this genus was used for oil production in the near east.[44] The use of this oil remains unclear.

The number of novel saponins that were isolated and characterized by the group of S. Kirmizigul from Turkey is outstanding (references 23-30). These compounds were found active in many medicinal/biological tests, especially antibacterial and cytotoxic activities. Based on the fact that saponins are known for their high cytotoxic effect,[45] and that they can be important prodrugs,[46] we find these dicoveries of very high impotance for drug development.

Comparison of our TPC and antioxidant capacity of the extracts of *C. tenuis* with those of Alali and his colleagues (ref. 13) reveal the fact that our results are slightly higher. As far as we can explain this, the difference might emerge from two reasons: our plant collection area is wetter than the harvest area of F. Alali in Jordan, and, seasonal variation. Our harvest was done in late March, while authors of reference 13 do not indicate their harvest time. Our plant materials were collected in the time when TPC is highest according to many published studies.[47]

Our antifungal activity findings are relatively high. All extracts had antifungal activities, when ethanolic extracts were most active, and that of *C. joppensis* is the highest. Even compared with reportedly very active extracts of plants with well known antifungal activity,[48,49] our findings are easily comparable. But also if we compare our results with the findings of S. Kirmizigul and her colleages (ref. 26), that tested the antifungal activity of three pure triterpenoid glycosides isolated from *C. transsylvanica*, our results are higher. These compounds have saponin typical structure with carboxylic acid residue. The structure of one of these compounds is shown in Figure 3.[50] To summarize our results, we present them in Figure 4.

Suggestions for further research

Both the plants, *Carthamus tenuis* and *Cephalaria joppensis* were very limitedly studied or not at all in terms of medicinal activities. Research of these plants should be widely expanded. The very limited studies so far focused on total phenolic content (with contradictions) and antioxidant capacity. Other properties such as antibaterial, antidiabetic, anticancer … etc. should be investigated. The antifungal activity of both plants is remarkable. This property should be studied in depth. The knowledge of the chemical compositions of both plants is very limited or does not exist. Both plants should be analyzed for active known, but especially for novel natural products.

References

[1]Yashin, A., Yashin, Y., Xia, X., Nemzer, B., *Antioxidants*, **2017**, *6*, 18 pages. DOI: 10.3390/antiox6030070

[2]Krishnaiah, D., Sarbatly, R., Nithyanandam, R., *Food Bioprod. Process.*, **2011**, *89*, 217-233. DOI: 10.1016/j.fbp.2010.04.008

[3]Piluzza, G., Bullitta, S., *Pharm. Biol*., **2011**, *49*, 240–247.DOI: 10.3109/13880209.2010.501083

[4]Balouiri, M., Sadiki, M., Ibnsouda, S. K., *J. Pharm. Anal*., **2016**, *6*, 71-79. http://dx.doi.org/10.1016/j.jpha.2015.11.005

[5]Panahirad, S., Zaare-Nahandi, F., Safafalizadeh, R., Alizadeh-Salteh, S., *J. Food Saf*., **2012**, *32*, 502-507. https://doi.org/10.1111/jfs.12013

[6]Sitalu, K., Babu, B. H., Latha, N. L., Rao, A. L., *Pak. J. Biol. Sci*., **2017**, *20*, 82-91. DOI: 10.3923/pjbs.2017.82.91

[7]Mohammadi, S., Aroiee, H., Aminifard, M. H., Tehranifar, A., Jahanbakhsh, V., *Arch. Phytopathol. Plant Protect*., **2014**, *47*, 1603-1610. https://doi.org/10.1080/03235408.2013.853456

[8]Maswada, H. F., Abdallah, S. A., *Pak. J. Biol. Sci*., **2013**, *16*, 1698-1705. DOI: 10.3923/pjbs.2013.1698.1705

[9]Vilatersana, R., Garnatje, T., Susanna, A., Garcia-Jacas, N., *Bot. J. Linean. Soc*., **2005**, *147*, 375-383. https://doi.org/10.1111/j.1095-8339.2005.00375.x

[10]Ronel, M., Lev-Yadun, S., *J. Arid Environ*., **2009**, *73*, 754-761. DOI: 10.1016/j.jaridenv.2009.02.009

[11]Baydoun, S., Chalak, L., Dalleh, H., Arnold, N., *J. Ethnopharmacol*., **2015**, *173*, 139-156. http://dx.doi.org/10.1016/j.jep.2015.06.052

[12]Alali, F. Q., Tawaha, K., El-Elimat, T., Syouf, M., El-Fayad, M., Abulaila, K., Nielsen, S. J., William D. Wheaton, W. D., Falkinham, J. O., Oberlies, N. H., *Nat. Prod. Res*., **2007**, *21*, 1121-1131. DOI: 10.1080/14786410701590285

[13]El-Hela, A. A., Ibrahim, T. A., Abdel-Hady, N., Al-Massarani, S., Abd-Allah, G.., *Planta Med*., **2013**, *79*, PN46.DOI: 10.1055/s-0033-1352389

[14]Kuete, V., Wiench, B., Hegazy, M. E., Mohamed, T. A., Fankam, A. G., Shahat, A. A., Efferth, T., *Planta Med.*, **2012**, *78*, 193-199.DOI: 10.1055/s-0031-1280319

[15]Ibrahim, T., El-Hela, A. A., Al-Massarani, S. Abo-Elfetoh, N. M.M Abdallah, G. M., *Indian J. Nat. Sci*., **2017**, *7*, 12130-12137. http://tnsroindia.org.in/JOURNAL/issue41/Front%20Page%20Issue%2041%20pdf.pdf

[16]Jamous, R. M., Ali-Shtayeh, M. S., Abu-Zaitoun, S. Y., Markovics, A., Azaizeh, H., *BMC Vet. Res.*, **2017**, *13*, 11 pages. DOI 10.1186/s12917-017-1237-7

[17]Arslan, Y., Arikahya Hacioglu, B., *Turk. J. Agric. For*., **2018**, *42*, 45-54. DOI: 10.3906/tar-1708-68

[18]Gokturk, R. S., Sumbul, H., *Turk. J. Bot*., **2014**, *38*, 927-968.DOI:10.3906/bot-1310-6

[19]Kislev, M. E., *Isr. J. Plant. Sci*., **2015**, *62*, 86-97. https://doi.org/10.1080/07929978.2015.1014261

[20]Hutchings, A., *Afr. Biodivers. Conser*., **1989**, *19*, 111-123. https://doi.org/10.4102/abc.v19i1.947

[21]Jarald, E., Joshi, S. B., Jain, D. C., *Iran. J. Pharmacol. Therap*., **2008**, *7*, 97-106. https://pdfs.semanticscholar.org/0df1/a47d25e9dd6a87d4d777c002238f4b463f78.pdf

[22]Altundag, E., Ozturk, M., *Procedia Soc. Behav. Sci*., **2011**, *19*, 756–777. DOI: 10.1016/j.sbspro.2011.05.195

[23]Sarikahya, N. B., Pekmez, M., Arda, N., Kayce, P., Yava, U. K., Kirmizigul, S., *Phytochem. Lett*., **2011**, *4*, 415-420. https://doi.org/10.1016/j.phytol.2011.05.006

[24]Sarikaya, N. B., Kirmizigul, S., *J. Nat. Prod*., **2010**, *73*, 825-830. DOI**:** 10.1021/np900724u

[25]Sarikaya, N. B., Kirmizigul, S.,*Turk. J. Chem*., **2012**, *36*, 323-334. DOI:10.3906/kim-1105-32

[26]Kirmizigul, S., Anil, H., Ucar, F., Akdemir, K., *Phytother. Res*., **1996**, *10*, 274-276. https://doi.org/10.1002/(SICI)1099-1573(199605)10:3<274::AID-PTR822>3.0.CO;2-V

[27]Capanlar, S., Kirmizigul, S., *Nat. Prod. Res*., **2010**, *24*, 1337-1346. https://doi.org/10.1080/14786410903381335

[28]Kayce, P., Sarikahya, N. B., Kirmizigul, S., *Phytochem. Lett*., **2014**, *10*, 324-329. https://doi.org/10.1016/j.phytol.2014.07.006

[29]Top, H., Sarikahya, N. B., Nalbantsoy, A., Kirmizigul, S., *Phytochem*., **2017**, *137*, 139-147. DOI: 10.1016/j.phytochem.2017.02.015

[30]Ozer, O., Sarikahya, N. B., Nalbantsoy. A., Kirmizigul, S., *Phytochem*., *152*, 29-35. DOI: 10.1016/j.phytochem.2018.04.015

[31]Kirmizigul, S., Boke, N., Sumbul, H., Gokturk, R. S., Arda, N., *Pure Appl. Chem.*, **2007**, *79*, 2297–2304.DOI: 10.1351/pac200779122297

[32]Sarikahya, N. B., Ucar, E. O., Kayce, P., Gokturk, R. S., Sumbul, H., Arda, N., Kirmizigul, S., *Rec. Nat. Prod*., **2015**, *9*, 116-123. http://www.acgpubs.org/RNP/2015/Volume9/Issue%201/10-RNP-1403-057.pdf

[33]Saikahya, N., Kayce, P., Tabanca, N., Estep, A. S., Becnel, J. J., Khan, I. A., Kirmizigul, S., *Nat. Prod. Commun*., **2015**, *10*, 1195-1198. https://www.ncbi.nlm.nih.gov/pubmed/26411009

[34]Sarikahya, N. B., Kayce, P., Halay, E., Gokturk, R. S., Sumbul, H., Kirmizigul, S., *Nat. Prod. Rese*., **2013**, *27*, 830–833. http://dx.doi.org/10.1080/14786419.2012.701216

[35]Vukicevic, D. R., Stevanovic, D. D., Gencic, M. S., Blagojevic, P. D., Radulovic, N. S., *Chem. Biodivers*., **2016**, *13*, 198-209. https://doi.org/10.1002/cbdv.201500050

[36]Godjevac, D., Vajs, V., Menkovic, N., Tesevic, V., Janackovic, P., Milosavljvic, S., *J. Serb. Chem. Soc*., **2004**, *69*, 883–886. https://www.shd.org.rs/JSCS/Vol69/No11/V69-No11-07.pdf

[37]Mbhele, N., Balogun, F. O., Kazeem, M. I., Ashafa, T., *Bangladesh J. Pharmacol*., **2015**, *10*, 214-221. DOI: 10.3329/bjp.v10i1.21716

[38]Miron, J., Weinberg, Z. G., Chen, Y., Miron, D., Raviv, Y., Bloch, A.,Yosef, E., Nikbahat, M., Zenou, A., Daklo, M., Nashef, K., Kushnir, U., *J. Dairy Sci*., **2012**, *95*, 4501-4509. https://doi.org/10.3168/jds.2011-5086

[39]Kumar, T., Jain, V., **2015**, *Scientifica*, Article ID 203679, 13 pages. http://dx.doi.org/10.1155/2015/203679

[40]Sharma, S. K., Singh, A. P., *J. Acupunct. Meridian Stud*., **2012**, 5, 112-118. DOI: 10.1016/j.jams.2012.03.002

[41]Sanders, E. R., *J. Vis. Exp*., **2012**, *63*, 3064-3081. DOI: 10.3791/3064

[42]Salhi, N., Saghir, S. A., Terzi, V., Brahmi, I., Ghedairi, N., Bissati, S., *BioMed Res. Int*., **2017**, Article ID 7526291, 6 pages. https://doi.org/10.1155/2017/7526291

[43]Saeidnia, S., Yassa, N., Rezaeipoor, R., Shafiee, A., Gohari, A. R., Kamalinejad, M., Goodarzy, S., *DARU*, **2009**, *17*, 37-41. http://applications.emro.who.int/imemrf/daru_2009_17_1_37.pdf

[44]Marinova, E., Riehl, S., *Veget. Hist. Archaeobot*., **2009**, *18*, 341–349.DOI: 10.1007/s00334-009-0212-z

[45]Podolak, I., Galanty, A., Sobolewska, D., *Phytochem. Rev*., **2010**, *9*, 425–474. DOI: 10.1007/s11101-010-9183-z

[46]Kumar, S. V., Saravanan, D., Kumar, B., Jayakumar, A.,*Asian Pac. J. Trop. Med*., **2014**, *7*, S54-S59. DOI: 10.1016/S1995-7645(14)60203-0

[47]Aoussar, N., Rhallabi, N., Mhand, R. A., Manzali, R., Bouksaim, M., Douira, A., Mellouki, F., *J. Saudi Soc. Agric. Sci*., **2018**, *In press*.

[48]Cortes-Rojas, D. F., Fernandes de Souza, C. R., Pereira Oliveira, W., *Asian Pac. J. Trop. Biomed*., **2014**, *4*, 90-96. DOI: 10.1016/S2221-1691(14)60215-X

[49]Rawal, P., Adhikari, R. S., *Adv. Appl. Sci. Res*., **2016**, *7*, 5-9. http://www.imedpub.com/articles/evaluation-of-antifungal-activity-of-zingiber-officinale-against-fusarium-oxysporum-fsp-lycopersici.pdf

[50]Kirmizigul, S., Anil, H., *Phytochem*., **1994**, *35*, 1075-1076. https://doi.org/10.1016/S0031-9422(00)90676-9

Received: 24.06.2018
Accepted: 18.07.2018.

LOWBUSH BLUEBERRY EXTRACT PROTECTS NORMAL HUMAN (*HOMO SAPIENS* L.) EPIDERMAL KERATINOCYTES FROM DAMAGE BY UV-B IRRADIATION

Seiji Yamasaki,[a]* Kenji Mizoguchi,[a] Naohiro Kodama[a] and Joji Iseki[a]

Keywords: flavonoids, normal human epidermal keratinocytes (NHEKs), polyphenols, proanthocyanidins, ultraviolet-B (UV-B).

To search for natural materials that protect human skin from damage caused by ultraviolet-B (UV-B) irradiation, we prepared water extracts of the following four dry berries: lowbush blueberry (LBB) (*Vaccinium angustifolium* L.), highbush blueberry (HBB) (*Vaccinium corymbosum* L.), cranberry (CB) (*Vaccinium macrocarpon* Ait.) and grape (*Vitis vinifera* L.). Normal human epidermal keratinocytes (NHEKs) were pretreated with each of the extracts and then subjected to transient UV-B irradiation (15.0 W m^{-2}) for 80 s. The results showed that pretreatment of NHEKs with LBB extract significantly attenuated UV-B-induced damage. The concentrations of proanthocyanidins, total flavonoids and total polyphenols in LBB extract were higher than those in the other three berry extracts. Therefore, these compounds might mediate the protection of NHEKs from UV-B-induced damage.

* Corresponding Author
Tel: +81-940-35-1386
Fax: +81-940-35-1386
E-Mail: yamasaki@fukuoka-edu.ac.jp
[a] Laboratory of Plant Physiology, Department of Science Education, Faculty of Education, University of Teacher Education Fukuoka, 1-1 Akamabunkyomachi, Munakata, Fukuoka 811-4192, Japan

INTRODUCTION

Chlorofluorocarbons cause continual depletion of the stratospheric ozone layer, which increases the amount of solar ultraviolet-B (UV-B; 280–320 nm) irradiation [UV-B (+)] passing through to the earth's surface.[1] UV-B (+) is harmful to living organisms. UV-B is the chief cause of skin reddening and sunburn, which damages the skin's more superficial epidermal layers. Direct absorption of UV-B by DNA induces mutations and leads to the development of carcinomas in cutaneous spinous cells.[2,3] Protection from UV-B (+) is crucial and is primarily achieved by the application of topical sunscreen treatments. Sunscreen contains UV-light absorbers and UV-light scattering agents. UV-light absorbers are usually phenolic compounds found in various oils whereas UV-light scattering agents are minerals such as titanium oxide or zinc oxide. However, these components sometimes cause allergies. Thus, it is essential to identify natural and safe compounds that do not cause allergies and that still protect skin from UV-B-mediated damage.

Red and purple berries, such as lowbush blueberry (LBB) (*Vaccinium angustifolium* L.), highbush blueberry (HBB) (*Vaccinium corymbosum* L.), cranberry (CB) (*Vaccinium macrocarpon* Ait.) and grape (*Vitis vinifera* L.) provide a readily available source of dietary phenolic compounds. Berries also contain many flavonoids.[4-6] A flavonoid fraction from CB extract inhibits the proliferation of human tumor cell lines.[7] Flavonoids from LBB and CB inhibit matrix metalloproteinases (MMPs), which degrade the extracellular cell matrix (ECM) during cancer metastasis[8,9] and in human prostate cancer cells.[10,11] Monomeric flavonoids that form oligomers and polymers are called proanthocyanidins or condensed tannins. Feeding proanthocyanidins to hairless mice reduced UV-B-induced skin carcinogenesis.[12] These combined results suggest that flavonoids and proanthocyanidins have beneficial dietary activities that promote health. However, the full effects of these berry compounds have not been elucidated. Plant flavonoids absorb UV irradiation;[13-15] therefore, berry extracts may absorb UV irradiation when added to a topical treatment. Our aim is to determine whether the addition of berry extracts to topical treatments could protect human skin from UV-B (+).

Although water extracts of living tissues can result in low recovery rates, they are simple to prepare, easy to use and provide a safe and biologically compatible matrix for bioactive compounds. We previously prepared water extracts from the following four dry berries: LBB, HBB, CB and grape (designated as the 'berry extract' in the present study). We showed that these four berry extracts efficiently absorb UV radiation, primarily UV-B.[16] Pretreatment of cucumber (*Cucumis sativus* L.) cotyledons with LBB, HBB and CB extracts attenuates UV-B-induced damage without causing any side effects.[16] We used high-performance liquid chromatography (HPLC) to analyze 51 polyphenols in the four berry extracts. The LBB extract contained primarily chlorogenic acid, caffeic acid and protocatechuic acid; the HBB extract contained primarily chlorogenic acid, caffeic acid and syringic acid; and the CB extract contained primarily protocatechic acid, myricetin and *p*-coumaric acid.[16] We proposed that these compounds contributed to the protection of cucumber plants against UV-B-induced damage.[16]

Similar to the UV-B protective effects of LBB, HBB and CB extracts in cucumber cotyledons, pretreatment of human skin with these extracts might also offer protection against UV-B-induced damage without any side effects. With the aim of developing a safe sunscreen for use in humans in the present study, we investigated whether the four berry extracts could protect human cells from UV-B-induced damage. First, we pretreated normal human (*Homo sapiens* L.) epidermal keratinocytes (NHEKs) with the four berry extracts, and then tested the effects of transient UV-B (+) on

NHEK survival. Second, we performed a spectrophotometric analysis to determine the concentrations of proanthocyanidins, total flavonoids and total polyphenols in the four berry extracts. Finally, we discuss the potential defense mechanisms elicited by the berry extracts in NHEKs in response to UV-B (+).

EXPERIMENTAL

Preparation of berry extracts

Commercially produced dry fruits of lowbush blueberry (LBB) (*Vaccinium angustifolium* L.), highbush blueberry (HBB) (*Vaccinium corymbosum* L.), cranberry (CB) (*Vaccinium macrocarpon* Ait.) and grape (*Vitis vinifera* L.) were purchased from the local supermarket Aeon (Aeon Co., Ltd., Chiba, Japan) in Fukuoka prefecture on September 27, 2012 and July 11, 2013, and were used before their expiry dates. For each of the four species, 5 g dried berries were ground using a mortar and pestle at room temperature, and then 15 ml of distilled water (pH 7.5) was added. Samples were placed at 4 °C, and the ground tissue was extracted into distilled water for 14 h. Then, samples were centrifuged at 6,000 rpm for 15 min at 4 °C. The crude supernatant was transferred to a new tube and centrifuged at 12,000 rpm for 10 min at 4 °C, and the clear supernatant was collected. This clear supernatant is designated as the berry extract. The Brix value of the four berry extracts was measured with a pocket sugar content meter (APAL-J; Atago Co., Ltd., Tokyo, Japan). The Brix values of LBB, HBB, CB and grape extracts were 19.4 %, 18.7 %, 22.4 % and 21.6 %, respectively. The extraction efficiencies [(collected extract weight / dried fruit weight) × Brix] of LBB, HBB, CB, and grape extracts were 45.7 %, 42.4 %, 43.25 and 56.1 %, respectively. The four berry extracts were stored at 4 °C during the experiment.

Analysis of berry extract dose-response effects on normal human epidermal keratinocytes (NHEKs) under normal light radiation [UV-B (–)]

The maximum amount of each berry extract that could be added to NHEKs (KK-4109; Kurabo Industries, Ltd., Osaka, Japan) without affecting cell viability under UV-B (–) was investigated by ACEL, Inc. (Kanagawa, Japan). NHEKs (2×10^4) were transferred to 100 µl keratinocyte basal medium (KBM, HuMedia-KG2; Kurabo Industries, Ltd., Osaka, Japan) in 32 wells of a 96-well culture plate (MS-8096F; Sumitomo Bakelite Co., Ltd., Tokyo, Japan), and cells were cultured in a dark humidified (5 % CO_2 atmosphere) incubator for 24 h at 37 °C. Cell growth and proliferation were confirmed. Then, 100 µl KBM per culture well was replaced with 100 µl KBM supplemented with 0 % (defined as a control in this study), 0.00064 %, 0.0032 %, 0.016 %, 0.08 %, 0.4 %, 2 % or 10 % (v/v) of each berry extract (n=4). One culture plate was used for each of the four berry extracts (a total of four culture plates were used for the experiment). The cells were cultured for 24 h at 37 °C before assessing cell viability using the Cell Count Reagent SF colorimetric assay (Nacalai Tesque, Inc., Kyoto, Japan). Briefly, 10 µl Cell Count Reagent SF was added to each well and incubated for 2 h at 37 °C. Then, cell viability was assessed colorimetrically by measuring the optical density at 450 nm (OD_{450}) using a microplate reader (Precision Microplate Reader; Molecular Devices Co., Tokyo, Japan). In this assay, the relative number of viable cells was expressed as the change in OD_{450} over a period of 1 h ($OD_{450}\ h^{-1}$).

Investigation of UV-B-induced lethality in NHEKs

The effect of transient UV-B irradiation [UV-B (+)] on NHEK survival was tested by ACEL, Inc. (Kanagawa, Japan). First, the time required for UV-B (+) to cause cell death in approximately 50 % of the NHEKs (LD_{50}) was determined as follows. The NHEKs (2×10^4) were transferred to 100 µl KBM per well in 6 wells in the middle of a 96-well culture plate, and cells were cultured in a dark humidified (5 % CO_2 atmosphere) incubator for 24 h at 37 °C. Cell growth and proliferation were confirmed. Then, the culture plates were placed 8 cm below a UV lamp (UVLMS-38; Funakoshi, Co., Ltd., Tokyo, Japan) with the following intensities of UV-A, UV-B and UV-C: 2.4, 15.0 and 1.7 W m^{-2}, respectively. UV-A, UV-B and UV-C intensities were measured with a digital UV intensity meter (UVX radiometer; Funakoshi, Co., Ltd.) equipped with a sensor for UV-A (Radiometer Sensor UVX-36, 365 nm; Funakoshi, Co., Ltd.), UV-B (Radiometer Sensor UVX-31, 310 nm; Funakoshi, Co., Ltd.) or UV-C (Radiometer Sensor UVX-25, 254 nm; Funakoshi, Co., Ltd.). Thus, the UV lamp primarily radiates UV-B. This UV lamp was adopted as a transient emitter of UV-B (+) for the present study. The culture plates were irradiated with the UV lamp for 0, 20, 100, 200 or 1,000 s, and then cultured again in a dark humidified (5 % CO_2 atmosphere) incubator for 24 h at 37 °C. Therefore, a total of five culture plates were needed for the study. Cell viability was evaluated after 24 h using the Cell Count Reagent SF colorimetric assay described in the previous section.

Effect of transient UV-B (+) on NHEKs that were pretreated with berry extracts

The effect of transient UV-B (+) on the survival of NHEKs that had been pretreated with berry extracts was investigated by ACEL, Inc. (Kanagawa, Japan). The experimental strategy is illustrated in Figure 1. For UV-B (–) of NHEKs, 2×10^4 cells were cultured in 100 µl KBM per well in 8 wells in the middle of a 96-well culture plate in a dark humidified (5 % CO_2 atmosphere) incubator for 24 h at 37 °C, and cell growth and proliferation were confirmed. Then, the culture medium in 4 wells was replaced with 100 µl KBM supplemented with berry extract at the maximum concentration that did not affect viability (as determined above), and cells were again cultured under the same conditions for 24 h (Figure 1). The remaining four wells were used as controls. Because there were four berry extracts, a total of four culture plates were needed. Cell viability was evaluated after 24 h using the Cell Count Reagent SF colorimetric assay as described above. For transient UV-B (+) of NHEKs, the same protocol as for UV-B (–) was used with the following modification: the time for replacement of KBM with KBM containing berry extracts was different. KBM medium was replaced at 6 h before, 10 min before and 10 min after transient UV-B (+) (Figure 1). Transient UV-B (+) of NHEKs was conducted 24 h after the start of the experiment (Figure 1). Briefly, 2×10^4 cells were

cultured in 100 µl KBM per well in 16 wells in the middle of a 96-well culture plate in a dark humidified (5 % CO_2 atmosphere) incubator at 37 °C (Figure 1). Then, the culture medium in 4 wells was replaced with 100 µl KBM supplemented with berry extract at the maximum concentration that did not affect viability (as determined above) at each of three different times [6 h before, 10 min before and 10 min after transient UV-B (+)], and cells were again cultured under the same conditions (Figure 1). Therefore, a total of 12 wells were needed. The remaining four wells were used as controls. Because there were four berry extracts, a total of four culture plates were required. Cell viability was evaluated using the Cell Count Reagent SF colorimetric assay as described above.

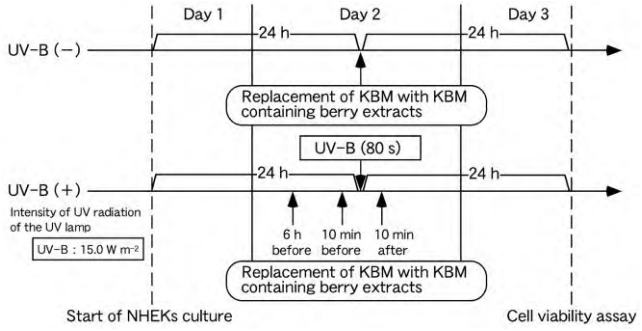

Figure 1. Illustration of the experimental protocol for assessing the effects of UV-B (–) and transient UV-B (+) on the viability of NHEKs that were treated with berry extracts. Standard KBM medium was removed and replaced with KBM containing berry extracts 6 h before, 10 min before and 10 min after transient UV-B (+) for 80 s.

Quantitative spectrophotometric analysis of proanthocyanidin concentrations in berry extracts

Proanthocyanidin concentrations in the berry extracts were analyzed according to a modified method which was reported previously.[17] Briefly, 1 ml berry extract was added to 4 ml of 0.07 % (w/v) iron (II) sulfate solution, and the reactions were incubated at 95 °C for 1 h. Then, 4 ml of 0.6 N hydrochloric acid:*n*-butanol (1:1, v/v) was added, and the sample absorbance was measured at 550 nm with ultraviolet and visible spectrophotometry (UVIDEC-4; Jasco Co., Tokyo, Japan). Delphinidin solution was used to prepare a standard calibration curve, and proanthocyanidin concentration was calculated with respect to the delphinidin calibration curve (µg $µl^{-1}$). The proanthocyanidin concentration in each berry extract was expressed as the average of three replicates.

Quantitative spectrophotometric analysis of the total flavonoid concentration in berry extracts

The total flavonoid concentration was analyzed according to the method which was reported previously.[18] Briefly, 1 ml berry extract was added to 4 ml distilled water and 0.3 ml of 5 % (w/v) sodium nitrite solution, and the reaction was allowed to stand for 5 min at room temperature. Then, 0.3 ml of 10 % (w/v) aluminum chloride solution was added and the tube was vortexed. After 1 min, 2 ml of 1.0 M sodium hydroxide solution was added, and the tube was vortexed again. Then, 2.4 ml of distilled water was added, and the sample absorbance was measured at 510 nm with ultraviolet and visible spectrophotometry (UVIDEC-4; Jasco Co., Tokyo, Japan). A calibration curve was prepared using (+)-catechin, and the total flavonoid concentration was calculated with respect to the (+)-catechin calibration curve (µg $µl^{-1}$). Total flavonoid concentration in each berry extract was expressed as the average of three replicates.

Quantitative spectrophotometric analysis of the total polyphenol concentration in berry extracts

The total polyphenol concentration was analyzed according to the method of Folin-Denis.[19] Briefly, 50 µl berry extract was added to 4 ml distilled water and 1 ml phenol reagent (a 5-fold dilution of Folin-Ciocalteu reagent with distilled water). After vortexing, 1 ml of 10 % (w/v) sodium carbonate solution was added and the tube was vortexed again. Then, the samples were allowed to stand in the dark for 1 h at room temperature. Sample absorbance was measured at 760 nm with ultraviolet and visible spectrophotometry (UVIDEC-4; Jasco Co., Tokyo, Japan). A calibration curve was prepared using (+)-catechin solution, and the total polyphenol concentration was calculated with respect to the (+)-catechin calibration curve (µg $µl^{-1}$). Total polyphenol concentration in each berry extract was expressed as the average of three replicates.

Statistical analysis

NHEK cell viability and the concentrations of proanthocyanidins, total flavonoids and total polyphenols in each berry extract were expressed as the mean ± standard error. Statistically significant differences were assessed by Dunnett's test (http://www.gen-info.osaka-u.ac.jp/MEPHAS/dunnett.html, March 6, 2017).

RESULTS

Pretreatment of NHEKs with berry extract protects against transient UV-B-induced cell death.

First, we determined the maximum concentrations of berry extracts (expressed as % of pure extract) that did not reduce NHEK cell viability more than 70 % of the value in control NHEKs under UV-B (–). The maximum concentrations of LBB, HBB, CB and grape extracts that did not affect NHEK cell viability were 2 %, 10 %, 10 % and 10 % (v/v), respectively. Because excessive dilution of the KBM media inhibits cell growth, the maximum percentage of extract that could be added to the cells was limited to 10 %. Second, the time for UV-B (+) that caused cell death in approximately 50 % of the NHEKs (LD_{50}) was determined; this time was 80 s (Figure 2).

We have confirmed that the cell viability of NHEKs pretreated with berry extracts (Figures 3Ab–Db) was more than 70 % of that of control NHEKs under UV-B (–) (Figures 3Aa–Da). The decrease in cell viability of NHEKs pretreated with berry extracts (Figures 3Ab–Db) suggests that these four berry extracts are toxic to cells.

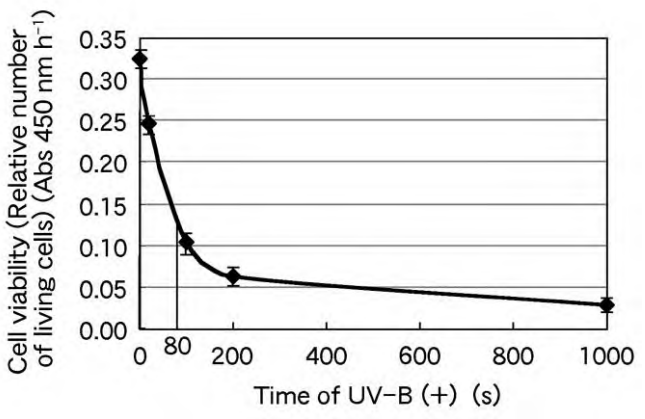

Figure 2. Effect of transient UV-B (+) at 15.0 W m^{-2} on NHEK viability. Values represent the average of six replicates (six wells in the culture plate).

The decline in cell viability of NHEKs treated with transient UV-B (+) (Figures 3Ac–Dc) was less than 50 % of that of NHEKs treated with UV-B (–) (Figures 3Aa–Da). Cell viability of NHEKs pretreated with 2 % LBB extract 6 h before transient UV-B (+) (Figure 3Ad) was higher than that of NHEKs treated with transient UV-B (+) ($P < 0.01$) (Figure 3Ac).

Cell viability of NHEKs pretreated with 2 % LBB extract 10 min before transient UV-B (+) (Figure 3Ae) was higher than that of NHEKs treated with transient UV-B (+) ($P < 0.01$) (Figure 3Ac). By contrast, cell viability of NHEKs treated with 2 % LBB extract 10 min after transient UV-B (+) (Figure 3Af) was not significantly different from that of NHEKs treated with transient UV-B (+) (Figure 3Ac).

Cell viability of NHEKs treated with 10 % HBB extract at 6 h and 10 min before (Figure 3Bd, Be) and 10 min after (Figure 3Bf) transient UV-B (+) was not higher than that of NHEKs treated only with transient UV-B (+) (Figure 3Bc). Similarly, cell viability of NHEKs treated with 10 % CB extract 6 h and 10 min before (Figure 3Cd, Ce) and 10 min after (Figure 3Cf) transient UV-B (+) was not more significant than that of NHEKs treated only with transient UV-B (+) (Figure 3Cc). Cell viability of NHEKs treated with 10 % grape extract 6 h and 10 min before (Figure 3Dd, De) and 10 min after (Figure 3Df) transient UV-B (+) was not higher than that of NHEKs treated only with transient UV-B (+) (Figure 3Dc). These results indicate that pretreatment of NHEKs with LBB extract protected the cells from UV-B-induced damage.

Spectrophotometric analysis of compounds in the berry extracts

To evaluate the presence of compounds that absorb UV radiation in the berry extracts, the concentrations of proanthocyanidins, total flavonoids and total polyphenols were analyzed. The proanthocyanidin concentrations in LBB, HBB, CB and grape extracts were 27.7 ± 0.44, 14.5 ± 0.63, 18.0 ± 1.1 and 6.1 ± 0.2 μg ml^{-1}, respectively (Figure 4A). Therefore, the proanthocyanidin concentration in LBB extract was 1.91-, 1.54- and 4.57-fold greater than those in HBB ($P < 0.01$), CB ($P < 0.01$) and grape ($P < 0.01$) extracts, respectively. The total flavonoid concentrations in LBB, HBB, CB and grape extracts were 150.8 ± 7.8, 83.2 ± 7.9, 92.4 ± 4.3 and 37.4 ± 3.5 μg ml^{-1}, respectively (Figure 4B). Therefore, the total flavonoid concentration in LBB extract was 1.81-, 1.63- and 4.03-fold greater than those in HBB ($P < 0.01$), CB ($P < 0.01$) and grape ($P < 0.01$) extracts, respectively.

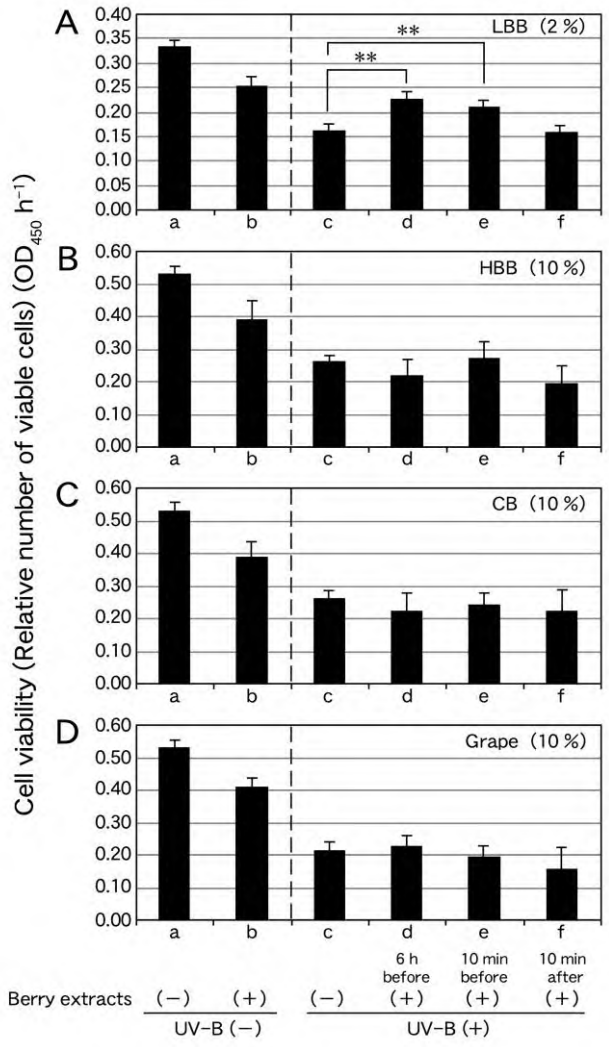

Figure 3. Effect of transient UV-B (+) (80 s) on the viability of NHEKs treated with extracts of 2 % LBB **(A)**, 10 % HBB **(B)**, 10 % CB **(C)** and 10 % grape **(D)** 6 h before, 10 min before and 10 min after UV-B (+). The vertical axis of the graph indicates relative numbers of viable cells expressed as OD_{450} h^{-1}. Values represent the average of four replicates (four wells in the culture plate). (**a**) NHEK viability under UV-B (–); (**b**) NHEK viability after treatment with 2 % LBB **(A)**, 10 % HBB **(B)**, 10 % CB **(C)** or 10 % Grape **(D)** extract under UV-B (–); (**c**) NHEK viability after transient UV-B (+); (**d**) NHEK viability after pretreatment with 2 % LBB (**A**), 10 % HBB (**B**), 10 % CB (**C**) or 10 % Grape (**D**) extract 6 h before transient UV-B (+); (**e**) NHEK viability after pretreatment with 2 % LBB (**A**), 10 % HBB (**B**), 10 % CB (**C**) or 10 % Grape (**D**) extract 10 min before transient UV-B (+); and (**f**) NHEK viability after treatment with 2 % LBB (**A**), 10 % HBB (**B**), 10 % CB (**C**) or 10 % Grape (**D**) extract 10 min after transient UV-B (+). Statistically significant differences were determined by Dunnett's test (**$P < 0.01$ vs. column c).

The total polyphenol concentrations in LBB, HBB, CB and grape extracts were 851.2 ± 5.8, 477.4 ± 6.9, 450.2 ± 12.6 and 460.3 ± 9.0 μg ml^{-1}, respectively (Figure 4C). Therefore, the total polyphenol concentration in LBB extract was 1.78-, 1.89- and 1.85-fold greater than those in HBB (*P*

< 0.01), CB (P < 0.01) and grape (P < 0.01) extracts, respectively. This concentration of total polyphenols is consistent with that of our previous study.[16] These combined results indicate that the concentrations of proanthocyanidins, total flavonoids and total polyphenols in the LBB extract were all substantially higher than those in the other three berry extracts.

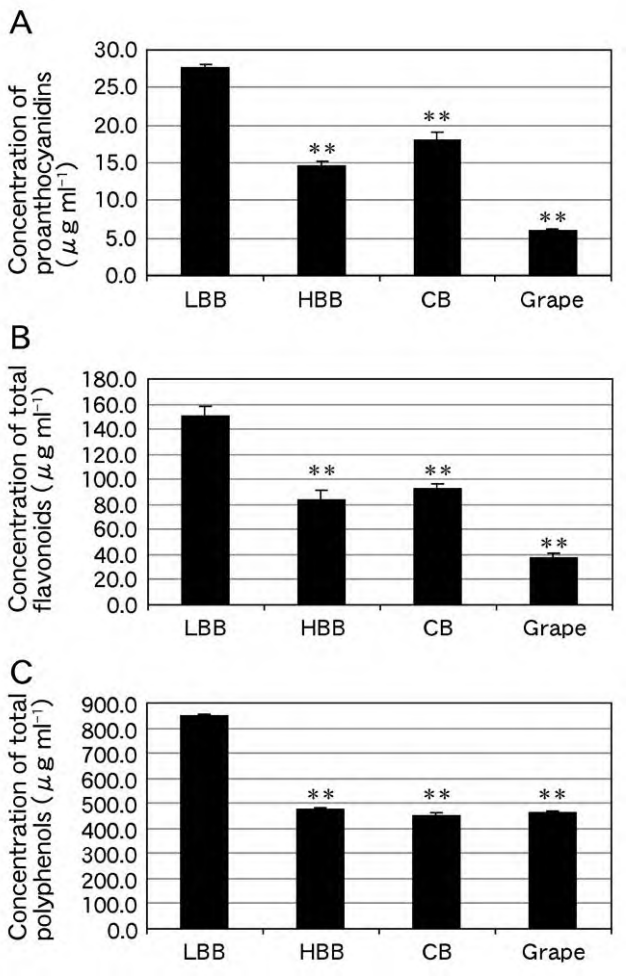

Figure 4. Concentrations of **(A)** proanthocyanidins, **(B)** total flavonoids and **(C)** total polyphenols in LBB, HBB, CB and grape extracts. Statistically significant differences were determined by Dunnett's test (**P < 0.01 vs. column LBB).

DISCUSSION

In this study, we prepared water extracts from four dry berries, LBB, HBB, CB and grape. Although the four berry extracts efficiently absorb UV-B primarily,[16] they showed slight toxicity against NHEKs under UV-B (–) (Figure 3Aa, Ab–Da, Db). Of the four berry extracts, pretreatment of NHEKs with LBB extract attenuated UV-B-induced damage (Figure 3A). These results indicate that LBB extract confers protection against UV-B-induced damage to human epidermal cells despite its cell toxicity.

We showed that concentrations of proanthocyanidins, total flavonoids and total polyphenols in the LBB extract were higher than those in the other three berry extracts (Figure 4). Therefore, the concentrations of proanthocyanidins, total flavonoids and total polyphenols are positively correlated with protection against UV-B-induced damage to NHEKs. In higher plants, flavonoids and proanthocyanidins are major UV-absorbing compounds.[13-15] Therefore, it is possible that flavonoids and proanthocyanidins in the LBB extract absorb UV-B irradiation, thereby protecting NHEKs from UV-B-induced damage. Proanthocyanidins also have high antioxidant and radical scavenging activity,[20-22] which is usually higher than that of vitamins C and E, the antioxidant and radical scavenging gold standards. It is conceivable that UV-B-induced ROS oxidize proanthocyanidins and this protects NHEKs from excess ROS, thereby attenuating UV-B-induced damage. To confirm the exact roles of proanthocyanidins and total flavonoids in protecting NHEKs from UV-B-induced damage, it will be necessary to analyze the effect of UV-B irradiation on NHEKs treated with these substances at concentrations similar to those found in LBB extract.

Alternatively, if the exact concentrations of proanthocyanidins and total flavonoids found in LBB extract are the cause to protect NHEKs from UV-B-induced damage, pretreatment of NHEKs with diluted LBB extract containing these substances at concentrations similar to those found in HBB, CB or Grape extract would not attenuate UV-B-induced damage. Such analysis might also provide useful information.

The LBB extract may contain other unidentified polyphenol compounds that attenuate UV-B-induced damage in NHEKs. We previously conducted an HPLC analysis of 51 polyphenols in the four berry extracts and showed that the most abundant compounds in LBB extract were caffeic acid, protocatechuic acid, syringic acid, vanillic acid and quercetin.[16] It is known that these compounds efficiently absorb UV-B light.[23-25] Caffeic acid is a nonflavonoid catecholic compound and is present in many plants.[26] Catecholic acids are reported to have anti-inflammatory, antimutagenic, antioxidant and anticarcinogenic activities.[26] Syringic acid and vanillic acid have been identified as antioxidants in medicinal mushroom (*Inonotus obliquus*).[27] Quercetin is one of the most abundant natural flavonoids and is a powerful antioxidant and metal ion chelator.[24] Thus, caffeic acid, syringic acid, vanillic acid and quercetin have verified antioxidant activities. It is possible that these five compounds contribute to the attenuation of UV-B-induced damage in NHEKs by a mechanism similar to that of proanthocyanidins as described above.

Of the four berry extracts, we showed that pretreatment of NHEKs with LBB extract attenuated UV-B-induced damage, although LBB extract has NHEK cell toxicity (Figure 3A). We also showed that pretreatment of cucumber (*Cucumis sativus* L.) cotyledons with LBB, HBB and CB extracts attenuated the damage induced by UV-B (+) without causing any side effects.[16] Thus, LBB extract was the most effective protector of NHEKs against UV-B(+), whereas LBB, HBB and CB extracts were the most effective protectors of cucumber cotyledons against UV-B(+). These results suggest that the compounds involved in protection from UV-B radiation might differ in plants and humans. Further work is required to identify the specific compounds involved in attenuating UV-B-induced damage and to determine the underlying mechanisms. Also, the precise nature of the compounds causing toxicity to NHEKs in LBB extract should be clarified. Alternatively, because the

ingestion of LBB and LBB extracts is not known to have toxic side effects, a patch test of LBB extract on the human skin should be conducted. This work has potential applications for developing a topical treatment to protect against UV-B radiation in humans.

CONCLUSION

To search for natural materials that protect human skin from damage caused by UV-B irradiation, we prepared water extracts of the following four dry berries: LBB, HBB, CB and grape. Pretreatment of NHEKs with LBB extract significantly attenuated UV-B-induced damage. The concentrations of proanthocyanidins, total flavonoids and total polyphenols in LBB extract were higher than those in the other three berry extracts. These compounds might mediate the protection of NHEKs from UV-B-induced damage.

ACKNOWLEDGEMENTS

This work was partially supported by the Japan Society for the Promotion of Science, a Grant-in-Aid for Scientific Research (C) (no. 15K07292 to S.Y.), the 5th Nissan Science Foundation, and the Saito Gratitude Foundation.

REFERENCES

[1]Rozema, J., van de Staaij, J., Björn, L. O., Caldwell, M., *Trends Ecol. Evol.*, **1997**, *12(1)*, 22-28. https://doi.org/10.1016/S0169-5347(96)10062-8

[2]Wikonkal, N. M., Brash, D. E., *Dermatol. Symp. Proc.*, **1999**, *4(1)*, 6-10. https://doi.org/10.1038/sj.jidsp.5640173

[3]Lisby, S., Gniadecki, R., Wulf, H. C., *Exp. Dermatol.*, **2005**, *14(5)*, 349-355. https://doi.org/10.1111/j.0906-6705.2005.00282.x

[4]Singh, A. P., Wilson, T., Kalk, A. J., Cheong, J., Vorsa, N., *Food Chem.*, **2009**, *116(4)*, 963-968. https://doi.org/10.1016/j.foodchem.2009.03.062

[5]Ivanova, V., Stefova, M., Chinnici, F., *J. Serb. Chem. Soc.*, **2010**, *75(1)*, 45-59. http://eprints.ugd.edu.mk/id/eprint/314

[6]Rodriguez-Mateos, A., Cifuentes-Gomez, T., Tabatabaee, S., Lecras, C., Spencer, J. P., *J. Agric. Food Chem.*, **2012**, *60(23)*, 5772-5778. https://pubs.acs.org/doi/10.1021/jf203812w

[7]Ferguson, P. J., Kurowska, E., Freeman, D. J., Chambers, A. F., Koropatnick, D. J., *J. Nutr.*, **2004**, *134(6)*, 1529-1535. https://doi.org/10.1093/jn/134.6.1529

[8]Stetler-Stevenson, W. G., Yu, A. E., *Semin. Cancer Biol.*, **2001**, *11(2)*, 143-152. https://doi.org/10.1006/scbi.2000.0365

[9]Pupa, S. M., Menard, S., Forti, S., Tagliabue, E., *J. Cell. Physiol.*, **2002**, *192(3)*, 259-267. https://doi.org/10.1002/jcp.10142

[10]Matchett, M. D., MacKinnon, S. L., Sweeney M. I., Gottschall-Pass, K. T., Hurta, R. A. R., *Biochem. Cell Biol.*, **2005**, *83(5)*, 637-643. https://doi.org/10.1139/o05-063

[11]MacLean, M. A., Matchett, M. D., Amoroso, J., Neto, C., Hurta, R., *FASEB J.*, **2007**, *21(6)*, 791.5. https://www.islandscholar.ca/islandora/object/ir:892

[12]Mittal, A., Elmets, C. A., Katiyar, S. K., *Carcinogenesis*, **2003**, *24(8)*, 1379-1388. https://doi.org/10.1093/carcin/bgg095

[13]Bieza, K., Lois, R., *Plant Physiol.*, **2001**, *126(3)*, 1105-1115. https://doi.org/10.1104/pp.126.3.1105

[14]Hada, H., Hidema, J., Maekawa, M., Kumagai, T., *Plant Cell Environ.*, **2003**, *26(10)*, 1691-1701. https://doi.org/10.1046/j.1365-3040.2003.01087.x

[15]Fujibe, T., Saji, H., Arakawa, K., Yabe, N., Takeuchi, Y., Yamamoto, K. T., *Plant Physiol.*, **2004**, *134(1)*, 275-285. https://doi.org/10.1104/pp.103.033480

[16]Yamasaki, S., Mizoguchi, K., Kodama, N., Iseki, J., *J. Agr. Res. Quart.*, **2017**, *51(3)*, 241-250. https://doi.org/10.6090/jarq.51.241

[17]Kayano, S., Fukutsuka, N., Suzuki, T., *J. Agr. Food. Chem.*, **2003**, *51(5)*, 1480-1485. https://pubs.acs.org/doi/pdf/10.1021/jf025929c

[18]Kim, D. O., Chun, O. K., Kim, Y. J., *J. Agr. Food. Chem.*, **2003**, *51(22)*, 6509-6515. https://pubs.acs.org/doi/abs/10.1021/jf0343074

[19]Ono, K., Huang, S. A., Res. Bull., *Gifu City Women's College*, **2001**, *51*, 135-138. https://ci.nii.ac.jp/els/contents110000473993.pdf?id=ART0000857907

[20]Baguchi, D., Garg, A., Krohn, R. L., Baguchi, M., Tran, M. X., Stohs, S. J., *Res. Commun. Mol. Pathol. Pharmacol.*, **1997**, *95(2)*, 179-189. https://www.ncbi.nlm.nih.gov/pubmed/9090754

[21]Ho, K. Y., Huang, J. S., Tsai, C. C., Lin, T. C., Hsu, Y. F., Lin, C. C., *J. Pharm. Pharmacol.*, **1999**, *51(9)*, 1075-1078. https://doi.org/10.1211/0022357991773410

[22]Beninger, C. W., Hosfield, G. L., *J. Agric. Food Chem.*, **2003**, *51(27)*, 7879-7883. https://pubs.acs.org/doi/full/10.1021/jf0304324

[23]Pearl, I. A., *J. Am. Chem. Soc.*, **1949**, *71(7)*, 2331-2333. https://pubs.acs.org/doi/pdfplus/10.1021/ja01175a700

[24]Svobodová, A., Psotová, J., Walterová, D., *Biomed. Papers*, **2003**, *147(2)*, 137-145. http://mefanet.upol.cz/BP/2003/2/137.pdf

[25]Savić, S. R., Stanojević, J. S., Marković, D. Z., Petronijević, Ž. B., *Hem. Ind.*, **2013**, *67(3)*, 411-418. http://www.ache.org.rs/HI/2013/No3/HEMIND_Vol67_No3_p411-418_Maj-Jun_2013.pdf

[26]Moridani, M. Y., Scobie, H., Jamshidzadeh, A., Salehi, P., O'brien, P. J., *Drug Metab. Dispos.*, **2001**, *29(11)*, 1432-1439. http://dmd.aspetjournals.org/content/dmd/29/11/1432.full.pdf

[27]Kumagai, A., Koizumi, Y., Kawagoe, M., Koyota, S., Sugiyama, T., *Akita J. Med.*, **2013**, *40*, 113-119. http://hdl.handle.net/10295/2341

Received: 24.06.2018
Accepted: 18.06.2018

ENVIRONMENTALLY FRIENDLY,ONE-POT SYNTHESES OF 2-(1H-BENZO[d]IMIDAZOLE-2-YL)-N-ARYLBENZAMIDES

V. Anitha Rani*[a]

Keywords: Green synthesis; 2-(1H-benzo[d]imidazole-2-yl)-N-arylbenzamides; glycerol; one-pot synthesis; anilines; o-phenylenediamine (OPDA); phthaldichloride.

Eco-friendly, one-pot three-component syntheses of 2-(1H-benzo[d]imidazole-2-yl)-N-arylbenzamideshave been developed by combining Phthaloyl dichloride with anilinesand o-phenylenediamine in glycerol without any external catalyst. These reactions involve easy workup, provide excellent yields and use glycerol as solvent at 100 °C for 60-90 min which are the merits of this preparation.

* Corresponding Authors
E-Mail: anitha1810@gmail.com
[a] Department of Chemistry, Institute of Aeronautical Engineering, Dundigal, Hyderabad-500043

Introduction

Development of efficientand environmentally friendly methods is an important challenge in modern organic syntheses.[1] In many synthetic organic processes, solvents represent a severe pollution problem. Thus, the replacement of hazardous solvents with relatively green solvents or the altogether elimination of use of hazardous solvents in chemical processes has been one of the key achievements of green chemistry.[2] Based on the principles of green chemistry, a green solvent should meet numerous criteria such as low toxicity, non-volatility, non-mutagenicity, non-flammability and widespread availability.[3] In the past decade, water,[4] glycerol,[5] polyethylene glycol[6]andionic liquids[7] have been used as green solvents in organic reactions. As a result, serious efforts are being made to develop glycerol as a solvent for most of the organic syntheses and processes wherever possible.

Hawkins[8] and Perry[9] reported the preparation of N-arylphthalamidic acids by the reaction of phthalic anhydride with arylamines at room temperature in chloroform. Young et al reported[10] the preparation of N-(2-aminophenyl)phthalamidic acid and N-(2-aminophenyl)-phthalimide by the reaction of phthalic anhydride with o-phenylenediamine in DMF. Perry et al[11] prepared these compounds in chloroform. Keeping the above results in mind, we now wish to report our synthetic studies on reactions of phthaloyl dichloride **l** with anilines and with o-phenylenediamine **3.**

Results and discussion

As illustrated in Scheme 1, a mixture of phthaloyl dichloride **1**, aniline **2a** and o-phenylenediamine **3** was heated at 100 °C in glycerol for 60 min resulting in the formation of 2-(1H-benzo[d]imidazole-2-yl)-N-phenylbenzamide **4a** (Table 1, entry 1). Then, this one-pot reaction of **1** (1 mmol)**, 2a** (1 mmol) and **3** (1 mmol) was optimized by doing a series of experiments in the presence of different solvents at different temperatures (Table 1). However, it is greatly notable that the one-pot reaction in glycol at 100 °C for 60 min gave reasonably high yield (80 %) of the product **4a** compared to other solvents such as PEG-600, ethylene glycol, DMF, DMSO and polyphosphoric acid (PPA) (Table 1, entry 11**).**

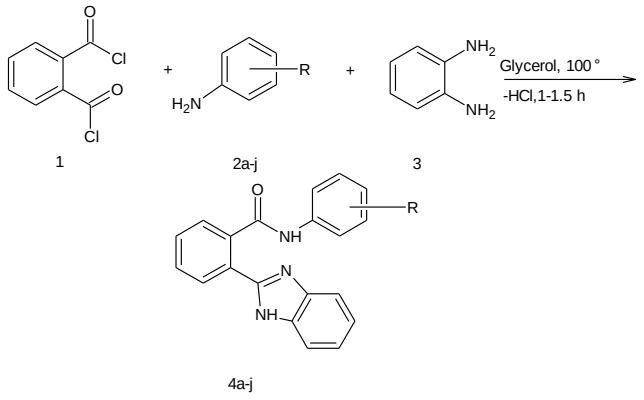

Scheme 1. One-pot synthesis of compounds **4a-4j** (R=H(a), p-Cl(b), p-Me(c), o-Me(d), p-Br(e), p-I(f), p-MeO(g), p-OH(h), p-NO_2(i), m-NO_2(j)

Table 1. Effect of solvent and Temperature on one-pot reaction of phthaloyl dichloride, aniline and o-phenylenediamine

Entry	Solvent	Temp., °C	Time, min	Yield of 4a, %
1	Glycerol	100	60	80
2	Glycerol	RT	240	-
3	PEG-600	RT	300	-
4	PEG-600	100	150	60
5	Ethyleneglycol	RT	300	-
6	Ethyleneglycol	100	150	55
7	DMF	RT	300	40
8	DMF	100	150	45
9	DMSO	RT	300	30
10	DMSO	100	180	35
11	PPA	100	90	20

Using the above-stated optimised conditions, the synthesis of **4a-4j** was carried out by heating the mixture of **1, 2a-2j** and **3** in glycerolat 100 °C for 60-90 min. Products were obtained in good yield and no side products were detected.

Their structures have been established on the basis of spectral properties such as IR, NMR and mass spectra. (Scheme 1) (Table 2).

Table 2. Characterization data, reaction time and yields of **4a-4j** obtained from **1, 2a-2j and 3.**

Entry	Starting material	Product obtained	Time, min	Yield, %*
1	**2a**	**4a**	60	80
2	**2b**	**4b**	65	80
3	**2c**	**4c**	70	75
4	**2d**	**4d**	80	75
5	**2e**	**4e**	85	80
6	**2f**	**4f**	90	80
7	**2g**	**4g**	80	75
8	**2h**	**4h**	65	80
9	**2i**	**4i**	75	80
10	**2j**	**4j**	75	85

*Yields of crude products

Two possible reaction routes can be proposed to account for the formation of **4** in the one-pot synthesis from **1, 2** and **3.**One among them is when phthaldichloride**1** reacts with aniline **2** to form the imide intermediate **5** by liberating hydrogen chloride. Then **5** was attacked byo-phenylenediamine**3** to form **4**.In the second probable reaction route, reaction of phthaldichloride**1** with o-phenylenediamine**3** yields the intermediate **6** by liberation hydrogen chloride. Then, **6** was attacked by **2** to form **4**.Intermediate **6** was prepared separately by the reaction between **1** and **3**, then then treatment of **6**with **2** in water gave **4**.

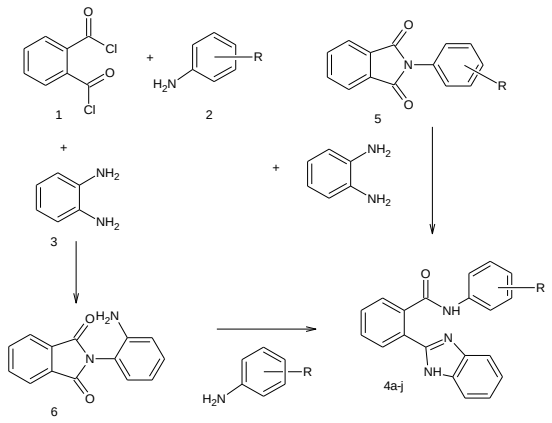

Scheme 2. Possible reaction routes to form compounds **4** from compounds **1**, **2** and **3**.

Experimental section

Melting points are uncorrected and were determined in open capillary tubes in sulphuric acid bath. TLC was run on silica gel – G and visualization was done using iodine or UV light. IR spectra were recorded using Perkin–Elmer 1000 instrument in KBr pellets. ^{1}H NMR spectra were recorded in DMSO–d_6 using TMS as internal standard using 400 MHz spectrometer. Mass spectra were recorded on Agilent-LCMS instrument under CI conditions and given by Q+1 values only. Starting materials **1** and **2** were obtained from commercial sources and used as such.

General procedure for preparation of 4a-j from 1, 2a-j and 3 by one-pot synthesis

A mixture of **1** (10 mM), **2a-2j** (10 mM), **3** (10 mM), and glycerol (20 ml) was heated at 100 °C for 60-90 min. At the end of this period, a colourless solid separated out from reaction mixture which was collected by filtration. The isolated solid was washed with water (10 ml) and dried. The product was recrystallized from a suitable solvent to obtain **4a-4j**.

2-(1H-Benzo[d]imidazole-2-yl)-N-phenylbenzamide (4a)

Melting point: >250 °C; IR (KBr): 3038-3353 cm^{-1} (broad, medium, -NH- and -OH groups put together), 1703 cm^{-1} (sharp, strong, -CO- of acid group), 1690 cm^{-1} (sharp, strong, -CO- of acid group), 1632 cm^{-1} (sharp, strong, -CO- of amide group); ^{1}H NMR δ_H(400 MHz; DMSO-d_6; Me_4Si) 7.1-8.1 (m, 13H, Ar-**H**), 10.3(s, 1H, -CO-N**H**, D_2O exchangeable), 12.7(s, 1H, -N**H**, D_2O exchangeable); HRMS calcd for $C_{20}H_{15}N_3O$ $[M+H]^+$: 314.32326, Found: 314.32329.

2-(1H-Benzo[d]imidazole-2-yl)-N-(4-chlorophenyl)benzamide (4b)

Melting point: >250 °C; IR (KBr): 3036-3355 cm^{-1} (broad, medium, -NH- and -OH groups put together), 1705 cm^{-1} (sharp, strong, -CO- of acid group), 1692 cm^{-1} (sharp, strong, -CO- of acid group), 1634 cm^{-1} (sharp, strong, -CO- of amide group); ^{1}H NMR δ_H(400 MHz; DMSO-d_6; Me_4Si) 7.0-8.0 (m, 12H, Ar-**H**), 10.3(s, 1H, -CO-N**H**, D_2O exchangeable), 12.5 (s, 1H, -N**H**, D_2O exchangeable); HRMS calcd for $C_{20}H_{14}ClN_3O$ $[M+H]^+$: 348.32326, Found: 348.32329.

2-(1H-Benzo[d]imidazole-2-yl)-N-(4-methylphenyl)benzamide (4c)

Melting point: >250 °C**;** IR (KBr): 3035-3355 cm^{-1} (broad, medium, -NH- and -OH groups put together), 1708 cm^{-1} (sharp, strong, -CO- of acid group), 1692 cm^{-1} (sharp, strong, -CO- of acid group), 1635 cm^{-1} (sharp, strong, -CO- of amide group); ^{1}H NMR δ_H(400 MHz; DMSO-d_6; Me_4Si) 2.4 (s, 3H, C**H**$_3$), 7.0-8.0 (m, 12H, Ar-**H**), 10.3(s, 1H, -CO-N**H,** D_2O exchangeable), 12.6 (s, 1H, -N**H,** D_2O exchangeable); HRMS calcd for $C_{21}H_{17}N_3O$ $[M+H]^+$: 328.32326, Found: 328.32329.

2-(1H-Benzo[d]imidazole-2-yl)-N-(2-methylphenyl)benzamide (4d)

Melting point: > 250 °C; IR (KBr): 3032-3350 cm^{-1} (broad, medium, -NH- and -OH groups put together), 1700 cm^{-1} (sharp, strong, -CO- of acid group), 1692 cm^{-1} (sharp, strong, -CO- of acid group), 1633 cm^{-1} (sharp, strong, -CO- of amide group); ^{1}H NMR δ_H(400 MHz; DMSO-d_6; Me_4Si) 2.3 (s, 3H, C**H**$_3$), 7.0-8.0 (m, 12H, Ar-**H**), 10.4 **(**s, 1H, -CO-**NH,**

D_2O exchangeable), 12.6(s, 1H, -N**H**, D_2O exchangeable); HRMS calcd for $C_{21}H_{17}N_3O$ $[M+H]^+$: 328.32326, Found: 328.32329.

2-(1H-Benzo[d]imidazole-2-yl)-N-(4-bromophenyl)benzamide (4e)

Melting point: > 250 °C; IR (KBr): 3040-3357 cm^{-1} (broad, medium, -NH- and -OH groups put together), 1713 cm^{-1} (sharp, strong, -CO- of acid group), 1695 cm^{-1} (sharp, strong, -CO- of acid group), 1635 cm^{-1} (sharp, strong, -CO- of amide group); ^1H NMR δ_H(400 MHz; DMSO-d_6; Me_4Si) 7.0-8.0 (m, 12H, Ar-**H**), 10.4(s, 1H, -CO-N**H**, D_2O exchangeable), 12.6 (s, 1H, -N**H**, D_2O exchangeable); HRMS calcd for $C_{20}H_{14}BrN_3O$ $[M+H]^+$: 392.32326, Found: 392.32329.

2-(1H-Benzo[d]imidazole-2-yl)-N-(4-iodophenyl)benzamide (4f)

Melting point: 240-242 °C; IR (KBr): 3031-3351 cm^{-1} (broad, medium, -NH- and -OH groups put together), 1701 cm^{-1} (sharp, strong, -CO- of acid group), 1691 cm^{-1} (sharp, strong, -CO- of acid group), 1639 cm^{-1} (sharp, strong, -CO- of amide group); ^1H NMR δ_H(400 MHz; DMSO-d_6; Me_4Si) δ 7.0-8.0 (m, 12H, Ar-**H**), 10.2(s, 1H, -CO-N**H**, D_2O exchangeable), 12.8 (s, 1H, -N**H**, D_2O exchangeable); HRMS calcd for $C_{20}H_{14}IN_3O$ $[M+H]^+$: 440.32326, Found: 440.32329.

2-(1H-Benzo[d]imidazole-2-yl)-N-(4-methoxyphenyl)benzamide (4g)

Melting point: >250 °C; IR (KBr): 3030-3350 cm^{-1} (broad, medium, -NH- and -OH groups put together), 1700 cm^{-1} (sharp, strong, -CO- of acid group), 1691 cm^{-1} (sharp, strong, -CO- of acid group), 1631 cm^{-1} (sharp, strong, -CO- of amide group); ^1H NMR δ_H(400 MHz; DMSO-d_6; Me_4Si) δ 2.7 (s, 3H, C**H**$_3$), 7.0-8.0 (m, 12H, Ar-**H**), 10.5(s, 1H, -CO-N**H**, D_2O exchangeable), 12.7 (s, 1H, -N**H**, D_2O exchangeable); HRMS calcd for $C_{21}H_{17}N_3O_2$ $[M+H]^+$: 344.32326, Found: 344.32329.

2-(1H-Benzo[d]imidazole-2-yl)-N-(4-hydroxyphenyl)benzamide (4h)

Melting point: >250 °C; IR (KBr): 3030-3343 cm^{-1} (broad, medium, -NH- and -OH groups put together), 1701 cm^{-1} (sharp, strong, -CO- of acid group), 1689 cm^{-1} (sharp, strong, -CO- of acid group), 1635 cm^{-1} (sharp, strong, -CO- of amide group); ^1H NMR δ_H(400 MHz; DMSO-d_6; Me_4Si) 7.0-8.0 (m, 12H, Ar-**H**), 8.5(s, 1H, -O**H**, D_2O exchangeable), 10.2(s, 1H, -CO-N**H**, D_2O exchangeable), 12.4(s, 1H, -N**H**, D_2O exchangeable); HRMS calcd for $C_{20}H_{15}N_3O_2$ $[M+H]^+$: 330.32326, Found: 330.32329.

2-(1H-Benzo[d]imidazole-2-yl)-N-(4-nitrophenyl)benzamide (4i)

Melting point: >250 °C; IR (KBr): 3031-3351 cm^{-1} (broad, medium, -NH- and -OH groups put together), 1700 cm^{-1} (sharp, strong, -CO- of acid group), 1694 cm^{-1} (sharp, strong, -CO- of acid group), 1632 cm^{-1} (sharp, strong, -CO- of amide group); ^1H NMR δ_H(400 MHz; DMSO-d_6; Me_4Si) δ 7.0-8.0 (m, 12H, Ar-**H**), 10.4(s, 1H, -CO-N**H**, D_2O exchangeable), 12.7(s, 1H, -N**H**, D_2O exchangeable); HRMS calcd for $C_{20}H_{14}N_4O_3$ $[M+H]^+$: 359.32326, Found: 359.32329.

2-(1H-Benzo[d]imidazole-2-yl)-N-(3-nitrophenyl)benzamide (4j)

Melting point: >250 °C; IR (KBr): 3039-3359 cm^{-1} (broad, medium, -NH- and -OH groups put together), 1709 cm^{-1} (sharp, strong, -CO- of acid group), 1699 cm^{-1} (sharp, strong, -CO- of acid group), 1638 cm^{-1} (sharp, strong, -CO- of amide group); ^1H NMR δ_H(400 MHz; DMSO-d_6; Me_4Si) δ 7.0-8.0 (m, 12H, Ar-**H**), 10.2(s, 1H, -CO-N**H**, D_2O exchangeable), 12.8(s, 1H, -N**H**, D_2O exchangeable); HRMS calcd for $C_{20}H_{14}N_4O_3$ $[M+H]^+$: 359.32326, Found: 359.32329.

Conclusion

In summary, a green synthetic method have been developed for the synthesis of **4a-4j** with good yield in glycerol through a one-pot, three-component synthesis.

Acknowledgement

Authors are very thankful to the authorities of Jawaharlal Nehru Technological University Hyderabad.

References

[1]Baker, R. T., Tumas, W., Toward Greener Chemistry**,** *Science.*, **1999**, *284*, 1477; https://doi.org/10.1126/science.284.5419.1477; Anastas, P. T., Introduction: Green Chemistry, *Chem. Rev.*, **2007**, *107*, 2167; https://doi.org/10.1021/cr0783784; Horvath, I. T., Green Chemistry, *Acc. Chem. Res.*, **2002**, *35*, 685. https://doi.org/10.1021/ar020160a

[2]Lindström, U. K. Stereoselective Organic Reactions in Water, *Chem. Rev.*, **2002,** *102*, 2751; https://doi.org/10.1021/cr010122p; Li, C. J., Organic Reactions in Aqueous Media with a Focus on Carbon−Carbon Bond Formations: A Decade Update, *Chem. Rev.*, **2005**, *105*, 3095; https://doi.org/10.1021/cr030009u; Tan, J. N., Li, H., Gu, Y., Water mediated trapping of activemethylene intermediates generated by IBX-induced oxidation of Baylis–Hillman adducts with nucleophiles, *Green Chem.*, **2010**, *12*, 1772; https://doi.org/10.1039/c0gc00274g; Solhy, A., Elmakssoudi, A., Tahir, R., Karkouri, M., Larzek, M., Bousmina, M., Zahouily, M., Clean chemical synthesis of 2-amino-chromenes in water catalyzed by nanostructured diphosphate $Na_2CaP_2O_7$, *Green Chem.*, **2010**, *12*, 2261. https://doi.org/10.1039/c0gc00387e;

[3]Capello, C., Fisher, U., Kungerbühler, K., What is a green solvent ? A comprehensive framework for the environmental assessment of solvents, *Green Chem.*, **2007,** *9*, 927. https://doi.org/10.1039/b617536h

[4]Li, C. J., Chen, L., Organic chemistry in water, *Chem. Soc. Rev.*, **2006**, *35*, 68**.** https://doi.org/10.1039/B507207G

[5]Safaei, H., Shekouhy, R. M., Rahmanpur, S., Shirinfeshan, A., Glycerol as a biodegradable and reusable promoting medium

for the catalyst-free one-pot three-component synthesis of *4H*-pyrans, *Green Chem.*, **2012,** *14,* 1696.https://doi.org/10.1039/c2gc35135h

[6]Chen, J., Spear, S. K., Huddleston, J. G., Rogers, R. D., Polyethyleneglycol and solutions of polyethyleneglycol as green reaction media, *Green Chem.*, **2005**, *7,* 64. https://doi.org/10.1039/b413546f

[7]Plechkova, N. V., Seddon, K. R., Applications of ionic liquids in the chemical industry, *Chem. Soc. Rev.*, **2008**, *37,* 123–150. https://doi.org/10.1039/B006677J

[8]Hawkins, M. D., Intramolecular catalysis. Part III. Hydrolysis of 3′- and 4′-substituted phthalanilic acids [*o*-(*N*-phenylcarbamoyl)benzoic acids], *J. Chem. Soc., Perkin Trans.2,* **1976**, 642. https://doi.org/10.1039/P29760000642

[9]Perry, C. J., Parveen, Z., The cyclisation of substituted phthalanilic acids in acetic acid solution. A kinetic study of substituted *N*-phenylphthalimide formation, *J. Chem. Soc., Perkin Trans. 2.* **2001,** 512. https://doi.org/10.1039/b008399m

[10]Young, P. R., Polyimidazopyrrolone model compounds, *J. Heterocycl. Chem.*, **1972**, *9,* 371. https://doi.org/10.1002/jhet.5570090232

[11]Perry, C. J., A new kinetic model for the acid-catalysed reactions of N-(2-aminophenyl)phthalamic acid in aqueous media, *J. Chem. Soc., Perkin Trans. 2*, **1997**, 977. https://doi.org/10.1039/a606699b

Received: 14.05.2018.
Accepted: 12.08.2018.

POLARON ON HARMONIC LATTICE IN ELECTRIC FIELD GENERATION OF COHERENT OSCILLATIONS

T. Yu. Astakhova[a]* and G. A. Vinogradov[a]

Keywords: Polaron, charge transfer, electron-lattice interaction, electron-phonon interaction, SSH.

The dynamics of a polaron on a one-dimensional harmonic lattice in an applied constant electric field has been considered. The calculations were performed with parameters close to those of polyacetylene and DNA. The polaron in a constant field goes to a stationary state, characterized by a constant profile and velocity. In this case, the energy got by the polaron from the electric field is transformed into longitudinal coherent lattice vibrations. For several thousand lattice sites, these oscillations have constant frequency and wave number, and these values depend weakly on the electric field.

* Corresponding Authors
Fax: +7(495) 9390838, +7(916) 1360239
E-Mail: astakhova@deom.chph.ras.ru
[a] Emanuel Institute of Biochemical Physics, Russian Academy of Sciences, Moscow, Russian Federation
119334, 4 Kosygina st, Moscow, Russia

INTRODUCTION

Presently, nano-sized electronic devices is widely used in various fields[1-10] and their uses have been reviewed also. [11,12] It is supposed that polarons are charge carriers in nonmetallic systems. Really, a minimum energy state of a charged elastic lattice with electron-phonon interaction corresponds typically to polaron formation.

Historically, polaron studies on one-dimensional lattices started with the modelling of a charged soliton in polyacetylene (PA).[13-17] First, an analysis of the effect of an external electric field on a charged soliton was done .[18] Later, the study of polaron in an external electric field was conducted.[19]

The energy and charge transfer in biological macromolecules, such as DNA and polypeptides, has been intensively investigated for a long time. The conduction mechanism picture in such systems evolved from the Marcus theory[20] to the tunneling[21] and hopping mechanism.[22] Further, the polaron mechanism of conductivity was proposed. Conwell and coworkers first applied polaron paradigm to DNA.[23-26] Later, various models and approximations of the polaron charge transport in DNA were developed.[27-37]

One of the most common methods for calculating the electronic structure and transport properties is the tight-binding approximation (TBA),[38,39] otherwise called the Huckel method. In this approximation, the wave function is represented as a linear combination of localized states. In the particular case of molecular systems, this is a linear combination of atomic orbitals. The most popular method for describing the electron-phonon interaction is the Su-Schrieffer-Heeger (SSH) approximation, first used to describe charged solitons in PA.[16,17]

The SSH model for PA includes minimum parameters necessary for polaron description. Namely, σ bonding is taken into account through harmonic interaction between nearest units (representing CH groups) of one dimensional lattice, and π electrons are treated in TBA. The units displacements are measured from positions of undimerized chain and dimerization is taken into account by the alternation of displacements sign. Another way to include dimerization is Brazovskii-Kirova symmetry breaking terms.[40,41] Subsequently, the SSH model became widely used for description not only for simple conjugated polymers but more complicated systems, for example, DNA,[23-26,42-44] polypyrrole[45] and paraphenylene polymers (PPP).[46] The electron-phonon coupling can be taken into account in a slightly different way also, as in the case of Frohlich or Holstein polarons[52-55] or in Davydov-Scott model.[57] However, in all models the general polaron behaviour is similar. Nonlinearity has also been included in dependence of the hopping integral on the distance between chain units.[58] Further, the polaron models were complicated by addition spin and Coulomb interactions for bipolarons,[40,46,47] thermal[48,59-61] and disorder[62,63] effects, and impurities.[64,65] Two-dimensional lattices including interchain interactions were also considered.[49-51,55,56] Higher order tight binding SSH model has been developed for DNA charge transport.[70]

Polarons as charge carriers can be accelerated under an external electric field.[19,68-70] The charge motion in semiconductors and insulators was first considered by Feynman.[71] It was found that the polaron transforms the energy of interaction with the electric field into vibrational energy. For Al_2O_3 the transferred energy is ~0.025 eV per 1 Å.

In the SSH model, the electric field can be taken into account either by vector potential or by a term which explicitly describes the voltage drop between neighbouring sites.[68,80] These descriptions are equivalent and interrelated through a gauge transformation.

It was found that polaron achieves maximum velocity in electric field. In simple SSH model without dimerization maximum polaron velocity is always less than the sound velocity. If dimerization is taken into account supersonic velocities can be achieved when optical mode is excited.[66,73] There is maximum electric field which destroys polaron.[72]

The reported value of the critical electric field in PA widely varies in the literature (10 mV/Å,[47,74,75] 4 mV/ Å,[50] 0.54 mV/Å[46] and 1.6 mV/Å[76] in polyparaphenylene). Critical field values for a number of inorganic polymers have reported[72] e.g., 3.9 mV/Å for PA, 1.3 mV/Å for polystannane, 1.3 mV/Å for polygermane, and 1.3 mV/Å for polysilane. In some papers the lattice vibrations following moving polaron in electric field are reported.[77,78] Above the critical field, the dissociated polaron propagates in the form of a free electron and performs spatial Bloch oscillations.[67] On the other hand, Bloch oscillations in the electric field can generator polarons in a 1D crystal.[79] Theoretical investigation of the simple SSH model with one electron on the harmonic lattice has been reported by Basko and Conwell.[80] Here, analytical dependence of the polaron velocity versus applied electric field has been presented. The critical electric field value is also estimated.

In present study, the polaron dynamics on harmonic lattice in an electric field is thoroughly investigated numerically in the framework of SSH model. A harmonic lattice with parameter close to polyacetylene and DNA has been considered. A weak logarithmic dependence of the stationary polaron velocity on the value of applied electric field is found. Mechanisms of energy transfer from a moving polaron to a lattice are discussed. The parameters of coherent vibrations generated by polaron moving in external electric field are investigated. Critical field for PA and DNA parameters are estimated. We found good agreement with the reported theoretical prediction.[80]

MODEL

We use the following generally accepted Hamiltonian,[68] where eqn. (2) describes the dynamics of regular harmonic lattice. Here, x_j and v_j are the deviation of the j-th particle from the equilibrium and its velocity, K is the rigidity, M is the particle mass.

$$H = H_{\mathrm{lat}} + E_{\mathrm{el}} \quad (1)$$

$$H_{\mathrm{lat}} = \frac{K}{2}\sum_{\mathrm{j}}\left(x_{\mathrm{j+1}} - x_{\mathrm{j}}\right)^2 + \frac{M}{2}\sum_{\mathrm{j}} v_{\mathrm{j}}^2 \quad (2)$$

The second, quantum term in eqn. (1) is the electronic part of the total Hamiltonian. It is written in the TBA approximation in an external constant electric field as eqn. (3).

$$H_{\mathrm{el}} = -\sum_{\mathrm{j}}\left[t_0 - \chi\left(x_{\mathrm{j+1}} - x_{\mathrm{j}}\right)\right]\left[\exp(\mathrm{i}\gamma A)c_{\mathrm{j}}^{+}c_{\mathrm{j+1}} + \mathrm{c.c.}\right] \quad (3)$$

Here, the electron-phonon interaction (EPI) is described in SSH approximation, t_0 is the equilibrium hopping integral, χ is the EPI parameter, and c_{j}^{+} /c_{j} are the creation/annihilation operators for the electron at the site j, and c.c. stands for complex conjugation.

As a rule, dimensionless quantities were used. For non-dimensionalization, four independent parameters should be chosen. It is convenient to choose M, K, t_0, and the electron charge e. The numerical values[70] of these parameters for DNA are $M = 4.35 \times 10^{-25}$ kg, $K = 13.6$ kg s^{-2}, $t_0 = 4.8 \times 10^{-20}$ kg m^2 s^{-2}, $e = 1.6 \times 10^{-19}$ C. At the non-dimensionalization, the numerical values of these parameters are taken to be unity. After that, all other parameters can be dimensionless. The dimensionless unit length is defined as $[[L]] = (t_0/K)^{1/2}$, and it corresponds to 0.59 Å. Similarly, the dimensionless time unit is defined as $[[t]] = (M/K)^{1/2}$, which corresponds to 0.18 ps. The dimensionless unit of energy is 0.3 eV. Dimensionless values of other parameters of the Hamiltonian are defined similarly: $\hbar \approx 10^{-2}$ and $\chi \approx 1.2$.

Since the numerical values of the parameters M, K and t_0 in PA differ from those in DNA,[67] the corresponding dimensionless parameters were renormalized. The length, time, and energy units are $[[L]]$=0.35 Å, $[[t]]$=8 fs, $[[E]]$=2.5 eV, respectively, and the EPI parameter $\chi\approx$0.4. Note that χ=0.4 is maximum value for which the continuum approximation works well. So, exact expressions for the polaron shape and the wave function are available.[81,82]

The external electric field is taken into account by a factor $\exp(\mathrm{i}\gamma A)$, where $\gamma = ea/\hbar c$ and e is the electron charge, a is the lattice constant, c is the light speed, ħ is Dirac's constant. The relation between the vector potential A and electric field E is $E = -1/c\,\mathrm{d}A/\mathrm{d}t$. It is convenient to write the exponential term as $\exp(-\mathrm{i}Bt)$, where $B = eEa/\hbar$. Below, we use B and call it an electric field parameter. For DNA and PA, the dimensionless value B=1 corresponds to $E \approx 1.1\times10^7$ V m^{-1} and $E \approx 6.8 \times 10^8$ V/m, respectively.

After non-dimensionalization we get the following evolutionary equations for both classical and quantum degrees of freedom where $F \equiv \exp(\mathrm{i}Bt)$.

$$\ddot{x}_{\mathrm{j}} = -\left(2x_{\mathrm{j}} - x_{\mathrm{j+1}} - x_{\mathrm{j-1}}\right) + \chi\left[F\psi_{\mathrm{j}}^{*}\psi_{\mathrm{j-1}} - F^{*}\psi_{\mathrm{j-1}}^{*}\psi_{\mathrm{j}} + F\psi_{\mathrm{j+1}}^{*}\psi_{\mathrm{j}} + F^{*}\psi_{\mathrm{j}}^{*}\psi_{\mathrm{j+1}}\right] \quad (4)$$

$$\dot{\psi}_{\mathrm{j}} = -\frac{i}{\hbar}\left\{\left[-1 + \chi\left(x_{\mathrm{j+1}} - x_j\right)\right]F\psi_{\mathrm{j+1}} + \left[-1 + \chi\left(x_{\mathrm{j}} - x_{\mathrm{j-1}}\right)\right]F^{*}\psi_{\mathrm{j-1}}\right\} \quad (5)$$

The time evolution of a polaron in electric field is obtained by numerical integration of eqns. (4) and (5) with free boundary conditions. The integration step Δt is determined by the most "fast" quantum dynamics for the wave function, and therefore $\Delta t = 10^{-4}$ is chosen.

POLARON IN ELECTRIC FIELD

The polaron on a harmonic lattice in an electric field reaches a steady state with a constant velocity and an unchanged profile of the polaron.[80] However, the stationary state setting time and the final polaron parameters depend strongly on the initial conditions.[69] Polaron evolution is also sensitive to the method of electric field switching. If the

switching time is small, a part of the electron density can decouple from the lattice deformation and the polaron can fail.

Initial conditions

Parameters of the polaron on a harmonic lattice without an electric field (velocity, amplitude and width) are uniquely related, and the choice, for example, of the velocity determines the polaron profile.

For small EPI parameter ($\chi \leq 0.4$) the continuum approximation is valid and analytical relations[83] for relative displacements of neighbouring particles $q_j \equiv (x_j - x_{j-1})$ and the wave function $\psi_j(t)$ are available (eqn. 6), where A and D are amplitudes of relative particles displacements and wave function, respectively, $1/d$ is a polaron width, j_0 is the initial polaron centre, v is the polaron velocity.

$$q_j = -\frac{A}{\cosh^2[d(j-j_0-v_0 t)]},$$

$$\psi_j = \frac{B}{\cosh[d(j-j_0-v_0 t)]} \qquad (6)$$

The following three equations relate polaron parameters.

$$d = \sqrt{\chi A}\ , v_0 = \left[1 - \sqrt{\chi^3/A}\right]^{1/2} \text{ and}$$

$$B = \sqrt{d/2} \qquad (7)$$

According to eqn. (7), polaron can be determined by any one parameter. It is convenient to choose the velocity v as a free parameter.

The polaron velocity on a harmonic lattice varies from zero to the nearly sound velocity, v_{snd}. Therefore, when modelling a polaron evolution in an electric field, the initial polaron velocity can be chosen in the range $0 < v_0 < v_{snd}$. Another simulation parameter is the electric field strength (dimensionless parameter B in (eqns. 4 and 5) and the method of the field switching-on (Figure 1).

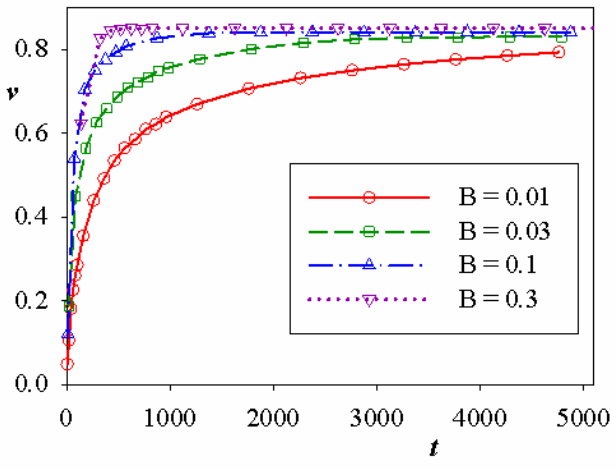

Figure 1. The dependence of polaron velocity v on time t for different values of electric field parameter B. Initial polaron velocity is zero. The field switching-on rate is 1/1250, $\chi = 0.4$.

Let us consider the setting of a stationary polaron velocity depending on the electric field for initially standing polaron. The time dependence of polaron velocity for different B is shown in figure 1. Here, $\chi = 0.4$, which corresponds to the PA. In all cases, the field grows linearly ($B = ct$) for a period of time τ up to the maximum value B_{max}, and $c = B_{max}/\tau = 1/1250$. In figure 1, all dependencies start at $t = \tau$, when the field reaches its maximum value. At small electric field, the polaron accelerates further after reaching B_{max} as it doesn't reach the maximum possible velocity. Hereafter, the polaron velocity is measured in the sound velocity.

For $\chi = 0.4$, the stationary dimensionless polaron velocity $v_{st} \approx 0.86$, which is $\approx 1.3 \times 10^4$ m s^{-1} in dimensional units. The dependence of the steady-state polaron velocity on the applied electric field is considered in more detail below. Polaron behaviour similar, to that in Figure 1, is also observed for $\chi = 1.2$, which corresponds to the DNA. Here, however, the stationary dimensionless velocity is less and $v_{st} \approx 0.6$, which corresponds to $\approx 1.1 \times 10^3$ m/s.

In the examples considered above, the total density of the wave function is localized on the polaron and is equal to the total charge of the electron. However, for some initial conditions, a part of the electron density can partially decouple from the lattice deformation,[67] and the polaron, being stable, carries a partial charge less than unity. The decoupled part of the wave function density is randomly distributed along the lattice (Figure 2).

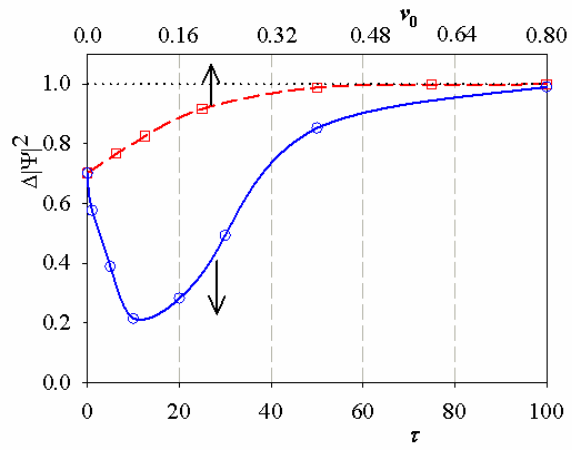

Figure 2. A fraction of electron density localized on the polaron $\Delta|\Psi|^2$ as function of switching-on time τ (solid line, open circles); $\Delta|\Psi|^2$ *vs* initial polaron velocity v_0 (dashed line, open squares) at instant field switching-on; $\chi = 0.4$.

If at first the field increases linearly ($B = B_{max}t/\tau$ for $t \leq \tau$ and $B = B_{max}$ for $t > \tau$), then the fraction of the electron density $\Delta|\Psi|^2$ left at the polaron depends on τ nonmonotonically. The result is shown in figure 2 (solid curve and circles). Here, $B_{max} = 0.08$, $\chi = 0.4$, and the initial polaron velocity is zero. One can see that when the electric field is slowly switched on ($\tau > 100$), the polaron keeps practically 100 % of the wave function density. Another example of non-conservation of the wave function density is shown in the same figure (dashed lines and squares). Here the field is switched on instantly, but the initial polaron velocity changes from zero to $v_0 = 0.8$. Even if a part of the

charge leaves the polaron, it remains stable. But in this case its amplitude decreases, and the width increases because of the renormalization of the wave function on the polaron. Similar polaron behavior is observed for $\chi = 1.2$. However, in this case the polaron is more "compact" (it has a smaller width and a larger amplitude), the wave function is better attached to the polaron, and the polaron itself is more stable to the variation of the initial conditions.

Thus, figure 2 demonstrates the closer the initial conditions correspond to the stationary state of the polaron, the faster and more "confident" the polaron reaches this stationary, while maintaining the complete norm of the wave function. In all numerical simulation, only such initial conditions are used below, which provide at least 99 % localization of the wave function density at the polaron.

Stationary polaron velocity

Numerical simulations reveal that the relations between polaron parameters (amplitude, velocity, width) do not depend on the presence of the electric field. That is, the field initially only accelerates the polaron, and after that it moves at a constant velocity as if without the field. The influence of the electric field is discussed in more detail below.

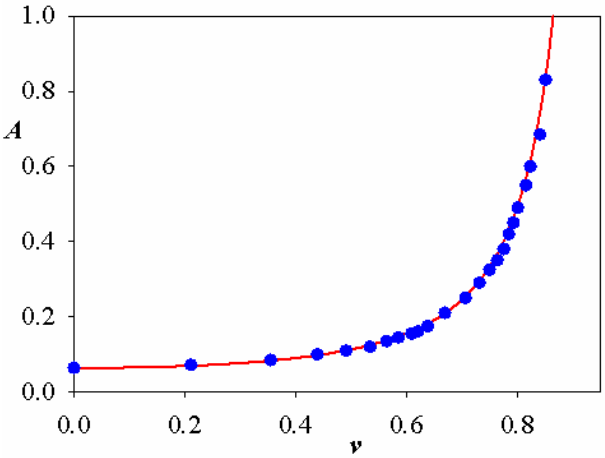

Figure 3. Amplitude of relative displacements A *vs* polaron velocity v without electric field (solid line is analytics[83]) and in electric field (circles, numerical simulation); $\chi = 0.4$

Figure 3 shows the relation between the amplitude and the velocity of the polaron in the electric field and without the field for the EPI parameter $\chi = 0.4$. Circles in figure 3corresponds to data in Figure 1 when the polaron accelerates in electric field of different values. For larger values of χ, e.g. $\chi = 1.2$, the continual approximation is not applicable because the corresponding polaron is narrow. However, as the polaron with $\chi = 1.2$ is much more stable in the electric field and quickly reaches the stationary state, the initial values of the polaron parameters are less significant. And it is reasonable to set initial conditions according to eqn. (6), choosing polaron parameters so that at least 99 % of the wave function density is localized at the polaron during the further evolution. In this case the wave function is the lowest-energy eigenfunction at the Hamiltonian diagonalization (eqn. 3).

The dependence of the steady-state velocity on the field strength B is weakly logarithmic. Figure 4 demonstrates less than 10 % difference in stationary polaron velocities within four orders of magnitude of the field strength. Therefore, in polyacetylene and DNA, the stationary polaron velocity slightly depends on the applied electric field. The small polaron velocity in very low field can be explained by the fact that the polaron has not yet reached a stationary state during the numerical simulation ($t \leq 10000$). Note, the dependences in Figure 4 are in good agreement with the dependences of the polaron velocity on the applied field.[80]

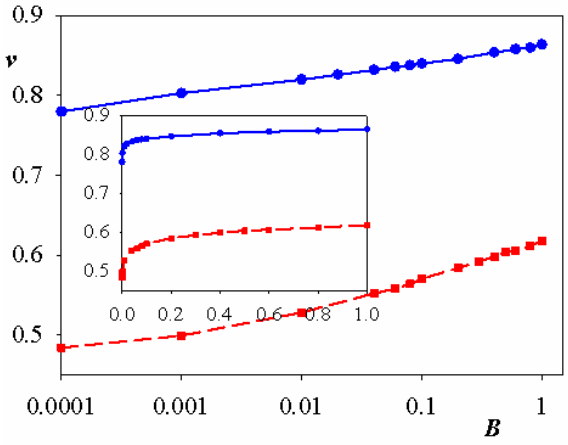

Figure 4. Stationary polaron velocity v *vs* electric field parameter B for $\chi = 1.2$ (dashed line and squares) and $\chi = 0.4$ (solid line and circles). The dimensionless velocity is measured in units of sound velocities. The inset shows dependencies in linear coordinates.

Generation of longitudinal coherent vibrations

The energy transferred from the electric field to the polaron, in general, can be used in several ways. First, this energy can be spent on accelerating the polaron and, accordingly, on increasing its kinetic energy. Secondly, energy can provide growth of potential energy due to a change in the polaron shape with an increase of the amplitude and a decrease of the width. Correspondingly, the electron energy changes due to the electron-phonon interaction. Finally, some of the energy can be transferred to lattice vibrations.

After the polaron reached a stationary state, the polaron continues to receive energy due to the interaction of the charge with the electric field. The constant power of this interaction is $p = fv_{st}$, where $f = eE$ (e is the polaron charge, E is the electric field strength, v_{st} is the stationary polaron velocity). In this case, the total energy of the "polaron + external field" system grows linearly with time. Since the polaron self-energy does not change, all the power consumed is converted only into lattice vibrational energy. Thus, the polaron velocity is determined by the balance of energies: the energy gained by the polaron in the electric field should be equal to the energy dissipated into the lattice.

The two top panels of figure 5 show snapshots of particles relative displacements $q_j \equiv (x_{j+1} - x_j)$ for $\chi = 0.4$ (left top panel) and $\chi = 1.2$ (right top panel). The polaron moves from left to right and is located on right ends. The lattice oscillations following the moving polaron can be divided into two regions. In region a, the oscillations are irregular

because they are generated during the field switching-on period. Region b can cover several thousand lattice periods and represents coherent oscillations. (Figure 6.)

The time dependence of chosen bond $q_{500} = x_{501} - x_{500}$ oscillations is shown in Figure 6. Polaron passes the bond at $t = 762$. After this, the bond oscillates with constant frequency and amplitude. The apparent amplitude modulation is due to the incommensurability of the oscillations period and the period of the particle displacement measurement, as illustrated in the inset to the figure.

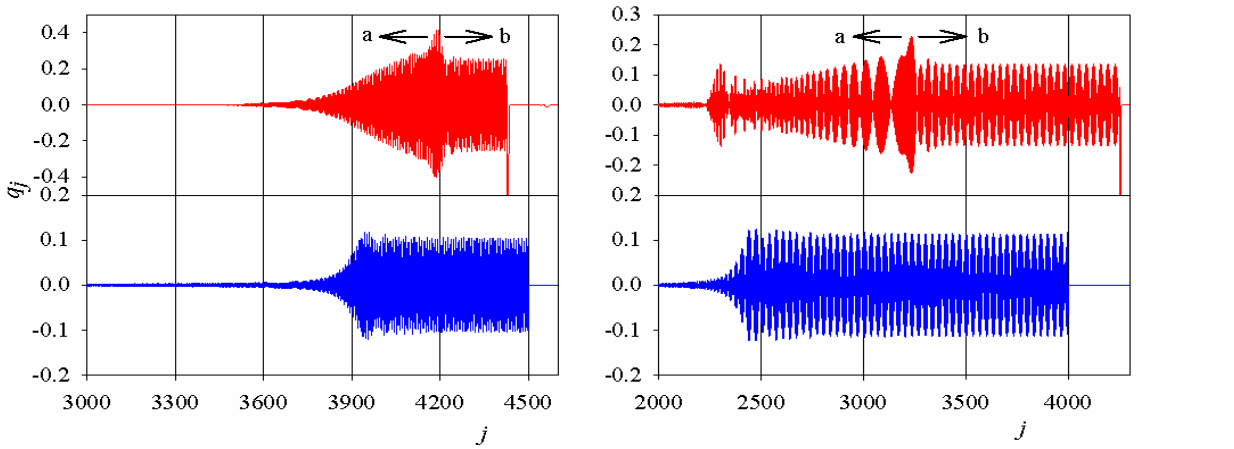

Figure 5. Snapshots of the relative displacements q_j at the time t. Upper row: polaron on the harmonic lattice in electric field. The left upper panel: $\chi = 0.4$, $v_0 = 0.8$, $B = 0.1$, $t = 2250$. The right upper panel: $\chi = 1.2$, $v_0 = 0.65$, $B = 1.0$, $t = 2825$. In both cases, the polaron was initially located at $j_0 = 2500$ and the field switching-on rate is $c = 1/1250$. Polarons are centered at $j = 4380$ and $j = 4420$ in the left and right panels, respectively. Lower row: the "demon" model (see Section 3.5). The lower left panel: $v_d = 0.862$, $t = 2320$. The right lower panel $v_d = 0.617$, $t = 2430$. In both cases, the excitation is initially localized at $j_0 = 2500$.

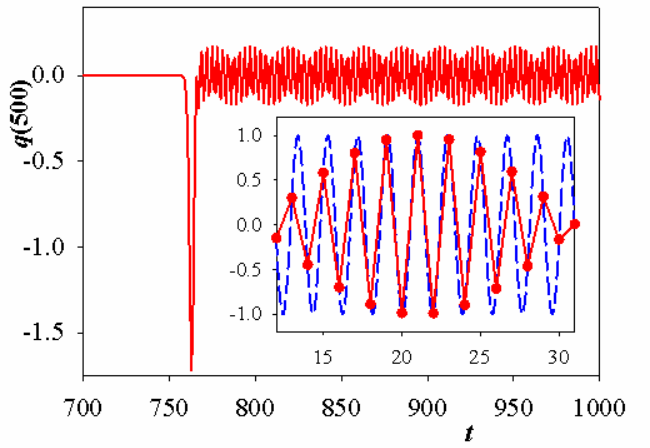

Figure 6. Relative displacement q_{500} *vs* time, $\chi = 1.2$. The inset illustrates the incommensurability of the true oscillations period (dashed line) and the period of numerical calculation (solid line).

Both space and time Fourie spectra have one peak corresponding to the wave number k (the wavelength $\lambda = 2\pi/k$), and frequency ω of the generated oscillations, respectively. Thus, moving polaron generates stable coherent oscillations described by the equation $q_j = C \sin(kj + \omega t + \varphi)$, where φ is the phase. The values of k and ω are determined by the polaron velocity and the amplitude is determined by the applied field strength, which is in agreement with the reported value.[80] The dependence of k and ω on polaron velocity is discussed below.

Spectral characteristics of generated coherent vibrations

In the previous section, it was shown that the generated vibrations have definite values of k and ω. Because of the fact that the field parameter B is uniquely related with the stationary polaron velocity (Figure 3), it is convenient to depict the spectral characteristics k and ω through the stationary polaron velocity v. These dependences are shown in figure 7.

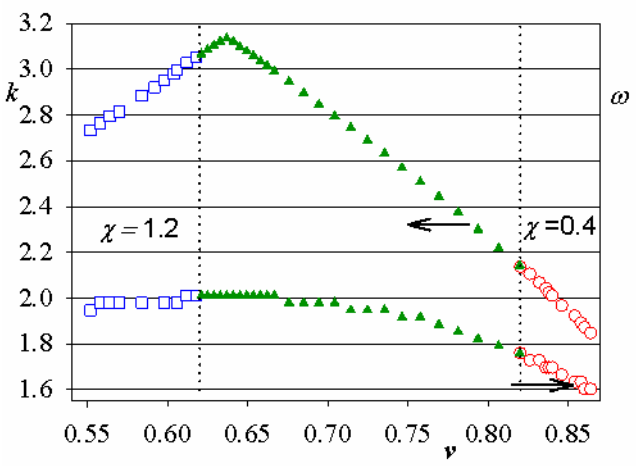

Figure 7. Dependences of the wave number k (upper curve and symbols) and the frequency ω (lower curve and symbols) on the polaron velocity for $\chi = 1.2$ (empty squares) and $\chi = 0.4$ (empty circles) and on the "demon" velocity (filled triangles). Symbols for the wave number refer to the left axis, and symbols for the frequency refer to the right axis.

It is seen that the wave numbers k of the oscillations generated by the polaron do not vary very much, $1.8 \le k \le 2.1$ for $\chi = 0.4$ in the velocity range $0.82 \le v \le 0.86$ (empty circles in Figure 7), and $2.7 \le k \le 3.1$

for χ=1.2 in the velocity range $0.55 \le v \le 0.62$ (empty squares in Figure 7). The character of k versus v dependences is different. The wave number increases with increasing speed for $\chi = 1.2$ (empty squares), and decreases for $\chi = 0.4$ (empty circles). The wavelength of the shortest-wave "optical" mode on the harmonic lattice is $\lambda = 2$ in the lattice constants, which corresponds to $k = \pi$. This means that for $\chi = 1.2$ the polaron excites the shortest-wave mode with $\lambda \approx 2.2$. For $\chi = 0.4$, the wavelength of the excited oscillations is slightly larger and $\lambda \approx 3.1$.

The oscillations frequencies are also not very different. The steps-like dependence of ω in Figure 7 is due to the finite value of the integration step. The decrease of the step increases the smoothness of the dependence of ω *vs* v. In dimensional units, the oscillation frequency is $\approx 2 \times 10^{12}$ Hz at the polaron velocity $v = 0.57$ ($\chi = 1.2$, DNA), and the frequency is $\approx 3 \times 10^{13}$ Hz at the polaron velocity $v = 0.86$ ($\chi = 0.4$, PA).

It was shown[80] that the wave number k depends on the polaron velocity v and it is determined by the following equation (mod 2π), where v_{snd} is the sound velocity and the frequency is determined by the dispersion equation

$$vk = v_{\mathrm{snd}} \sin(k/2) \qquad (8)$$

$$\varpi_k = v_{\mathrm{snd}} \left|\sin(k/2)\right| \qquad (9)$$

Our results are in good agreement with eqns. (8) and (9). Indeed, for $v = 0.8$ and $v = 0.65$ these equations give $k \approx 2.3$, $\omega \approx 1.8$ and $k \approx 3.1$, $\omega \approx 2.0$, respectively. These points fit well in figure 7.

"Demon" Model

As shown above, the moving polaron generates coherent vibrations, and the wave number and the frequency of these vibrations are determined by the applied field (or the polaron velocity). One can say that the polaron is an effective "generator" of stable coherent lattice vibrations, and thousands of lattice sites can participate in these oscillations.

The polaron velocities fall in a narrow range of values ($0.56 \le v \le 0.62$ and $0.82 \le v \le 0.86$ for DNA and PA, respectively). It is a question, whether generation of such oscillations is possible in some other way than by localized moving compression of special shape. If possible, what are the spectral characteristics of these oscillations over a wider range of velocities of the generating source, and what should be the profile of the generative force.

In light of these questions, eqn. (8) deserves special attention. The fact is that eqn. (4) can be rewritten as $d^2x_j/dt^2 = -(2x_j - x_{j+1} - x_{j-1}) + f_j(t)$, where $f_j(t)$ is a generic force. The force has a profile of a moving impulse, while the profile itself can be of arbitrary shape. In this case, the wave number is determined from the eqn. (8), and the frequency from the dispersion law (eqn. 9).

We propose a simple model called "demon". This is a dynamic model of the compression moving on harmonic lattice in the absence of EPI. The compression has a step-like shape with a width of one lattice period. The power transferred to the lattice is constant in time and depends on the deformation value. In this model, the demon velocity can vary within $0 < v_d < 1$, which is out of the limits of polaron velocities for two EPI parameters under consideration. We consider the "demon" velocity varying in the range $0.55 \le v_d \le 0.9$.

Two lower panels of figure 5 show snapshots of the relative displacements in the harmonic lattice with moving "demon". Comparison of upper and lower panels demonstrates that the oscillations generated by "demon" are very similar to those generated by polaron moving with the same velocity.

Analysis of the spectral characteristics of the generated oscillations shows that the "demon" and the polaron moving with the same velocity excite oscillations with the same wave numbers and frequencies. In figure 7, the frequency and the wave number in the "demon" model are shown by filled triangles. It is seen that in the ranges of polaron velocities, the dependencies for the "demon" model and for polaron in electric field completely coincide. In this case, the wave numbers obey eqn. (8), and the frequencies are calculated from eqn. (9).

Eqn. (8) has a simple physical meaning. For all values of polaron velocity, the equation has one solution which is in the range $0 \le k \le 2\pi$, and this solution corresponds to the wave with phase velocity equal to the velocity of the generating source ($v_{phase} = \omega/k$). It is obvious from combination of eqns. (8) and (9). For small velocities ($v \le 0.13$), eqn. (8) has more than one solutions. For example, for $v = 0.1$ there are three solutions, $k_1 = 5.705$, $k_2 = 14.136$, and $k_3 = 16.846$. One can easily check that all three waves with corresponding wave numbers are presented in the Fourie spectra of vibrations generated by "demon" moving with $v = 0.1$.

Critical electric field

The equations of motion (4) and (5) do not imply any limitation on value of electric field. Really, we did not find a maximum field in the range of reasonable values if appropriate initial conditions are chosen, in particular the field switching-on rate is rather low. The situation drastically changes if the field is switch on instantaneously, and it is the instantaneous field switching-on has a physical sense.

The theoretical estimation of critical field has been reported.[80] Estimations are based on the fact that, when the large field is switched on instantly, a tilted potential is formed. The heavy and slow lattice does not have time to readjust. However, the electron can tunnel through the potential.

The critical field is defined as a field, when the probability of tunneling per unit time Γ_{tun} is of the same order of magnitude as the reciprocal of the lattice readjusting time, Γ_{lat}. For analytical estimations the triangular barrier is considered. Then the tunnelling probability can be estimated by the WKB method.[84] In the case of initial standing polaron the barrier height (the electronic part of the polaron binding energy) is $e_b = \chi^4/(K^2 t_0)$[80,85] and tunnelling is

$$\Gamma_{\text{tun}} = 4\exp\left[-\frac{4e_b^{3/2}}{3t_0^{1/2}eEa}\right] \quad (10)$$

The lattice readjusting time is estimated as the time necessary for the sound to pass a distance equal to the sum of the polaron width and the barrier width. Then Γ_{lat} has the form

$$\Gamma_{\text{lat}} = \frac{v_{\text{snd}}}{e_b/eEa+1/\chi^2} \quad (11)$$

The critical field can be estimated as

$$\Gamma_{\text{lat}} = \Gamma_{\text{tun}} \quad (12)$$

Since the tunnelling has a physical meaning in the continuum limit the above relations are true when the continuum approximation works, i.e. for sufficiently small χ. As we have already noted, $\chi = 0.4$ is the limiting value of the electron-phonon interaction, when the continuum approximation is well applicable. So we can expect an agreement between analytical and numerical estimations of critical field. For $\chi = 0.4$, eqns. (10)-(12) give values $E^{\text{cr}} \approx 0.00071$ in dimensionless units, which corresponds to $B^{\text{cr}} = eaE^{\text{cr}}/\hbar \approx 0.076$.

In numerical experiment we determine the fraction of electron density remaining on the polaron $\Delta|\Psi|^2$ if the field is switched on instantly in the case of initial standing polaron (see figure 8). For field upto $B \approx 0.04$, almost 100 % of electron density is localized at the polaron. For higher values of B, $\Delta|\Psi|^2$ drastically decreases. We define the critical field as a field at which about 90 % of the total electron density remains on the polaron. Then numerical experiment gives $B_{\text{cr}}^{\text{num}} \approx 0.07$, which is in good agreement with analytical estimation. This value corresponds to $4.7 \cdot 10^7$ V/m in dimension units. (Figure 8)

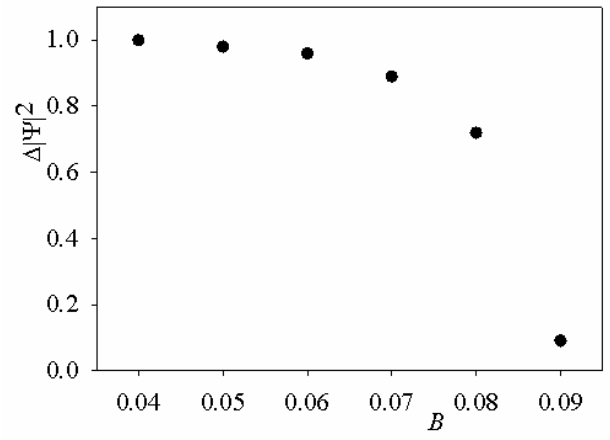

Figure 8. A fraction of electron density localized on the polaron $\Delta|\Psi|^2$ after the instantaneous switching-on of the electric field *vs* field parameter B; $\chi = 0.4$.

In the case of $\chi = 1.2$, we can hardly expect such a coincidence between theoretical prediction and numerical results, because for large values of χ, the continuum approximation does not work. However, some estimations can be done. For $\chi = 1.2$, the manually fitted parameters are $A \approx 0.78$ and $d \approx 0.7$ for standing polaron and the numerically calculated barrier height (the electronic part of the polaron coupling energy) is about 0.96. Then equations (10)-(12) give the magnitude of the critical field parameter $B_{1.2}^{\text{cr}} \approx 18$. This value is slightly higher than those estimated numerically $B_{1.2}^{\text{num}} \approx 13$. However, taking into account that equations (10)-(12) are derived in an approximation that does not work for $\chi = 1.2$, such a coincidence is surprising. Note, $B_{1.2}^{\text{num}}$ corresponds to $2 \cdot 10^8$ V/m for DNA.

CONCLUSIONS

Polarons on harmonic lattice with EPI parameter corresponding PA and DNA are very stable in a constant electric field.

The results of the numerical simulation are rather sensitive to the initial conditions and to the method of switching-on the electric field. The main criterion of the simulation correctness is the complete localization of the electron density on the polaron. With unsuccessful initial conditions, a part of the electron density decouples from the lattice deformation. In all presented results at least 99 % of the total electron density is localized on the polaron. In the case of complete localization of the electron density on the polaron, the results do not depend on the initial conditions and the method of switching-on the electric field.

The polaron moves with constant velocity in electric field. The dependence of the stationary velocity on the applied field is weakly logarithmic. Within four orders of magnitude of the field strength, stationary velocities vary ≤ 10 %. This means that in polyacetylene and DNA the dependence of the polaron velocity on the applied electric field is insignificant.

The parameters (amplitude, width, velocity) of a stationary moving polaron in an electric field coincide with the parameters of a polaron moving with the same velocity in the absence of an electric field, which indicates the adiabatic polaron movement.

Polaron moving in electric field generates coherent oscillations. The spectral characteristics of the generated oscillation are well described by a simple "demon" model. This means that any moving localized excitation of arbitrary shape generates coherent oscillations of the harmonic lattice. The phase velocity of generated oscillations is equal to the polaron/"demon" velocity.

For appropriate initial conditions, i.e. adiabatically slow field switching-on rate or initially moving polaron, we did not find maximum value of the electric field resulting in polaron destruction. However, in the case of instantaneous field switching-on, rather low fields destroy initially standing polaron. The estimated values of critical field are $4.7 \cdot 10^7$ V m^{-1} and $2 \cdot 10^8$ Vm^{-1} for polyacetylene and DNA, respectively.

The numerical results of present work are in good agreement with theoretical predictions reported earlier.[80]

References

[1]Friedman, K. A., Heller, A., On the Non-Uniform Distribution of Guanine in Introns of Human Genes: Possible Protection of Exons against Oxidation by Proximal Intron Poly-G Sequences, *J. Phys. Chem. B*, **2001**, *105*, 11859. DOI: 10.1021/jp012043n

[2]Endres, R. G., Cox D. L., Singh R. R. P., The quest for high-conductance DNA, *Rev. Mod. Phys.*, **2004**, *76*, 195. DOI: 10.1103/RevModPhys.76.195

[3]Fink, H.-W., Schonenberger, Ch., Electrical conduction through DNA molecules, *Nature*, **1999**, *398*, 407. DOI:10.1038/18855

[4]Porath, D., Bezryadin, A., de Vries, S., Dekker, C., Direct measurement of electrical transport through DNA molecules, *Nature*, **2000**, *403*, 635. DOI:10.1038/35001029

[5]Genereux, J. C., Barton, J. K., Mechanisms for DNA Charge Transport, *Chem. Rev.*, **2010**, *110*, 1642. DOI: 10.1021/cr900228f

[6]Genereux, J. C., Wuerth, S. M., Barton, J. K., Single-Step Charge Transport through DNA over Long Distances,, *J. Am. Chem. Soc*., **2011**, *133*, 3863. DOI: 10.1021/ja107033v

[7]Arikuma, Y., Nakayama, H., Morita, T., Kimura, S., Electron Hopping over 100 Å Along an α Helix, *Angew. Chem. Int. Ed*., **2010**, 49, 1800. DOI: 10.1002/anie.200905621

[8]Augustyn, K. E., Genereux, J. C., Barton, J. K., Distance-Independent DNA Charge Transport across an Adenine Tract, *Angew. Chem. Int. Ed.*, **2007**, *46*, 5731. DOI: 10.1002/anie.200701522

[9]Barton J. K., Olmon E. D., Sontz, P. A., Metal Complexes for DNA-Mediated Charge Transport, *Coordin. Chem. Rev*., **2011**, *255*, 619. DOI: 10.1016/j.ccr.2010.09.002

[10]Slinker, J. D., Muren, N. B., Renfrew, S. E., Barton, J. K., DNA charge transport over 34 nm, *Nat. Chem.*, **2011**, *3*, 228. DOI:10.1038/nchem.982

[11]Cordes, M., Giese, B., Electron transfer in peptides and proteins, *Chem. Soc. Rev*., **2009**, *38*, 892. DOI: 10.1039/B805743P

[12]Astakhova, T. Yu., Likhachev, V. N., Vinogradov, G. A., Long-range charge transfer in biopolymers, *Russ. Chem. Rev*., **2012**, *81*, 994. DOI: 10.1070/RC2012v081n11ABEH004308

[13]Su, W. P., Schrieffer, J. R., Heeger, A. J., Solitons in Polyacetylene, *Phys. Rev. Lett*., **1979**, *42*, 1698. DOI: 10.1103/PhysRevLett.42.1698

[14]Su, W. P., Schrieffer, J. R., Heeger, A. J., Soliton excitations in polyacetylene, *Phys. Rev. B*, **1980**, *22*, 2099. DOI: 10.1103/PhysRevB.22.2099

[15]Su, W. P., Schrieffer, J. R., Soliton dynamics in polyacetylene, *Proc. Natl. Acad. Sci. USA*, **1980**, *77*, 5626. DOI: 10.1073/pnas.77.10.5626

[16]Su, W. P., Schrieffer, J. R., Fractionally Charged Excitations in Charge-Density-Wave Systems with Commensurability 3, *Phys. Rev. Lett.*, **1981**, *46*, 738. DOI: 10.1103/PhysRevLett.46.738

[17]Takayama, H., Lin-Liu, Y. R., Maki K., Continuum model for solitons in polyacetylene, *Phys. Rev. B*, **1980**, *21*, 2388. DOI: 10.1103/PhysRevB.21.2388

[18]Wilson, E. G., *J. Phys. C*, A new theory of acoustic solitary-wave polaron motion, **1983**, *16*, 6739. DOI: 10.1088/0022-3719/16/35/008

[19]Arikabe Y., Kuwabara, M., Ono, Y., Dynamics of an Acoustic Polaron in One-Dimensional Electron-Lattice System, *J. Phys. Soc. Jpn*., **1996**, *65*, 1317. DOI: 10.1143/jpsj.65.1317

[20]Marcus, R. A., Electron Transfer Reactions in Chemistry: Theory and Experiment, *Angew. Chem., Int. Edit*., **1993**, *32*, 1111. DOI: 10.1002/anie.199311113

[21]Sartor, V., Boone, E., Schuster, G. B., Long-Distance Radical Cation Migration through A/T Base Pairs in DNA: An Experimental Test of Theory, *J. Phys. Chem. B*, **2001**, *105*, 11057. DOI: 10.1021/jp011354v

[22]Meggers, E., Michel-Beyerle, M. E., Giese, B., Sequence Dependent Long Range Hole Transport in DNA, *J. Am. Chem. Soc*., **1998**, *120*, 12950. DOI: 10.1021/ja983092p

[23]Conwell, E. M., Rakhmanova, S. V., Polarons in DNA, *Proc. Natl. Acad. Sci. USA*, **2000**, *97*, 4556. DOI: 10.1073/pnas.050074497

[24]Rakhmanova, S. V., Conwell, E. M., Polaron Motion in DNA, *J. Phys. Chem. B*, **2001**, *105*, 2056. DOI: 10.1021/jp0036285

[25]Conwell, E. M., Basko, D. M., Hole Traps in DNA, *J. Am. Chem. Soc*., **2001**, *123*, 11441. DOI: 10.1021/ja015947v

[26]Conwell, E. M., Charge transport in DNA in solution: The role of polarons, *Proc. Natl. Acad. Sci*., 2005, *102*, 8795. DOI: 10.1073/pnas.0501406102

[27]Komineas, S., Kalosakas, G., Bishop, A. R., Effects of intrinsic base-pair fluctuations on charge transport in DNA, *Phys. Rev. E*, **2002**, *65*, 061905. DOI: 10.1103/PhysRevE.65.061905

[28]Kalosakas, G., Rasmussen, K. O., Bishop, A. R., Charge trapping in DNA due to intrinsic vibrational hot spots, *J. Chem. Phys*., **2003**, *118*, 3731. DOI: 10.1063/1.1539091

[29]Chang, C.-M., Castro Neto, A. H., Bishop, A.R., Long-range charge transfer in periodic DNA through polaron diffusion, *Chem. Phys.*, **2004**, *303*, 189. DOI: 10.1016/j.chemphys.2004.05.015

[30]Berashevich, J. A., Bookatz, A. D., Chakraborty, T., The electric field effect and conduction in the Peyrard–Bishop–Holstein model, *J. Phys.- Condens. Mat.*, **2008**, *20*, 035207. DOI: 10.1088/0953-8984/20/03/035207

[31]Berashevich, J. A., Chakraborty, T., Electronic parameters for the hole transfer in DNA duplex oligomers, *Chem. Phys. Lett*., **2007**, *446*, 159. DOI: 10.1016/j.cplett.2007.08.045

[32]Hawke, L. G. D., Kalosakas, G., Simserides, C., Electronic parameters for charge transfer along DNA, *Eur. Phys. J. E*, **2010**, *32*, 291. DOI: 10.1140/epje/i2010-10650-y

[33]Yamada, H., Starikov, E. B., Hennig, D., Quantum diffusion in polaron model of poly(dG)-poly(dC) and poly(dA)-poly(dT) DNA polymers, *Eur. Phys. J. B*, **2007**, *59*, 185. DOI: 10.1140/epjb/e2007-00274-4

[34]Kalosakas, G., Charge transport in DNA: Dependence of diffusion coefficient on temperature and electron-phonon coupling constant, *Phys. Rev. E*, **2011**, *84*, 051905. DOI: 10.1103/PhysRevE.84.051905

[35]Kucherov, V. M., Kinz-Thompson, C. D., Conwell, E. M., Polarons in DNA Oligomers, *J. Phys. Chem. C*, **2010**, *114*, 1663. DOI: 10.1021/jp908809t

[36]Qu Z., Kang, D. W., Jiang, H., Xie, S. J., Temperature effect on polaron dynamics in DNA molecule: The role of electron-base interaction, *Physica B*, **2010**, *405*, S123. DOI: 10.1016/j.physb.2009.12.020

[37]Triberis, G., Simserides, C., Karavolas, V., A small polaron hopping model for multiphonon-assisted transport along DNA molecules,in the presence of disorder, *Physica E*, **2006**, *32*, 592. DOI: 10.1016/j.physe.2005.12.111

[38]Cuniberti, G., Fagas, G., Richter, K., Fingerprints of mesoscopic leads in the conductance of a molecular wire, *Chem. Phys*., **2002**, *281*(*2-3*), 465. DOI: 10.1016/S0301-0104(02)00341-5

[39]Todorov, T. N., Tight-binding simulation of current-carrying nanostructures, *J. Phys.-Condens. Mat.*, **2002**, *14*(*11*), 3049. DOI: 10.1088/0953-8984/14/11/314

[40]Lima, M. P., e Silva, G. M., Dynamical evolution of polaron to bipolaron in conjugated polymers, *Phys. Rev. B*, **2006**, *74*, 224304. DOI: 10.1103/PhysRevB.74.224304

[41]e Silva, G. M., Electric-field effects on the competition between polarons and bipolarons in conjugated polymers, *Phys. Rev.* B, **2000**, *61*, 10777. DOI: 10.1103/PhysRevB.61.10777

[42]Peng, C., Jian, W., GuiQing, Zh., ChengBu, L., Hole polarons in poly(G)-poly(C) and poly(A)-poly(T) DNA molecules, *Sci. China Ser. B*, **2008**, *51*, 1182. DOI: 10.1007/s11426-008-0128-y

[43]Basko, D. M., Conwell, E. M., Self-trapping versus trapping: Application to hole transport in DNA, *Phys. Rev. E*, **2002**, *65*, 061902. DOI: 10.1103/PhysRevE.65.061902

[44]Zheng, B., Wu, J., Sun, W., Liu, Ch., Trapping and hopping of polaron in DNA periodic stack, *Chem. Phys. Lett*, **2006**, *425*, 123. DOI:10.1016/j.cplett.2006.05.022

[45]Lin, X., Li, J., Smela, E., Yip, S., Polaron-induced conformation change in single polypyrrole chain: An intrinsic actuation mechanism, *Int. J. Quantum Chem.*, **2005**, *102*, 980. DOI: 10.1002/qua.20433

[46]Falleiros, M. B., e Silva, G. M., Polaron and bipolaron stability on paraphenylene polymers, *J. Mol. Model*., **2017**, *23*, 59. DOI: 10.1007/s00894-017-3215-1

[47]Ma, H., Schollwock, U., Dynamical simulations of polaron transport in conjugated polymers with the inclusion of electron-electron interactions, *J. Phys. Chem. A*, **2009**, *113*(*7*), 1360. DOI: 10.1021/jp809045r

[48]Ribeiro, L. A., da Cunha, W. F., de O. Neto, P. H., Gargano, R., e Silva, G. M., Effects of temperature and electric field induced phase transitions on the dynamics of polarons and bipolarons, *New J. Chem.*, **2013**, *37*, 2829. DOI: 10.1039/c3nj00602f

[49]Hultell, M., Stafstrom, S., Polaron dynamics in highly ordered molecular crystals**,** *Chem. Phys. Lett*., **2006**, *428*, 446. DOI:10.1016/j.cplett.2006.07.042

[50]Johansson, A., Stafstrom, S., Polaron Dynamics in a System of Coupled Conjugated Polymer Chains**,** *Phys. Rev. Lett.*, **2001**, *86*, 3602. DOI: 10.1103/PhysRevLett.86.3602

[51]Johansson, A., Stafstrom, S., Soliton and polaron transport in *trans*-polyacetylene, *Phys. Rev. B*, **2002**, *65*, 045207. DOI: 10.1103/PhysRevB.65.045207

[52]Alexandrov, A. S., Yavidov, B. Ya., Small adiabatic polaron with a long-range electron-phonon interaction, *Phys. Rev. B*, **2004**, *69*, 073101. DOI: 10.1103/PhysRevB.69.073101

[53]Diaz, E., Lima, R. P. A., Dominguez-Adame, F., Bloch-like oscillations in the Peyrard-Bishop-Holstein model, *Phys. Rev. B*, **2008**, *78*, 134303. DOI: 10.1103/PhysRevB.78.134303

[54]Hague, J. P., Kornilovitch, P. E., Alexandrov, A. S., Samson, J. H., Effects of lattice geometry and interaction range on polaron dynamics, *Phys. Rev. B*, **2006**, *73*, 054303. DOI: 10.1103/PhysRevB.73.054303

[55]Mozafari, E., Stafstrom, S., Polaron dynamics in a two-dimensional Holstein-Peierls system, *J. Chem. Phys.*, **2013**, *138*, 184104. DOI: 10.1063/1.4803691

[56]Wei, J. H., Liu, X. J., Berakdar, J., Yan, YiJing, Pathways of polaron and bipolaron transport in DNA double strands, *J. Chem. Phys.*, **2008**, *128*, 165101. DOI: 10.1063/1.2902279

[57]Luo, J., Piette, B. M. A. G., A generalised Davydov-Scott model for polarons in linear peptide chains, *Eur. Phys. J. B*, **2017**, *90*, 155. DOI: 10.1140/epjb/e2017-80209-2

[58]Hennig, D., Neibner, C., Velarde, M. G., Ebeling, W., Effect of anharmonicity on charge transport in hydrogen-bonded systems, *Phys. Rev. B*, **2006**, *73*, 024306. DOI: 10.1103/PhysRevB.73.024306

[59]da Cunha, W. F., Neto, P. H. de O., Gargano, R., e Silva, G. M., Temperature effects on polaron stability in polyacetylene, *Int. J. Quantum Chem.*, **2008**, *108*, 2448. DOI: 10.1002/qua.21798

[60]Zhang, Y. L., Liu, X. J., An, Z., Temperature dependence of polaron stability in conjugated polymers, *Europhys. Lett*, **2015**, *111*, 17009. DOI: 10.1209/0295-5075/111/17009

[61]Yao, Y., Qiu, Y., Wu, Ch.-Q., Dissipative dynamics of charged polarons in organic molecules, *J. Phys.- Condens. Matter*, **2011**, *23*, 305401. DOI: 10.1088/0953-8984/23/30/305401

[62]Ojeda J. H., Lima, R. P. A., Dominguez-Adame, F., Orellana, P. A., Trapping and motion of polarons in weakly disordered DNA molecules, *J. Phys.- Condens. Matter*, **2009**, *21*, 285105. DOI:10.1088/0953-8984/21/28/285105

[63]Zhang, G., Cui, P., Wu, J., Liu, Ch., Structural fluctuation effect on the polaron in DNA, *Physica B*, **2009**, *404*, 1485. DOI:10.1016/j.physb.2009.01.004

[64]Yan, Y. H., An, Z., Wu, C.Q., Dynamics of polaron in a polymer chain with impurities, *Eur. Phys. J. B*, **2004**, *42*, 157. DOI: 10.1140/epjb/e2004-00367-6

[65]Wang, Y. D., Zhang, X. G., Meng, Y., Di, B., Zhang, Y. L., An, Z., Dynamic recombination of polaron pair with impurity in conjugated polymers, *Org. Electron.*, **2017**, *49*, 286. DOI: 10.1016/j.orgel.2017.06.067

[66]Johansson, A, Stafstrom, S., Nonadiabatic simulations of polaron dynamics, *Phys. Rev. B*, **2004**, *69*, 235205. DOI: 10.1103/PhysRevB.69.235205

[67]Li, Y., Liu, X.-J., Fu, J.-Y., Liu, D-Sh., Xie, Sh.-J., Mei, L.-M., Bloch oscillations in a one-dimensional organic lattice, *Phys. Rev. B*, **2006**, *74*, 184303. DOI: 10.1103/PhysRevB.74.184303

[68]Ono, Y., Terai, A., Motion of Charged Soliton in Polyacetylene Due to Electric Field, *J. Phys. Soc. Jpn*., **1990**, *59*, 2893. DOI: 10.1143/JPSJ.59.2893

[69]Liu, X., Gao, K., Fu, J., Li, Y., Wei, J., Xie, Sh., Effect of the electric field mode on the dynamic process of a polaron, *Phys. Rev. B*, **2006**, *74*, 172301. DOI: 10.1103/PhysRevB.74.172301

[70]Zhang, G., Hu, H., Cui, S., Lv, Z., Higher order tight binding Su–Schrieffer–Heeger method and its applications in DNA charge transport, *Physica B*, **2010**, *405*, 4382. DOI:10.1016/j.physb.2010.07.047

[71]Thornber, K. K., Feynman, R. P., Velocity Acquired by an Electron in a Finite Electric Field in a Polar Crystal, *Phys. Rev. B*, **1970**, *1*, 4099. DOI: 10.1103/PhysRevB.1.4099

[72]Ribeiro, L. A., da Cunha, W. F., Fonseca, A. L. de A., e Silva, G. M., Bloch oscillations in organic and inorganic polymers, *J. Chem. Phys*., **2017**, *146*, 144903. DOI: 10.1063/1.4979950

[73]da Silva, M. V. A., Neto, P. H. de O., Cunha, W. F. da, Gargano, R., e Silva, G. M., Supersonic quasi-particles dynamics in organic semiconductors, *Chem. Phys. Lett.*, **2012**, *550*, 146. DOI: 10.1016/j.cplett.2012.09.012

[74]Rakhmanova, S. V., Conwell, E. M., Polaron dissociation in conducting polymers by high electric fields, *Appl. Phys. Lett*., **1999**, *75*, 1518. DOI: 10.1063/1.124741

[75]Rakhmanova, S. V., Conwell, E. M., Nonlinear dynamics of an added carrier in trans-polyacetylene in the presence of an electric field, *Synthetic Met.*, **2000**, *110*, 37. DOI: 10.1016/S0379-6779(99)00261-1

[76]Mahani, M. R., Mirsakiyeva, A., Delin, A., Breakdown of Polarons in Conducting Polymers at Device Field Strengths, *Phys. Chem. C*, **2017**, *121*, 10317. DOI: 10.1021/acs.jpcc.7b02368

[77]Yu, J. F., Wu, C. Q., Sun, X., Nasu, K., Breather in the motion of a polaron in an electric field, *Phys. Rev. B*, **2004**, *70*, 064303. DOI: 10.1103/PhysRevB.70.064303

[78]Vidmar, L., Bonca, J., Mierzejewski, M., Prelovsek, P., Trugman, S. A., Nonequilibrium dynamics of the Holstein polaron driven by an external electric field, *Phys. Rev. B*, **2011**, *83*, 134301. DOI: 10.1103/PhysRevB.83.134301

[79]Nazareno, H. N., de Brito, P. E., Bloch oscillations as generators of polarons in a 1D crystal, *Physica B*, **2016**, *494*, 1. DOI: 10.1016/j.physb.2016.04.029

[80]Basko, D. M., Conwell, E. M., Stationary Polaron Motion in a Polymer Chain at High Electric Fields, *Phys. Rev. Lett*., **2002**, *88*, 056401. DOI: 10.1103/PhysRevLett.88.056401

[81]Likhachev, V. N., Astakhova, T. Yu., Vinogradov G.A., Поляроны в одномерной решетке. I. Неподвижный полярон*Russ. Khim. Fiz.*, **2013**, *32*, 3. DOI: 10.7868/S0207401X13040092

[82]Carstea, A. S., Integrable systems related to Su-Schrieffer-Heeger lattices, *Chaos Soliton Fract*, **2009**, 42, 923. DOI: 10.1016/j.chaos.2009.02.034

[83]Astakhova, T. Yu., Likhachev, V. N., Vinogradov, G. A., Polaron on a one-dimensional lattice: II. A moving polaron, *Russ. J. Phys. Chem. B*, **2013**, *7*, 521. DOI: 10.1134/S199079311305028X

[84]Landau, L. D., Lifshitz, E. M., *Quantum Mechanics, Non-relativistic Theory, Second edition, revised and enlarged*, Pergamon Press, **1965**, 174-175.

[85]Landau, L. D., Lifshitz, E.M., *Quantum Mechanics, Non-relativistic Theory, Second edition, revised and enlarged*, Pergamon Press, **1965**, 72-73.

Received: 01.06.2018.
Accepted: 17.08.2018.

POTENTIOMETRIC STUDY FOR RAPID CONTINUOUS MONITORING OF TRACE LEVEL THIOCYANATE USING SOLID AND CONVENTIONAL TYPES PVC MEMBRANE SENSORS

Saad S. M. Hassan[a]*, Ayman H. Kamel[a]*, Heba Abd El-Naby[a] and M. Abdelwahab Fathy[a]

Key words*:* Potentiometry, conventional sensors, solid state; thiocyanate, flow injection analysis, biological fluids.

A comparative study using two different thiocyanate electrode designs was conducted; a solid type electrode (type A) and conventional liquid inner contact electrode (type B). The fabrication of these electrodes was based on Al (III) [4-(2-Pyridylazo) resorcinol] (Al/PAR) and Mg (II) phthalocyanine (MgPC) complexes as a charged carrier, aliquate 336S and TDMAC as ion exchangers in plasticized poly (vinyl chloride) membrane. Electrodes type (A) revealed significantly enhanced response towards SCN^- ions with displayed near-Nernstian slope of -53.7 - -55.8 mV decade^{-1} over the concentration range 5.0x10^{-6}-1.0x10^{-2} mol L^{-1} and a detection limit of 0.4-3.7 µg mL^{-1}. Type (B) sensors revealed near-Nernstian potential response to SCN^- with a slope of -45.9 - -62.4 mV decade^{-1} over a linear range of 5.0x10^{-5}-1.0x10^{-2} mol L^{-1} and a detection limit of 0.12-0.3 µg mL^{-1}. Membrane sensors based on (Al/PAR) and (MgPC) using the so called "fixed interference method" (FIM) exhibited a good selectivity over different anions which differ significantly from the classical Hofmeister series. All sensors were integrated in a flow system for continuous monitoring of thiocyanate under hydrodynamic mode of operation. The sensors revealed a frequency of ~ 54 samples h^{-1}. Application of the proposed sensors for SCN^- determination in biological fluid samples such as saliva collected from some non-smoker and smoker donors. Determination of cyanide content in electroplating wastewater samples after its conversion into thiocyanate was also applied. The results obtained from the proposed sensors were agreed with that obtained using the standard methods of thiocyanate and cyanide analysis.

* Corresponding Authors
Fax: +20 2 26822991
E-Mail: saadsmhassan@yahoo.com (S.S.M. Hassan); ahkamel76@sci.asu.edu.eg (Ayman H. Kamel)
[a] Department of Chemistry, Faculty of Science, Ain Shams University, Cairo, Egypt

INTRODUCTION

Potentiometric ion-sensors have become a versatile instrument in chemical analysis because of their wide applications in different fields such as clinical diagnostics and environmental monitoring.[1-5] Ease of use, simplicity, ease of manipulation and no sample pre-treatment have replaced for long other wet analytical methods, because they offer high precision and rapidity, low cost, high selectivity and enhanced sensitivity over a wide linear range of concentrations. From all of the above, potentiometric sensors can be used as appropriate devices for process control.

Good analytical performances were noticed for conventional potentiometric sensors such as potential stability, short response time and high selectivity. On the other hand, low detection limit and lack of miniaturization were also noticed. Significant progress, concerning construction and analytical parameters of potentiometric sensors could be noticed in the last three decades.[6-9] This goal has been achieved in potentiometric sensors having a liquid internal contact by reducing zero-current trans-membrane ion flux effects. For that, the primary ion activity in the internal filling solution is kept at a low level by using ion buffers[10,11] or ion-exchange resins.[12] A carefully designed internal solution reduces trans-membrane concentration gradients through the partial exchange of primary ions by interfering ones on the inner membrane side.[13] However, a significant drawbacks of these sensors are miniaturization and difficulty in use due to the presence of this internal filling solution. This requires avoiding leakage via alignment of the sensor in a vertical position, refilling the solution; moreover, there are problems with shape tailoring.

A new trial regarding solution-free sensors was proposed, based on inclusion of additional layer between the membrane and support, called solid contact ion selective electrodes (SC-ISEs).[14] The first reported SC-ISEs were commonly referred to as coated-wire electrodes (CWEs).[15] In which, a sensing polymeric membrane is directly coated onto an electronic conductor. These sensors have a high potential drift due to the “blocked” interface between the sensing membrane and the electronic conductor.[16] These initial detections soonheless led to dense research to introduce materials that facilitate the charge transfer at the interface between the ion conducting membrane and the electronic conductor "ion-to-electron transduction". The most promising “ion-to-electron transducers” introduced to date include conducting polymers[17–20] and different carbon structures such as carbon nanotubes,[21, 22] graphene,[23–25] and colloid-imprinted mesoporous carbon.[26]

For biomedical analysis, relevant contributors to the potential at the membrane of sample interface are thiocyanate itself and interfering ions. For most applications, a solvent polymeric membrane is used. Perm-selectivity is a necessary condition for thiocyanate and is achieved by

incorporating cationic sites in the membrane, addition of an ion complexing agent or ionophore to the membrane. Many ionophores have been used for thiocyanate monitoring using solid contact potentiometric electrodes. [27-32] Although these sensors exhibit an anti-Hoffmeister selectivity order, they suffer from strong interference by I^-, CN^-, NO_2^-, IO_4^-, ClO_4^-, Br^-, and N_3^-. In addition, some of these sensors suffer from the disadvantages of limited range of the linear response, and a long response time.

In this work, a comparative study concerning slopes, detection limits, concentration ranges and selectivity for a potentiometric determination of SCN^- using ion selective membrane was made between two types of transducers: high double layer capacitance (Solid contact) e.g graphite/graphene sensors type (A) and classical inner filling solution (Liquid contact) sensors type (B).

Herein, we present a novel potentiometric thiocyanate membrane sensors based on the Al(III) [4-(2-Pyridylazo) resorcinol] (Al/PAR) and Mg (II) phthalocyanine (MgPC) complexes as a charged carrier, aliquate 336S and TDMAC as ion exchangers in plasticized poly (vinyl chloride) membrane are described and developed. These sensors were used for thiocyanate determination in saliva and urine fluids, and for the determination of cyanide in waste-water and electroplating samples after conversion into thiocyanate.

EXPERIMENTAL

An Orion (Cambridge, MA, USA) Model 720/SA pH /mV meter was used for all potential measurements. Thiocyanate membrane sensor in conjunction with an Orion double-junction Ag /AgCl reference electrode (Model 90-20) filled with 10% (w/v) KNO_3 were used for cell construction. For pH measurements, Ross glass electrode (Orion 81-02) was used.

Continuous monitoring of SCN^- using flow system was carried out using a two-channel peristaltic pump (Ismatech Ms-REGLO) integrated with an Omnifit injection valve (Omnifit, Cambridge, UK) with a sample loop of 500 µL volume. The potential readings were contineously recorded through the interface ADC 16 (Pico Tech, UK) and Pico Log software (version 5.07).

All UV/Vis measurements were conducted using spectrophotometer (Shimadzo, model 1601, Japan) under the recommended conditions of the standard method used for thiocyanate assessment.[33]

4-(2- monosodium salt monohydrate (PAR), tri-dodecyl methyl ammonium chloride (TDMAC), high molecular weight poly (vinyl chloride) (PVC), grapheme and *o*-nitrophenyloctyl ether (*o*-NPOE) were used as received from Fluka (Ronkonoma, NY). Tetrahydrofurane (THF) and Mg (II) phthalocyanine (MgPC) were purchased from Sigma (St. Louis, MO). Aliquat 336 was purchased from Acros. Aluminium potassium sulfate was purchased from (BDH chemicals Ltd). The buffer used in this work was 0.1 mol L^{-1} acetate buffer, pH 5.0.

Preparation of AL/PAR complex

Al/PAR ionophore (Figure 1) was prepared and structurally characterized using elemental and spectral analysis. To a solution containing 4-(2-pyridylazo) resorcinol monosodium salt monohydrate (PAR), (3.5 mmol) in 20 mL ethyl alcohol, $K[Al(SO_4)_2].12H_2O$ (1.5 mmol) was added. A solid precipitate was immediately produced, stirred at room temperature for 30 min, collected by filtration and washed with de-ionized water. The crude precipitate was re-crystallized from ethanol to give fine dark red crystals.

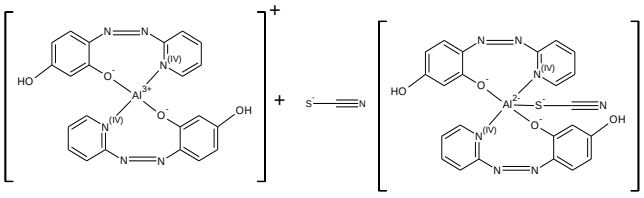

Figure 1. Chemical structure of Al (III)–PAR complex.

Sensor preparation and emf measurements

Liquid contact sensors were prepared as described previously.[34, 35] A 2.0 mg portion of the ionophore was mixed with 126 mg of the plasticizer, 66 mg of PVC, 1.0 mg TDMAC and dissolved in 3 mL THF in a glass ring (2.2 cm diameter). The cocktail left to stand overnight for solvent evaporation at room temperature. The master membrane was sectioned with a cork borer (10 mm diameter) and glued using THF to PVC tubing (~3 cm length, 8 mm; internal diameter). The PVC tube was attached to a 1 mL micropipet tip. The blue tip was internally filled with 10^{-2} mol L^{-1} thiocyanate solution. Homemade Internal reference electrode Ag/AgCl (1.0 mm diameter) was immersed in the internal reference solution. The conditioning solution was 10^{-2} mol L^{-1} SCN^- solution for 12 h and was stored in the same solution when not in use.

Solid contact sensors were fabricated as described previously[36] and as shown in Figure 2. A solid electrical contact is made from graphene which is characterized with high double layer capacitance. The epoxy metal mixture, used as supporting conductor, was obtained by pressing out an equal amount of both components onto the enclosed mixing tray. These two equal parts were mixed well with a synthetic spatula until a paste is obtained with a homogeneous color. This resulting paste was then mixed with graphite powder 1:1 mass ratio, introduced to the electrode body which is made from polypropylene and a copper disk with diameter 5.5 mm welded to a copper wire and immersed inside the paste. The electrodes were left to dry in air for 24 h. A volume of 10 µL of graphene solution (dissolved after sonication in THF) was applied onto the conductive layer. After dry, a volume of 20 µL of the membrane cocktail is applied at once by drop casting above the graphene layer. The membranes were left to dry at ambient temperature for 2 h before use. These solid contact electrodes were conditioned in a $1.0x10^{-2}$ mol L^{-1} aqueous SCN^- solution for 2 h before using and were stored dry when not in use.

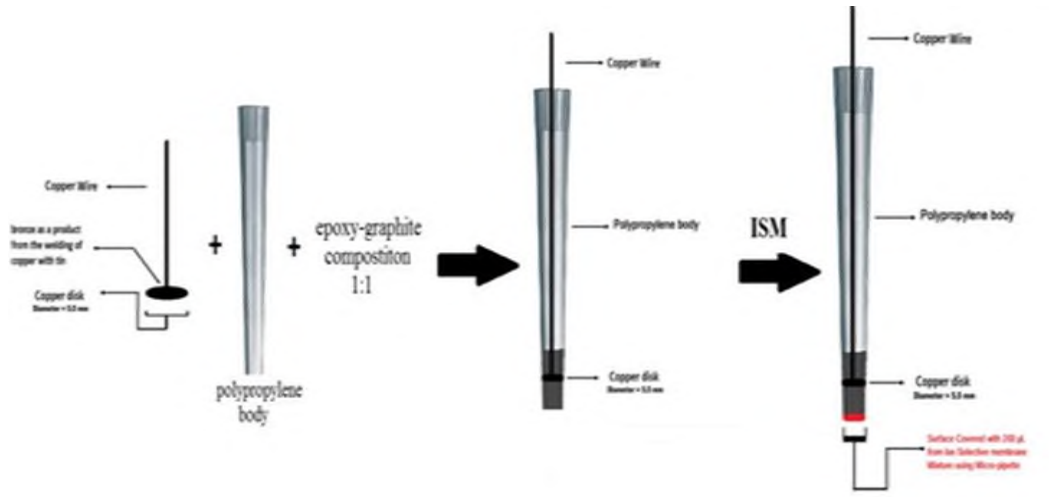

Figure 2. Fabrication of a SC-ISE high double layer capacitance based on epoxy-graphite composite.

Table 1. Potentiometric response characteristics of SCN^- membrane sensors type (A) and (B) in 0.1 mol L^{-1} acetate buffer pH (5.0).

Parameter	Sensors type (A)				Sensors type (B)			
	Sensor I	**Sensor II**	**Sensor III**	**Sensor IV**	**Sensor I**	**Sensor II**	**Sensor III**	**Sensor IV**
Slope, (mV decade^{-1})	-53.7 ± 0.6	-55.3 ± 0.9	-54.7 ± 1.5	-55.8 ± 0.95	-46.4 ± 1.1	-56.1 ± 1.7	-55.1 ± 0.78	-62.4 ± 0.5
Correlation coefficient, (r)	0.9998	0.9999	0.9998	0.99997	0.9988	0.9998	0.9996	0.9995
Linear range, mol L^{-1}	$5.0x10^{-6}$ - $1.0x\ 10^{-2}$	$5.0x\ 10^{-5}$ - $1.0x\ 10^{-2}$	$5.0x10^{-5}$ - $1.0x10^{-2}$	$5.0x10^{-5}$ - $1.0x10^{-2}$	$5.0x10^{-5}$ - $1.0x10^{-2}$	$5.0x10^{-5}$ - $1.0x10^{-2}$	$5.0x10^{-5}$ - $1.0x10^{-2}$	$5.0x10^{-6}$ - $1.0x10^{-2}$
Detection limit, mol L^{-1}	$1.45x10^{-6}$	$2.68x10^{-6}$	$7.56x10^{-6}$	$3.88x10^{-6}$	$5.0x10^{-6}$	$2.9\ x10^{-6}$	$5.3x10^{-6}$	$2.0\ x10^{-6}$
Working range, (pH)	3.5 – 10.0	4.5-10.0	3.0 – 10.0	4.0 – 10.0	4.0 – 7.0	2.5 – 8.0	4.0 – 10.0	4.0 – 10.0
Response time, (s)	10	15	30	10	10	10	10	10
Life span, (week)	12	12	12	8	12	12	12	8
Intercept	-201.7	-148.2	-182.8	-233.4	-21.4	-46.0	-65.6	-110.8
Standard deviation σv(mv)	0.6	0.9	1.5	0.95	1.1	1.7	0.78	0.5

The sensors were calibrated under a static mode of operation by transferring (0.5-1.0) mL aliquots of a $1.0\ x\ 10^{-1}$-$1.0\ x\ 10^{-4}$ mol L^{-1} aqueous solution of SCN^- to a 25 mL beaker containing 10.0 mL of 0.1mol L^{-1} acetate buffer of pH 5.0. The potential readings were recorded after stabilization to ±1 mV.

Determination of SCN^- content in saliva

Different saliva samples were collected from cigarette smokers and non-smokers into polyethylene tubes. The samples were immediately centrifuged and stored at 4 ºC. A 1 mL aliquot of the sample was transferred into 10 mL measuring flask and diluted with 0.1 mol L^{-1} acetate buffer (pH= 5.0). The proposed sensor in conjunction with the reference electrode were immersed in the solution, and the potential readings were recorded after stabilization.

Cyanide determination

An aliquot of 10 mL of standard 1.0 mol L^{-1} CN^- test solution was boiled for 30 min using a hot plate with 1.0 g potassium polysulfide, pH adjusted at 10 by ammonia solution to prevent formation of volatile HCN. The solution was cooled, transferred into a 100 mL measuring flask and completed to the mark with 0.1 mol L^{-1} acetate buffer of pH 5.0. Further dilutions ($1.0x10^{-2}$-$1.0x10^{-4}$) were made by the same buffer solution. The solutions were shaken well and (0.5-1.0) mL aliquots of a $1.0\ x\ 10^{-1}$-$1.0\ x\ 10^{-4}$ mol L^{-1} of converted CN^- solution were transferred into a 25 mL beaker. The potential changes after each addition was recorded, and a calibration curve was constructed by plotting the potential reading against the concentration of cyanide ions.

RESULTS AND DISCUSSIONS

Characterization of Al/PAR complex

4-(2-Pyridylazo)resorcinol monosodium salt monohydrate (PAR) reacts with $K[Al(SO_4)_2].12H_2O$ to form an orange complex. The precipitate was isolated and characterized by elemental analysis. Al/PAR, K[Al/PAR], $K[Al(C_{11}H_7N_3O_2)_2].2H_2O$; yield 80 %, orange, m.p. >300 ºC. Anal.: Calcd. for $K[Al(C_{11}H_7N_3O_2)_2].2H_2O$: C, 49.34; H 3.36; N 15.70. Found: C 46.25; H 3.58; N 14.88. The conductivity measurements showed a conductance value of 17.36 µs cm^{-1} indicating the non-electrolytic nature of the

complex. The IR spectra of both PAR and Al/PAR complex are shown in Figure S1. The IR spectrum of the free ligand displayed strong bands at 3419 cm^{-1}, 1491.8 cm^{-1}, 1325.5 cm^{-1} and 1213.4cm^{-1} due to O-H, C=C, C-N and C-O. In the IR spectrum of Al/PAR, these bands are shifted to 3437.96 cm^{-1}, 1477.65 cm^{-1}, 1285.83cm^{-1} and 1192.18 cm^{-1}, respectively. This confirms the complexation between Al^{3+} ion and the PAR ligand. Mass spectroscopy analysis with molecular weight 536.0 confirmed the formation of 2:1 complex as shown in Figure S2.

Performance characteristics of thiocyanate sensors

Development of new potentiometric ion-sensors with better designs is a prospering area of research. An improvement in detection limit is more likely by introduction of solid inner contact instead of the traditional internal filling solution of the membrane. This may ideally give rise to a more reliable and robust sensors.

We have designed and characterized these new sensors, a conventional and solid contact types for thiocyanate monitoring and then compared their properties in light of these considerations. The optimum membrane composition was 33.0 wt % PVC, 1.0 wt % sensing material, 66.0 wt % of the plasticizer, and 0.5 wt % TDMAC as cation excluder in case of Al (III)–PAR complex and MgPC, whereas 33.0 wt % PVC, 1.0 wt % sensing material, 66.0 wt % of the plasticizer in case of aliquat and TDMAC ion exchangers. The response characteristics of thiocyanate sensors based on these ionophores were given in Table 1. Sensors based on Al(III)–PAR/TDMAC complex (sensor I) revealed a potentiometric response towards SCN^- ions with near-Nernstian slope of -53.7±0.6 and -46.4±1.1 mV $decade^{-1}$ (r^2 = 0.9998 and 0.9988) and a detection limit of $1.45x10^{-6}$ and $5.0x10^{-6}$ mol L^{-1} for type (A) and (B) sensors, respectively. For sensors based on MgPC/TDMAC (sensor II) exhibited a Nernstian potentiometric slope of -55.3±0.9 and -56.1±1.7 mV $decade^{-1}$ (r^2 = 0.9999 and 0.9998) with a detection limit of $2.7x10^{-6}$ and $2.9x10^{-6}$ mol L^{-1} for type (A) and (B) sensors, respectively. For sensor III based on aliquat exhibited a potentiometric response with near-Nernstian slope of -54.7±1.5 and -55.1±0.8 mV $decade^{-1}$ (r^2 = 0.9998 and 0.9996) and a detection limit of $7.56x10^{-6}$ and $5.3x10^{-6}$ mol L^{-1} for type (A) and (B) sensors, respectively. Sensors based on TDMAC only (sensor IV) exhibited a potentiometric response towards SCN^- ions with near-Nernstian slope of -55.8±0.9 and -62.4±0.5 mV $decade^{-1}$ (r^2 = 0.9999 and 0.9995) and a detection limit of $3.9x10^{-6}$ and $2.0x10^{-6}$ mol L^{-1} for type (A) and (B) respectively. Potentiometric responses of these sensors are shown in Figure 3.

The pH effect on the potentiometric response of the sensors was studied over the pH range of 2 to 11 at fixed concentrations of thiocyanate (1.0×10^{-3} and 1.0×10^{-2} mol L^{-1}). The pH of these solutions was adjusted by adding NaOH and/or HCl. The solid contact sensors exhibited wider pH range 3.5-10, 4.5-10, 3.5-10 and 4-10 for sensor I, II, III, and IV, respectively.

For conventional sensors, they were pH independent in the pH range 4.0-7.0, 2.5-8.0, 4.0-10, 5.0-9.0 and 4.0-7.0 for sensor I, II, III, IV and V, respectively. The potentials of all sensors considerably declined with negative drift at higher pH values probably due to an increase of the OH^- competition with the SCN^- anion. The sensors were stored and conditioned in 10^{-2} mol L^{-1} SCN^- solution of pH 5.0. With all sensors examined, the detection limits, response times, linear ranges and calibration slopes were reproducible within ±3 % of their original values over a period of at least 12 weeks for both sensors types.

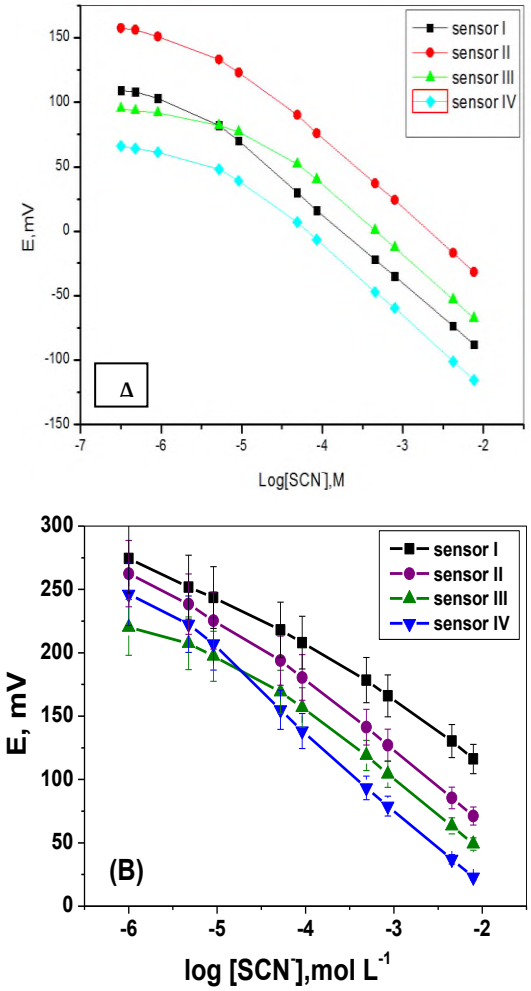

Figure 3. Calibration plot of thiocyanate sensors type (A) and type (B) I, II, III and IV; in 0. 1 mol L^{-1} acetate buffer pH 5.0

One of the important features of the electrochemical sensor is the response time which can be evaluated by measuring the time required to achieve a steady-state potential with in ±0.2 mV of the final equilibrium value after successive immersion in a series of SCN^- solution, each having a 10-fold difference from low to high concentrations. The time required to achieve a steady potential response (±3 mV) using the proposed sensors in 10^{-6} to 10^{-4} mol L^{-1} SCN^- solutions with a rapid 10-fold increase in concentration was < 20 s and < 10 s for sensors type (B) and type (A), respectively. Replicate calibrations for each sensor indicated low potential drift, long-term stability and negligible change in the response of the sensors.

Effect of foreign ions on thiocyanate sensors

Selectivity of the sensors was assessed by means of potentiometric selectivity coefficients ($K^{POT}_{SCN,J}$), calculated by the fixed interference method (FIM).[37] The potential

measurements determined by using a solution contain a fixed activity of the interfering ion (10^{-3} mol L^{-1}) on acetate buffer pH 5.0 and varying the activity of the primary ion. The logarithmic values of log $K^{POT}_{SCN,J}$ were indicated in Table 2.

The selectivity order for type (A) sensors were illustrated as follow: For sensor I, the selectivity order as follow sensor I revealed a selectivity pattern $SCN^- > I^- > IO_4^- > S_2O_3^{2-} > NO_3^- > Br^- > NO_2^- > S^{2-} > CN^- > SO_3^{2-} > Cl^- > F^- > ClO_4^- > SO_4^{2-}$, sensor II: $SCN^- > IO_4^- > I^- > S_2O_3^{2-} > NO_3^- > CN^- > S^{2-} > Br^- > ClO_4^- > F^- > NO_2^- > SO_3^{2-} > Cl^- > SO_4^{2-}$, sensor III: $SCN^- > IO_4^- > I^- > S_2O_3^{2-} > NO_3^- > S^{2-} > CN^- > SO_3^{2-} > SO_4^{2-} > Br^- > ClO_4^- > NO_2^- > Cl^- > F^-$ and sensor IV: $SCN^- > I^- > IO_4^- > S_2O_3^{2-} > NO_3^- > CN^- > Br^- > SO_3^{2-} > NO_2^- > F^- > ClO_4^- > Cl^- > SO_4^{2-} > S^{2-}$.

Table 2. Effect of foreign ions on SCN^- membrane sensors type (A) and (B) by using FIM.

Interfering anion	log $K^{POT}_{SCN^-}$, B							
	Sensor type (A)				Sensor type (B)			
	Sensor I	Sensor II	Sensor III	Sensor IV	Sensor I	Sensor II	Sensor III	Sensor IV
SCN^-	0	0	0	0	0	0	0	0
Br^-	-2.34	-2.44	-2.27	-2.15	-1.66	-1.7	-1.8	-1.83
Cl^-	-2.84	-2.64	-2.36	-2.38	-1.66	-1.63	-1.77	-2.05
ClO_4^-	-2.93	-2.44	-2.24	-2.36	-1.11	-1.28	-1.35	-1.1
CN^-	-2.52	-2.16	-2.01	-1.95	-1.42	-1.5	-1.65	-1.88
F^-	-2.85	-2.50	-2.39	-2.29	-1.63	-1.74	-1.81	-2.16
I^-	-0.75	-0.68	-0.78	-0.67	-0.67	-0.6	-0.63	-0.5
NO_2^-	-2.41	-2.52	-2.25	-2.29	-1.53	-1.58	-1.7	-1.83
NO_3	-1.81	-1.71	-1.59	-1.72	-1.26	-1.36	-1.42	-1.38
S_2^{2-}	-2.46	-2.42	-1.91	-2.55	-2.16	-2.5	-2.1	-2.25
$S_2O_3^{2-}$	-1.55	-1.48	-1.19	-1.38	-1.43	-1.98	-1.59	-1.51
SO_3^{2-}	-2.62	-2.51	-2.08	-2.24	-2.22	-2.11	-1.89	-2.01
SO_4^{2-}	-2.94	-2.64	-2.18	-2.54	-2.54	-2.24	-2.07	-2.34
IO_4^-	-1.12	-0.50	-0.33	-0.73	-1.012	-0.73	-0.42	-0.62

Table 4. Determination of thiocyanate in saliva samples using type (A) sensors I, II, III and IV.

No. of smoked cigarettes Day^{-1}	Spectrophotometry* [Saliva-SCN^-] mol L^{-1}	Potentiometry* [Saliva-SCN^-] mol L^{-1}			
		Sensor I	Sensor II	Sensor III	Sensor V
0	8.59×10^{-5}	8.47×10^{-5}	8.9×10^{-5}	8.7×10^{-5}	8.49×10^{-5}
15 - 20	7.46×10^{-4}	7.2×10^{-4}	7.62×10^{-4}	7.5×10^{-4}	7.35×10^{-4}
20 - 25	9.34×10^{-3}	9.27×10^{-3}	9.5×10^{-3}	9.4×10^{-3}	9.3×10^{-3}

*Average of 5 measurements

For Sensors type (B) they exhibited selectivity order as follow: sensor I revealed a selectivity pattern $SCN^- > I^- > IO_4^- > ClO_4^- > NO_3^- > CN^- > S_2O_3^{2-} > NO_2^- > F^- > Cl^- > Br^- > S^{2-} > SO_3^{2-} > SO_4^{2-}$, sensor II: $SCN^- > I^- > IO_4^- > ClO_4^- > NO_3^- > CN^- > NO_2^- > Cl^- > Br^- > F^- > S_2O_3^{2-} > SO_3^{2-} > SO_4^{2-} > S^{2-}$, sensor III: $SCN^- > I^- > IO_4^- > ClO_4^- > NO_3^- > S_2O_3^{2-} > CN^- > NO_2^- > Cl^- > Br^- > F^- > SO_3^{2-} > SO_4^{2-} > S^{2-}$ and sensor IV: $SCN^- > I^- > IO_4^- > ClO_4^- > NO_3^- > S_2O_3^{2-} > NO_2^- > Br^- > CN^- > SO_3^{2-} > Cl^- > F^- > S^{2-} > SO_4^{2-}$ and all the results are summarized in Table 2. As noticed from the results, sensor I exhibited better selectivity towards the lipophilic anions such as I^-, ClO_4^-, IO_4^- and NO_3^- than other sensors. Finaly we can conclude that, the selectivity is mainly depending on the membrain composition but the electrode configuration has no observed effect on the selectivity pattern of all proposed sensors.

Hydrodynamic monitoring of thiocyanate

Flow-through analysis using potentiometric detectors showed high advantages such as low cost, simple instrumentation and automation. In addition, the transient nature of the signal in flow injection analysis is help to overcome the effects of interfering ions if the electrode's response to the target analyte is faster than those interfering ions.[38] A tubular-type detector incorporating Al (III)–PAR/TDMAC (sensor I), MgPC/TDMAC (sensor II) and Aliquat sensor (III) based membrane sensors were prepared and used under the hydrodynamic mode of operation for continuous SCN^- quantification. A triplicate transient peaks were obtained from the flow injection analysis system under optimal experimental conditions and are shown in Figures 4A, 4B and 4C.

Table 3. Potentiometric response characteristics of SCN^- membrane type (B) sensors I, II and III using FI operation.

Parameters	Sensor I	Sensor II	Sensor III
Slope	-46.5±0.2	-52.0±0.3	-53.3±0.1
Correlation coefficient, (*r*)	0.998	0.9999	0.9996
Linear range mol L^{-1}	1.0 x10^{-4} – 1.0 x 10^{-1}	1.0 x10^{-4} – 1.0 x 10^{-1}	1.0 x10^{-4} – 1.0 x 10^{-1}
Detection limit mol L^{-1}	1.0 x 10^{-5}	1.0 x 10^{-5}	1.0 x 10^{-5}
Life span (week)	12	12	12
Intercept	-14.7	-29	-41.5
Flow rate mL min^{-1}.	4.0	4.0	4.0

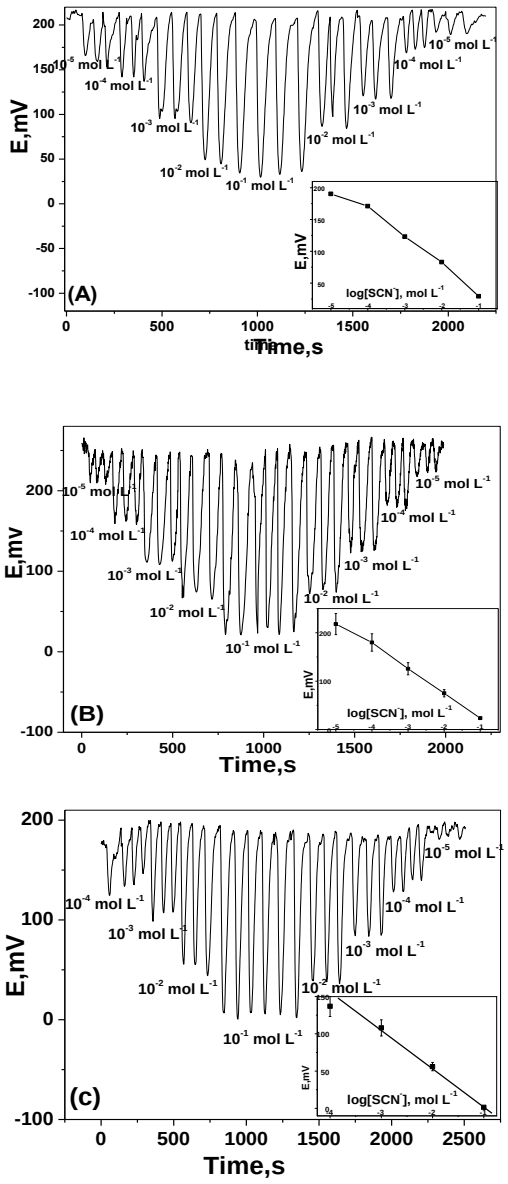

Figure 4. Transient potentiometric signals obtained in triplicate for sensor I (A) , sensor II (B) and sensor III (C). Conditions: carrier solution, 0.1 mol L^{-1} acetate buffer pH 5.0, flow rate 4.0 mLmin^{-1}; sample volume, 500 µL.

A linear relationship between the SCN^- concentrations and FIA signals was obtained over a concentration range of 1.0 x 10^{-5} to 1.0 x 10^{-1} mol L^{-1} using a 0.1 mol L^{-1} acetate buffer, pH 5.0. The general analytical features recorded under optimum flow conditions are presented in Table 3. The slope of the calibration plot was near-Nernstian (-46.5, -52.0 and -53.3 mV $decade^{-1}$), there lower limit of detection was 1.0 x 10^{-5} mol L^{-1}, and the sampling frequencies were about 44, 54 and 44 samples per hour respectively.

Thiocyanate determination in saliva

In the saliva of cigarette smokers, rhodanaze enzyme catalyzes the detoxification reaction of hydrogen cyanide forming thiocyanate. The possibility of using the proposed sensors to measure SCN^- concentration in human saliva samples was examined. Table 4 indicates that the concentrations of saliva-SCN^- in the groups under study fairly agreed with data obtained by the standard spectrophotometric method.[39]

The *F*-test showed no significant difference at the 95 % confidence level between the mean and the variance of the potentiometrric and spectrophotometric set of results. The calculated F-values (n = 5) were found to be in the range 1.1-5.2 compared with the tabulate value (6.39) at the 95 % confidence limit. 1

Cyanide determination in electroplating baths

Determination of cyanide ion after its conversion to thiocyanate ion using the potassium polysulfide treatment was investigated. Such a conversion is well-documented,[40] and occurs according to the following reaction:

$$K_2S_x + CN^- \rightarrow SCN^- + K_2S_{x-1}$$

Table 5. Potentiometric determination of cyanide in electroplating baths after conversion into thiocyanate using a thiocyanate PVC membrane type (B) sensor I, II and III.

ISE	Cyanide content (mol L^{-1})*			
	Batch		Flow	
	Waste-water	Electro-plating bath	Waste-water	Electro-plating bath
Sensor I	0.014	0.14	0.02	0.14
Sensor II	0.016	0.15	0.016	0.16
Sensor III	0.016	0.14	0.015	0. 14
Cyanide sensor[a]	0.015	0.14	-	-

*Average of 5 measurements; [2]Orion Cyanide solid state sensor

A linear calibration curve for CN^- ions (1.0 x 10^{-5}-1.0x10^{-2} mol L^{-1}) after conversion into SCN^- by a treatment with potassium polysulfide, followed by monitoring using the proposed sensors were obtained. The method was used for the potentiometric determination of free cyanide ions in industrial waste-water and electroplating samples obtained from an electroplating factory. These sensors are used under the hydrodynamic mode of operation for continuous monitoring of CN^- ions (1.0 x 10^{-4} - 1.0 x 10^{-1} mol L^{-1}) after conversion into SCN^- using a 0.1mol L^{-1} acetate buffer, pH 5.0 as a flow carrier. The obtained results agreed with data obtained using the solid state cyanide ion-selective electrode Table 5**.**

CONCLUSION

Two Types of potentiometric ISE (Solid type (A) and conventional type (B)) were studied to give a fast and simple method for determination of thiocyanate under static (manual) mode of operation and hydrodynamic (FIA) mode of operation for type (B). A new Al (III)–PAR complex was prepared and developed by using TDMAC as anionic additive. ISE type (A) improved the response of sensor I towards SCN^{-1} ion with lower detection limit $1.45x10^{-6}$ mol L^{-1} and slope of -53.7 mV $decade^{-1}$ while that of type (B) exhibit detection limit $5.0x10^{-6}$ mol L^{-1} and a Nernstian slope of -46.4 ± 1.1 mV $decade^{-1}$. So ISE type (A) can be preferred to use as a tool for low SCN^{-} concentration determination in biological fluids (saliva). ISE type (B) used for determination of CN^{-} ion in waste and electroplating.

REFERENCES

[1]Hassan, S. S. M.**,** Kamel, A. H., Abd El-Naby, H., Flow-Through Potentiometric Sensors for Alizarin Red S Dye and Their Application for Aluminum Determination, *J. Chin. Chem. Soc.*, **2014,** *61*, 295. https://doi.org/10.1002/jccs.201300293

[2]Hassan**,** S. S. M,. Kamel, A. H., Abd El-Naby, H., New potentiometric sensors based on selective recognition sites for determination of ephedrine in some pharmaceuticals and biological fluids, *Talanta*, **2013,** *103***,** 330**.** doi: 10.1016/j.talanta.2012.10.067.

[3]Hassan, S. S. M., Sayour, H. E. M., Kamel, A. H.**,** A simple-potentiometric method for determination of acid and alkaline phosphatase enzymes in biological fluids and dairy products using a nitrophenylphosphate plastic membrane sensor, *Anal. Chim. Acta*, **2009,** *640*, 75. https://doi.org/10.1016/j.aca.2009.03.019

[4]Kamel, A. H., New potentiometric transducer based on a Mn(II) [2-formylquinoline thiosemicarbazone] complex for static and hydrodynamic assessment of azides, *Talanta*, **2015**, *144*, 1085. DOI: 10.1016/j.talanta.2015.07.075

[5]van de Velde, L., d'Angremont, E. , Olthuis, W., Solid contact potassium selective electrodes for biomedical applications - a review, *Talanta*, **2016**, *160*, 56. DOI: 10.1016/j.talanta.2016.06.050

[6]Zou, X. U., Cheong, J. H., Taitt, B. J., Bühlmann, P., Solid contact ion-selective electrodes with a well-controlled Co(II)/Co(III) redox buffer layer, *Anal Chem.* **2013,** *85(19)*, 9350-5., DOI:10.1021/ac4022117

[7]Michalska, A**.,** All-Solid-State Ion Selective and All-Solid-State Reference Electrodes**,** *Electroanalysis*, **2012**, *24*, 1253. https://doi.org/10.1002/elan.201200059

[8]Kimmel, D. W., LeBlanc, G., Meschievitz, M. E., Cliffel, D. E., Electrochemical sensors and biosensors, *Anal. Chem.*, **2012**, *84*, 685. DOI: 10.1021/ac202878q

[9]Tymecki, L., Glab, S., Koncki, R., Miniaturized, Planar Ion-selective Electrodes Fabricated by Means of Thick-film Technology, *Sensors*, **2006**, *6*, 390. doi:10.3390/s6040390

[10]Sokalski, T., Ceresa, A., Zwickl, T., Pretsch, E., Large Improvement of the Lower Detection Limit of Ion-Selective Polymer Membrane Electrodes, *J. Am. Chem. Soc.*, **1997**, *119*, 11347. DOI: 10.1021/ja972932h

[11]Sokalski, T., Ceresa, A., Fibbioli, M., Zwickl, T., Bakker, E., Pretsch, E., Lowering the Detection Limit of Solvent Polymeric Ion-Selective Membrane Electrodes. 2. Influence of Composition of Sample and Internal Electrolyte Solution, *Anal. Chem.***,** **1999**, *71*, 1210. DOI: 10.1021/ac9809332

[12]Qin, W., Zwickl, T., Pretsch, E., Improved Detection Limits and Unbiased Selectivity Coefficients Obtained by Using Ion-Exchange Resins in the Inner Reference Solution of Ion-Selective Polymeric Membrane Electrodes, *Anal. Chem.***,** **2000**, *72*, 3236. **DOI:** 10.1021/ac000155p

[13]Ceresa, A., Radu, A., Peper, S., Bakker, E., Pretsch, E., Rational design of potentiometric trace level ion sensors. A Ag+-selective electrode with a 100 ppt detection limit, *Anal. Chem.*, **2002**, *74*, 4027. DOI: 10.1021/ac025548y

[14]Cadogan, A., Gao, Z., Lewenstam, A., Ivaska, A., Diamond, D., All-solid-state sodium-selective electrode based on a calixarene ionophore in a poly(vinyl chloride) membrane with a polypyrrole solid contact, *Anal. Chem.*, **1992**, *64*, 2496. DOI: 10.1021/ac00045a007

[15]Cattrall, R. W., Freiser, H., Coated wire ion-selective electrodes, *Anal. Chem.*, **1971**, *43*, 1905. DOI: 10.1021/ac60307a032

[16]Buck, R. P., Freiser, H. (Ed.), *Ion-Selective Electrodes in Analytical Chemistry*, Plenum, New York, **1980**, 58.

[17]Michalska, A., Optimizing the analytical performance and construction of ion-selective electrodes with conducting polymer-based ion-to-electron transducers, *Anal. Bioanal. Chem.*, **2006**, *384*, 391. DOI: 10.1007/s00216-005-0132-4

[18]Bobacka, J., Ivaska, A., Lewenstam, A., Potentiometric sensors based on poly(3,4-ethylenedioxythiophene) (PEDOT) doped with sulfonated calix[4]arene and calix[4]resorcarenes, *Electroanalysis*, **2002**, *15*, 366. DOI 10.1007/s10008-004-0597-7

[19]Mousavi, Z., Bobacka, J., Ivaska, A., Potentiometric Ag+ Sensors Based on Conducting Polymers: A Comparison between Poly(3,4 - ethylenedioxythiophene) and Polypyrrole Doped with Sulfonated Calixarenes , *Electroanalysis*, **2005**, *17*, 1609. https://doi.org/10.1002/elan.200503269

[20]Sutter, J., Radu, A., Peper, S., Bakker, E., Pretsch, E., Solid-contact polymeric membrane electrodes with detection limits in the subnanomolar range, *Anal. Chim. Acta.*, **2004**, *523*, 53. https://doi.org/10.1016/j.aca.2004.07.016

[21]Parra, E. J., Crespo, G. A., Riu, J., Ruiz, A., Rius, F. X., Ion-selective electrodes using multi-walled carbon nanotubes as ion-to-electron transducers for the detection of perchlorate., *Analyst*, **2009**, *134* , 1905. DOI: 10.1039/b908224g

[22]Rius-Ruiz, F. X., Crespo, G. A., Bejarano-Nosas, D., Blondeau, P., Riu, J., Rius, F. X., Disposable planar reference electrode based on carbon nanotubes and polyacrylate membrane, *Anal. Chem.***,** **2011**, *83*, 8810. DOI: 10.1021/ac200627h

[23]Ping, J., Wang, Y., Wu, J., Ying, Y., Development of an all-solid-state potassium ion-selective electrode using graphene as the solid-contact transducer, *Electrochem. Commun.*, **2011**, *13*, 1529.

[24]Li, F., Ye, J., Zhou, M., Gan, S., Zhang, Q., Han, D., All-solid-state potassium-selective electrode using graphene as the solid contact , *Analyst*, **2012**, *137*, 618. DOI: 10.1039/C1AN15705A

[25]Jaworska, E., Lewandowski, W., Mieczkowski, J., Maksymiuk, K., Michalska, A., Critical assessment of graphene as ion-to-electron transducer for all-solid-state potentiometric sensors., *Talanta*, **2012**, *97*, 414. DOI: 10.1016/j.talanta.2012.04.054

[26]Hu, J., Zou, X. U., Stein, A., Bühlmann, P., Ion-Selective Electrodes with Colloid-Imprinted Mesoporous Carbon as Solid Contact, *Anal. Chem.***,** **2014**, *86*, 7111. DOI: 10.1021/ac501633r

[27]Han, W., Hong, T., Lee, Y., Thiocyanate Ion Selective Solid Contact Electrode Based on Mn Complex of N,N'-BIs-(4-Phenylazosalicylidene)-O-Phenylene Diamine Ionophore, *Am. J. Anal. Chem.*, **2011**, *2*, 731. DOI: 10.4236/ajac.2011.26084

[28]Vlascici, D., Pica, E. M., Fagadar-Cosma, E., Cosma, V., Bizerea, O., Thiocyanate and fluoride electrochemical sensors based on nanostructurated metalloporphyrin systems, *J. Optoelectr. Adv. Mat.*, **2008,** *10*, 2303.

[29]Vlascici, D., Fagadar-Cosma, E. and Bizerea-Spiridon, O., A New Composition for Co(II)-porphyrin-based Membranes Used in Thiocyanate-selective Electrodes, *Sensors*, **2006**, *6*, 892. https://doi.org/10.3390/s6080892

[30]Shehab, O. R., Mansour, A. M., New thiocyanate potentiometric sensors based on sulfadimidine metal complexes: experimental and theoretical studies, *Biosen. Bioelect*., **2014**, *57*, 77. DOI: 10.1016/j.bios.2014.01.051

[31]Arvand, M., Zanjanchi, M. A., Heydari, L., Voltammetric Oxidation of Potassium Thiocyanate using $ErBa_2Cu_3O_7$ Modified Glassy Carbon Electrode, *Sens. Act. B*, **2007**, *122*, 301.

[32]Khorasan, J. H., Amin, M. K., Motagh, H., Tangestaninejad ,S., Moghadam, M., Manganese porphyrin derivatives as ionophores for thiocyanate-selective electrodes: the influence of porphyrin substituents and additives on the response properties, *Sens. Act. B*, **2002**, *87*, 448. https://doi.org/10.1016/S0925-4005(02)00294-0

[33]*Standard Methods for the Examination of Water and Wastewater*, 19th ed., American Public Health Association, Washington **1995**.

[34]Kamel, A. H., Khalifa, M. E., Abd El-Maksoud, S. A., Elgendy, F. A., Selective sensors for potentiometric assessment of iodide based on anion recognition through copper(II) dipeptide derivative complex, *Eur. Chem. Bull.*, **2016**, *5*, 368. DOI: 10.17628/ECB.2016.5.368

[35]Kamel, A. H., El-Naggar, A. M., Argig, A. A. A., Response characteristics of lead-selective membrane sensors based on a newly synthesized quinoxaline derivatives as neutral carrier ionophores, *Ionics*, **2017**, *23*, 3497. DOI https://doi.org/10.1007/s11581-017-2141-7

[36]Cammann, K., Working with lon-Selective Electrodes: Chemical Laboratory Practice, Springer-Verlag, Berlin, **1979**.

[37]Umezawa, Y., Buhlmann, P., Umezawa, K., Tohda, K., Amemiya, S., Potentiometric selectivity coefficients of ion-selective electrodes part I. Inorganic cations (technical report), *Pure Appl. Chem*., **2000,** *72*, 1851.

[38]Cammann, K., Flow injection analysis with electrochemical detection, *Fres, Z., Anal. Chem.*, **1988**, *329*, 691. DOI https://doi.org/10.1007/BF00624777

[39]Hovinen, J., Lahti, M., Vilpo, J., Spectrophotometric Determination of Thiocyanate in Human Saliva, *J. Chem. Educ*., **1999**, *76*, 1281. DOI: 10.1021/ed076p1281

[40]Demirata, B., Apak, R., Asfar, H., Tor, I., Spectrophotometric determination of organic nitrogen by a modified Lassaigne method and its application to meat products and baby food., *J. AOAC*, **2002**, *85*, 971.

Received: 04.06.2018.
Accepted: 17.08.2018.